Improving the Deterministic Reserve Requirements Method to Mitigate Wind Uncertainty

Thèse

Jules Bonaventure Mogo

Doctorat en génie électrique
Philosophiæ doctor (Ph. D.)

Québec, Canada

Improving the Deterministic Reserve Requirements Method to Mitigate Wind Uncertainty

Thèse

Jules Bonaventure Mogo

Sous la direction de:

Jérôme Cros, directeur de recherche

Innocent Kamwa, codirecteur de recherche

Résumé

Atténuation de l'Aléa Éolien par Optimisation de
l'Approche Deterministe de la Réserve d'Exploitation.

Les réseaux électriques sont sujets aux aléas divers pouvant éventuellement mettre en péril leur sûreté. Des événements résultants de l'aléa météorologique ou de la défaillance stochastique des composants du réseau tels qu'une fluctuation de températures hors saison ou la perte d'une unité de production, peuvent causer des déséquilibres inattendus entre l'offre et la demande et entraîner des délestages. Pour faire face à ces aléas, des marges de puissance ou 'réserve' sont ménagées par rapport au strict équilibrage de l'offre et de la demande prévisionnelle. Cependant, déterminer la quantité de réserve suffisante pour une opération fiable et rentable est un problème difficile à résoudre, particulièrement en présence d'incertitude croissante due à la libéralisation du marché de l'électricité et à la pénétration à grande échelle des éoliennes sur le réseau.

L'approche déterministe considère un niveau de réserve statique du jour pour le lendemain. L'énergie éolienne étant faiblement prévisible, de la réserve supplémentaire est requise pour pallier l'intermittence du vent. Parce que les éoliennes ne sont pas distribuables, les générateurs conventionnels ont été laissés sous pression en répondant aux variations larges et rapides de la charge nette du réseau. Étant données les contraintes de rampe qui limitent leur flexibilité, le bon fonctionnement du marché de l'électricité peut être altéré parce que les transactions d'énergie qui y sont contractées risquent de ne pas être réalisées en temps réel comme convenu pour des raisons de sécurité. Dans ce contexte, l'utilisation de l'approche déterministe à elle seule comme c'est le cas aujourd'hui, pourrait ne pas être économique ou fiable pour contenir les risques encourus; d'où la nécessité des méthodes sophistiquées basées sur une représentation plus complexe de l'incertitude.

Cette thèse propose des solutions viables et efficientes à l'incertitude croissante dans l'opération à court terme des réseaux électriques en présence d'éoliennes à grande échelle et dans un contexte de compétition. Le caractère conservatif de la méthode déterministe a été grandement amélioré par une génération de réserve supplémentaire, contrôlable, et qui tient en compte l'aspect stochastique des éoliennes. La mutualisation des capacités via l'interconnexion permet d'alléger la contrainte d'équilibrage du réseau et de réduire les secousses autour des générateurs conventionnels. Afin de faciliter les transactions d'énergie sur le marché, des règles ont été élaborées pour inciter la mise en disponibilité des générateurs à larges paliers de rampes. Un problème combiné de la programmation des centrales et de transit optimal de puissance incorporant tous les objectifs sus-cités a été formulé. Traduit en programmation mixte quadratique car générant des solutions faisables dont le niveau d'optimalité est connu, celui-ci a été utilisé pour investiguer divers effets de l'interconnexion sur la réduction des coûts d'exploitations associés à plus d'éoliennes sur le réseau. Enfin et surtout, la capacité de notre modèle à résister aux contingences a été validée avec un modèle qui tient compte de l'aspect aléatoire des composants du réseau à tomber en panne. Ce qui nous a permis d'ajuster notre stratégie du marché du jour pour le lendemain par rapport à celui du temps réel. Notre modèle se distingue par sa rapidité et sa capacité à révéler les coûts cachés de l'intégration des éoliennes dans les réseaux électriques.

Abstract

Power grids are subject to a variety of uncertainties that may expose them to potential safety issues. Interruptions in electricity supply for instance, may result from an unseasonable temperature fluctuations or a power station outage, which are events of stochastic nature involving the weather or the failure of a component in the grid. The result may be sudden imbalances in supply and demand, leading to load interruptions. To plan for such unforeseen events, the grid carries 'reserve', i.e., additional capacity above that needed to meet actual demand. However, scheduling the appropriate amount of reserve needed for a reliable and cost-effective grid operation is very challenging, especially in the context of increased uncertainties due to liberalization and the large-scale wind electric generators (WEGs) penetration to grid.

Traditional grids assume a fixed knowledge of system conditions for the next day. Wind power being very poor to predict, an extra reserve generation to accommodate its uncertainty is required. Because WEGs aren't built around spinning turbines, conventional units have been left stressed while responding to large and fast variations in the system net load. Given the temporal operating restrictions that limit their flexibility, the properly functioning of the electricity market can be altered as the energy transactions may not be carried out in real-time, exactly as agreed for security reasons. In this context, the use of the deterministic criteria alone as is the case today, may not be economical or reliable in limiting the risk of uncertainty; calling for sophisticated methods based on more-complex characteristics of uncertainty.

This thesis proposes reliable and sound solutions to the increased variability and uncertainty in short-term power grid operations emanating from increasing the share of WEGs in the generation mix and competition from electricity markets. The conservativeness of the deter-

ministic method has been greatly improved with an adjustable extra generation reserve that accounts for the stochastic feature of WEGs. An inherent flexibility–design that attempts to reduce the onus placed on conventional units to balance the system has been considered. In doing so, the jerkings around these units while responding to large and fast variations in the system net load have been considerably mitigated. Adequate market policies that incentivize flexible resources to make their units with higher ramp rates available to follow dispatch signals have been crafted, thereby avoiding potential reliability degradation or costly out-of-market actions. A combined Security Constrained Unit Commitment (SCUC) and Optimal Power Flow (OPF) optimization problem that encompasses all the above mentioned goals has been formulated. Translated into a Mixed Integer Quadratic Programming (MIQP) problem that can return a feasible solution with a known optimality level, the SCUC-OPF engine has been used to investigate various effects of grids integration on reducing the overall operating costs associated with more wind power in the system. Last but not least, the effectiveness of our model to withstand contingencies has been done with a probabilistic model benchmark that accounts for the random nature of grid failure. This allows the adjustment of the Day-Ahead Market (DAM) strategy with respect to the Real-Time Market (RTM). Our model is proven to be more acceptable as it is time-saving, and has particular implications for wind integration studies as it can reverse the hidden cost of integrating WEGs to grid.

Contents

List of Tables

List of Figures

Abbreviations

WEG	Wind Electric Generator
SCUC	Security-Constrained Unit Commitment
OPF	Optimal Power Flow
DAM	Day-Ahead Market
RTM	Real-Time Market
MIQP	Mixed Integer Quadratic Programming
ENTSO-E	European Network of Transmission System Operators for Electricity
SO	System Operator
LMP	Locational Marginal Price
GWEC	Global Wind Energy Council
EENS	Expected Energy Not Served
ISO	Independent System Operator
UC	Unit Commitment
CAISO	California Independent System Operator
PJM	Pennsylvania-New Jersey-Maryland
LAO	Last Accepted Offer
FRO	First Rejected Offer
LAB	Last Accepted Bid
LAB	First Rejected Bid
MCP	Market Clearing Point
PDF	Probability Density Function
CDF	Cumulative Distribution Function

Nomenclature

The notation used in this dissertation is listed below. They are stated per Chapter for quick reference. Others are defined as required in the text.

List of Symbols Used in Chapter 1

Indices:

G_g, D_g	Generator and corresponding offers/dispatchable load and corresponding bids.
g	Index over G_g or D_g, from 1 to N_G and 1 to N_D, respectively.
k, n, r	Indices of buses, r being the reference.
$k(g)$	Bus number corresponding to location of G_g or D_g.

Sets:

$\mathscr{G}$, $\mathscr{D}$	Set of G_g/D_g.
$\mathscr{B}$	Set of buses.
$\mathscr{L}$	Set of lines.

Constants:

$P^g_{G_{\min}}, P^g_{G_{\max}}$	Limits on generation level.
$P^g_{D_{\min}}, P^g_{D_{\max}}$	Limits on consumption level.
$\mathscr{X}$	Scaling factor between OPF results and the pricing rules.
$o^{g,LA}_p$	Price of last (partially or fully) accepted block for real power offer g.
$\mathscr{X}^{LAO}$	Scaling factor corresponding to the LAO pricing rule.

Variables:

P^g_G, P^g_D	Real power produce/consume by G_g/D_g.
λ^k_p	Nodal prices for active power at bus k as computed by the OPF.

λ_p^r	Equivalent value of λ_p^k at bus r.
x_p^k	Uniform price at bus k.
x_r^k	Equivalent uniform price at bus r.
θ_n	Phase angle at bus n.
$Flow_{nk}$	Power flow on lines $\in \mathscr{L}$.

List of Symbols Used in Chapter 2

Indices:

i	Index over data points, from 1 to n.
j	Index over bins, from 1 to N.
g	Index over WEGs, from 1 to N_w.
t	Index over time periods, from 1 to N_T.
R	Index over regions.

Sets:

RG^R	Set of renewable generators of region R.

Constants:

n	Number of data points.
N	Number of bins.
Δ_v	Width of bin j.
Δ_t	Time interval between forecasts.
k	Weibull shape parameter.
c	Weibull scale parameter $[m/s]$.
m	Number of segments on each CDF curve of the Weibull distribution.
ρ_{air}	Air density $[kg/m^3]$.
A_r	Rotor swept area exposed to the wind $[m^2]$.
C_p	Coefficient of performance.
η_g	Generator efficiency.
η_b	Gearbox/bearings efficiency.
C_v	Combined coefficient.

Variables:

v	Wind speed $[m/s]$.
n_j	Number of data points that falls inside bin j.
fr_j	Relative frequency associated with bin j.
f	Weibull probability density function.
F	Weibull cumulative distribution function.
P^{gt}	Output power of WEG g in time t.
E_t	The EENS at hour t.

List of Symbols Used in Chapter 3

Indices:

R	Index over regions.
g	Index over region R generators, from 1 to N_g^R.
t	Index over time periods, from 1 to N_T.
k,l,n	Indices of region R buses/loads, from 1 to N_b^R.
RR	Index over adjacent regions to region R.

Sets:

CG^R	Set of conventional generators of region R.
RG^R	Set of renewable generators of region R.
CG^{RR}	Set of conventional generators of region RR.
CG_n^R	Set of conventional generators located at bus n of region R.
RG_n^R	Set of renewable generators located at bus n of region R.
Φ_{nk}^R	Set of buses adjacent to bus n, all in region R.
Γ_{nl}^R	Set of buses of adjacent regions to region R, all connected to bus n of region R.
L^R	Set of internal lines of region R.
L_{tie}^R	Set of tie-lines of region R.

Constants:

c_g, b_g, a_g	Cost coefficients for unit g.
S_{on}^g, S_{off}^g	Startup/shutdown costs for unit g.
d_g	Spinning reserve cost for unit g.

e_{g_+}, e_{g_-}	Upward/downward load-following ramping reserve costs for unit g.
$VOLL$	Value of lost load.
R^{Rt}	Region R reserve requirement in time t.
D_n^{Rt}	Demand at bus n of region R in time t.
τ_+^g, τ_-^g	Minimum up/down times for unit g in number of periods.
x_{nk}	Reactance of line between buses n and k.
$f_{nk}^{max}, f_{nl}^{max}$	Maximum capacity of lines $\in L^R, L_{tie}^R$.
$\delta_{max}^g, \delta_{min}^g$	Upward/downward load-following ramping reserve limits for unit g.
$R_{max^+}^g, R_{max^-}^g$	Upward/downward spinning reserve capacity limit for unit g.
Δ_+^g, Δ_-^g	Upward/downward physical ramping limit on unit g.
P_{min}^g, P_{max}^g	Limits on the output power of unit g.
β_1	Scaling factor to dial in the amount of spinning reserve due to equipment unreliability.
β_2	Scaling factor to dial in the amount of expected energy not serve (EENS) due to the uncertainty of supply from WEGs.

Variables:

$\mathbf{X}$	The complete solution vector.
$E(\mathbf{X})$	The EENS considering a solution $\mathbf{X}$.
$TC(\mathbf{X})$	The total schedule cost for a solution $\mathbf{X}$.
P^{gt}	Output power of generator g in time t.
u^{gt}	Commitment state for unit g in period t.
v^{gt}, q^{gt}	Startup and shutdown states for unit g in period t.
r^{gt}	Reserve provided by unit g in time t.
$\delta_+^{gt}, \delta_-^{gt}$	Upward/downward load-following ramping reserve needed from unit g in period t for transition to period $t+1$.
LNS_n^{Rt}	Load shedding impose on load at bus n of region R in period t.
θ_n^{Rt}	Phase angle at bus n of region R in period t.
$Flow_{nk}$	Power flow on lines $\in L^R$.
$Flow_{nl}$	Power flow on lines $\in L_{tie}^R$.
r_{tie}^t	Regions RR contribution to region R reserve requirement in time t.

List of Symbols Used in Chapter 4

Indices:

R	Index over regions.
t	Index over time periods.
g	Index over region R generators.
c	Index over contingencies.
w	Index over scenarios.
k,l,n	Indices of region R buses/loads, from 1 to N_b^R.

Sets:

$\mathscr{T}$	Set of time periods considered, typically $\{1,...,N_T\}$.
$\mathscr{G}^{Rt}$	Set of region R generators at time t, typically $\{1,...,N_g^R\}$.
$\mathscr{G}^{Rtwc}$	Set of region R generators available for dispatch in contingency state c of scenario w at time t.
$\mathscr{C}^{tw}$	Set of contingencies considered in scenario w, typically $\{1,...,N_c\}$.
$\mathscr{W}^t$	Set of scenarios at time t, typically $\{1,...,N_w\}$.
$\mathscr{D}^{Rtwc}$	Set of region R demands in contingency state c of scenario w at time t.
$\mathscr{CG}^{Rt}$	Set of conventional generators of region R in time t.
$\mathscr{RG}^{Rt}$	Set of renewable generators of region R in time t.
$\mathscr{CG}_n^{Rtwc}$	Set of conventional generators located at bus n of region R in contingency state c of scenario w at time t.
$\mathscr{RG}_n^{Rtwc}$	Set of renewable generators located at bus n of region R in contingency state c of scenario w at time t.
Φ_{nk}^R	Set of buses adjacent to bus n, all in region R.
Γ_{nl}^R	Set of buses of adjacent regions to region R, all connected to bus n of region R.
L^R	Set of internal lines of region R.
L_{tie}^R	Set of tie-lines of region R.

Parameters:

c_g, b_g, a_g	Cost coefficients for unit g.
S_{on}^g, S_{off}^g	Startup/shutdown costs for unit g.
d_{g_+}, d_{g_-}	Costs for upward/downward contingency reserve purchase from unit g.

e_{g_+}, e_{g_-}	Costs for upward/downward load-following ramp reserve for unit g.
f_{g_+}, f_{g_-}	Costs for upward/downward deviations from active power contract quantity for unit g.
$VOLL$	Value of lost load.
π^{twc}	Probability of contingency c occurring in scenario w at time t. (π^{tw0} is the probability of no contingency, i.e., the base case of scenario w at time t.)
ρ^t	Probability of reaching period t. $\rho^t \equiv \sum_{w \in \mathscr{W}_{t-1}} \pi^{(t-1)w0} = \sum_{w \in \mathscr{W}_t,\ c \in \mathscr{C}_{tw}} \pi^{twc}$
D_n^{Rtwc}	Demand at bus n of region R in contingency state c of scenario w at time t.
τ_+^g, τ_-^g	Minimum up/down times for unit g in number of periods.
x_{nk}	Reactance of line between buses n and k.
$f_{nk}^{max}, f_{nl}^{max}$	Maximum capacity of lines $\in L^R, L_{tie}^R$.
$\delta_{max}^g, \delta_{min}^g$	Upward/downward load-following ramping reserve limits for unit g.
$R_{max^+}^g, R_{max^-}^g$	Upward/downward spinning reserve capacity limit for unit g.
Δ_+^g, Δ_-^g	Upward/downward physical ramping limit on unit g.
P_{min}^g, P_{max}^g	Limits on the output power of unit g.

Variables:

$\mathscr{X}$	The complete solution vector.
P_c^{gt}	Active power contract quantity for unit g at time t.
P^{gtwc}	Active injection for unit g in post-contingency state c of scenario w at time t.
P_+^{gtwc}, P_-^{gtwc}	Upward/downward deviation from active contract quantity for unit g in post-contingency state c of scenario w at time t.
u^{gt}	Commitment state for unit g in period t.
v^{gt}, q^{gt}	Startup and shutdown states for unit g in period t.
r_+^{gt}, r_-^{gt}	Upward/downward active contingency reserve provided by unit g in time t.
$\delta_+^{gt}, \delta_-^{gt}$	Upward/downward load-following ramping reserve needed from unit g in period t for transition to period $t+1$.
LNS_n^{Rtwc}	Load shedding impose on load at bus n of region R in contingency c of scenario w at period t.
θ_n^{Rtwc}	Phase angle at bus n of region R in contingency c of scenario w at period t.

This thesis is dedicated to my
beloved family.

If a man does not know to what port he is steering, no wind is favourable to him.

Lucius Annaeus Seneca

Acknowledgement

No act is more noble than a show of gratitude. I would like to express my appreciation to all those individuals and organizations who offered me constant support through out the realization of this work.

My deepest gratitude goes to my supervisor, Professor Innocent Kamwa for this research opportunity. I am indebted to him for his time, dedication and more especially his tremendous patience and sense of fairness. A big thank you also goes to Professor Jérôme Cros for accepting me as his student.

I am indebted to Professors Philippe Viarouge and Hoang Lehuy for providing me with high-quality technical education, for their fruitful scientific discussions and support.

This research was funded by the Canadian government through its discovery grant program, Natural Sciences and Engineering Research Council (NSERC) and HYDRO-QUEBEC through its research institute centre IREQ.

Special thoughts go to my late father, whose memory has inspired my achievements including this one. I wish to thank my mother for her quiet strength and presence. In a special way I thank Caroline, Thiery and William for being supportive during these difficult times. I equally wish to thank Cicinda and Ronny for being there for me throughout. My gratitude also goes to Ray Zimmerman for all these fruitful discussions and to Dolores Shulika for accepting to read every piece of this work.

None of this would have happened without the strength and support of my kids Tony Bryan, Caris, Kenneth and Warren. It was really challenging to write this other thesis and you gave me the strength to keep going each time I felt like giving up.

Foreword

This thesis consists of 4 chapters as follows:

- Chapters 1-2 have been written specifically for the thesis.
- Chapters 3 and 4 are published articles that I have written within the framework of this research work as the first author, while part of chapter 2 is made up of results that have also been published.

An introduction to operating reserve requirements for power system operations is provided in the general introduction. The types, characteristics and classification of operating reserves are given as well as an analysis of the impact of wind electric generator on the requirements of operating reserves. The research question, the thesis objective and a summary of the thesis contributions conclude this part of the dissertation.

Chapter 1 synthesizes and analyzes the relevant published works linked to this research. A critical evaluation of the different methodologies used in the available literature helps to identify the appropriate approach to be used in our investigations. This approach entails that the author systematically breaks down the relevant literature into its constituent parts and make connections between them. Decisions on the problems addressed in this thesis are taken in the electricity market, while risk mitigation remains the main concern of power grid operations. Chapter 1 provides the reader with a functional description of the wholesale electricity market, along with a tutorial example that shows how the tight coupling between grid and market operations are coordinated under the supervision of the independent system operator.

Chapter 2 deals with the modeling of wind electric generators and the management of the risk borne by the system through the inclusion of stochastic resources into the power grid. The Weibull distribution which models wind speed, and the power curve which displays the power

that will be available at each wind speed are used to estimate the average power produced by a wind electric generator. One of the important published findings of this research work is the establishment of a formula to supplement the $N-1$ security that accounts for the stochastic feature of wind power. The main features of the published work presented in chapters 3 and 4 as well as the information on the implementation of the methodology used are also presented here.

A security-constrained unit commitment and an optimal power flow suitable for power systems with a large share of wind energy, participating in the day-ahead market has been devised in chapter 3. The traditional spinning reserve requirement supplemented by an adjustable fraction of the expected shortfall from the supply of WEGs is computed using the stochastic feature of wind and loosely represented in the security constraint with scenarios. The optimization tool commits and dispatches generating units, while simultaneously determining the geographical procurement of the required spinning reserve and the load-following ramping reserve by mixed integer quadratic programming. Case studies are used to investigate various effects of grid integration on a reduction in the overall operation costs associated with more wind power in the system.

The findings of this chapter are published with Springer Nature/Journal of Modern Power and Clean Energy at https://doi.org/10.1007/s40565-019-0499-4. I achieved this under the supervision of Prof. I. Kamwa. Due to limited space, the RTS-96 test system results was not included in the paper, however these results have been included in this chapter. The article is also formatted in chapter 3 in order to meet the requirement of the Faculty for post-doctoral studies and higher learning.

Chapter 4 provides the model that has been used to validate the improved tool presented in Chapter 3. The uncertainty of component failures are represented with discrete probability and reserve requirement is endogenously determined. A comparative study of contingencies analysis makes it possible to adjust the scaling factors from the exogenous requirements and close the gap of operating cost between the day-ahead and real-time markets.

An article based on the findings of this chapter is under consideration and will be published with IET Generation, Transmission, and Distribution.

The conclusion of this dissertation and the topics for future research are provided in the last

part of the thesis.

List of Publications

A list of published and submitted articles in international scientific journals and conferences that are written based on results of this research is given as follows:

- J. B. Mogo, I. Kamwa and J. Cros, 2016, "Multi-Area Security-Constrained Unit Commitment and Reserve Allocation with Wind Generators", *2016 IEEE Canadian Conference on Electrical and Computer Engineering (CCECE)*, 1-6.

- MOGO, J.B. & KAMWA, I., "An Improved Deterministic Reserve Allocation Method for Multi-Area Unit Scheduling and Dispatch under Wind Uncertainty", *J. Mod. Power Syst. Clean Energy (2019),* https://doi.org/10.1007/s40565-019-0499-4.

- J. B. Mogo and I. Kamwa, "Reserve Allocation with Equipment Failure and Wind Uncertainty", Under consideration, to be published with IET Generation, Transmission, and Distribution.

General Introduction

0.1 What it Takes to Keep the Power Grid Stable

The function of a power grid is to supply electricity economically and with a reasonable assurance of continuity and quality (Billinton et al., 1991). However, due to numerous uncertainties inherent or extrinsic to the grid, it is subject to potential safety issues that could lead to power disruptions. Such issues include frequency and voltage reductions, unstable supply with erratic frequency and power fluctuations, or a total interruption of supply[1]. Indeed, interruptions of supply are caused by power outages, which are predominantly events of a stochastic nature involving the failure of one or several components in the grid. Thus, owing to the aspect of random grid failures, it is accepted that any grid will present a definite risk of suffering from a number of future power shortages. That is, imbalances[2] between power supply and demand leading to load interruptions.

If electricity could be stored economically, the assurance of continuity in supply would be relatively straightforward. Instead, electricity has a high temporal specificity that requires it to be produced and delivered practically on real-time. Accordingly, grid carries operating reserve or simply 'reserve', by keeping some margin of generation or demand reduction, so that it can be called on to deal with unexpected mismatch between generation and load. Ensuring that this gap is filled smoothly and instantaneously, relies on using the inertia of spinning turbines as shown in Figure 0.1, where, through the use of a speed governing mechanism, the deviation of the frequency from a set value (60 Hz in North America, 50 Hz in Europe and many other areas throughout the world) can be used as feedback to adjust the power

[1] The effects of interruption of supply in practice are most severe compared to other events, although they all impose costs on customers.

[2] An unbalance between supply and demand affects the frequency of the grid and lead to instability and equipment damage.

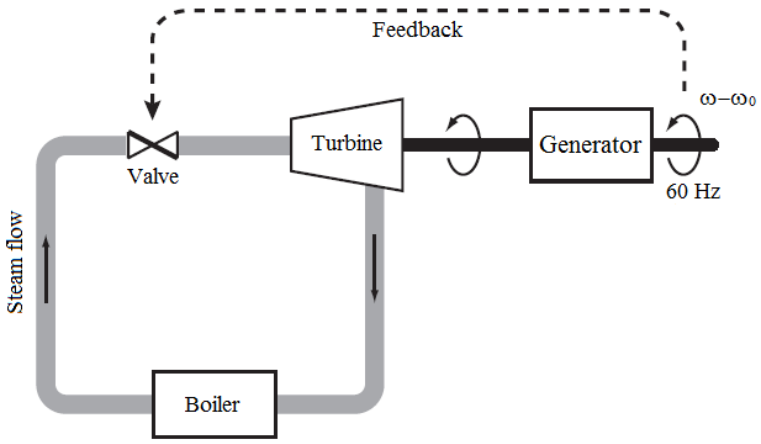

Figure 0.1: Frequency control of a steam turbine. The steam flow which determines the torque exerted by the turbine is continually adjusted using a valve, to keep the system frequency at 60 Hz.

production and ensure that balance is maintained.

Reserve[3] is an important aspect of power grid operations. The efficient management of reserve adds value to the service as it can improve the reliability and security of a power grid but also, provides substantial cost reductions; reason why all utilities have included reserve provision in their operating activities. However, despite its pervasive usage, there is no universal terminology and rule concerning what it stands for.

0.2 Operating Reserve: Types, Definitions and Classification

Operating reserve is the flexible demand reduction or the flexible unused available active power response capacity hold (either online or on stand-by) that can be called on at short notice to ensure the continuous balance of the grid during normal conditions and effective response to sudden changes in system conditions (Ela et al., 2011; Holttinen et al., 2012). This spare capacity represents the stand-by power necessary to keep the risk of power shortages at an acceptable level. However, its characterization can have different terminologies and definitions depending on the grid.

In China, the operating reserve is divided into load-following reserve, contingency reserve and maintenance reserve, where the load-following and contingency reserves constitute the spinning reserve, and the maintenance reserve constitutes the non-spinning reserve (Chen et al., 2013). The North American Electric Reliability Council (NERC) (NERC, 2009) classifies

[3]Power grids also require reactive power reserve as well to provide voltage support, however, it is out of the scope of this dissertation, therefore, the term operating reserve is used to refer solely to frequency control reserve, i.e., reserve accounting for active power dispatch.

operating reserve based on the imbalance driver as follows: regulating reserve, frequency responsive reserve, spinning reserve, non-spinning reserve and supplemental reserve. The European Network of Transmission System Operators for Electricity (ENTSO-E), in turn, follows a classification mostly based on the reserve procurement mechanism (ENTSO-E, 2009), i.e. frequency containment reserve, frequency restoration reserve and replacement reserve. For details concerning operating reserve definitions and reliability standards in North America and Europe, the reader should refer to (NERC, 2009; ENTSO-E, 2009), respectively.

To avoid any conflict of terminology we propose a coherent classification that attempts to clearly define operating reserve categories. The proposed classification is consistent with the analysis by (Ela et al., 2010, 2011) and is picturized in Figure 0.2, where the hierarchical diagram illustrates the reasons why operating reserve has been carried out, as well as the deployment speed (e.g., ramp rate and start-up time), deployment duration, direction of use (up or down), and type of control (e.g., control center activation, autonomous, automatic).

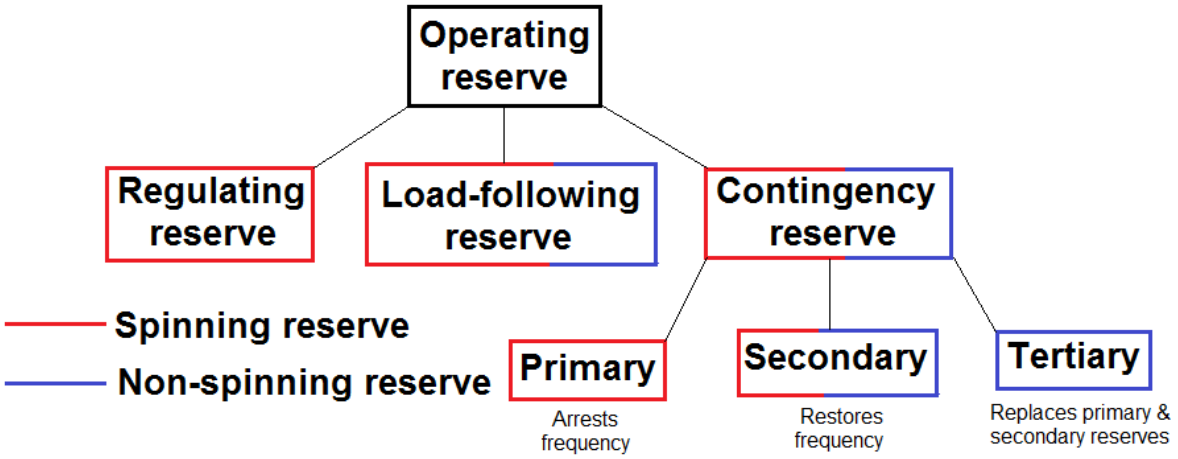

Figure 0.2: Operating reserve diagram.

If we define - a contingency as the unexpected failure or outage of a grid component such as a generator or transmission line, as well as significant unexpected load variations; - the spinning reserve as the portion of operating reserve consisting of generation synchronized to the grid and fully available to serve the load within the disturbance recovery period following a contingency, or load fully removable from the grid within the disturbance recovery period following a contingency; - the Non-spinning reserve as the portion of operating reserve consisting of generation not connected to the grid, but capable of serving demand within a specified time, or interruptible load that can be removed from the grid in a specified time, then spinning

and non-spinning reserve are characteristics of each of the other types of operating reserve, classified in Figure 0.2 and defined below:

0.2.1 Regulating Reserve

Regulating reserve, also known as regulation service or regulation is the reserve that can respond to System Operator (SO) requests to cover the continuous fast and frequent changes in load and generation that creates energy imbalance during normal conditions. Regulating reserve cannot be handled by manual SO actions. Technologies that are allowed to supply regulating reserve must be online units, operating under Automatic Generation Control (AGC) as shown in Figure 0.1. But in large interconnected grids with multiple balancing regions (e.g., North America and Continental Europe), normal imbalances usually do not trigger frequency response due to the size of the grid and the deadbands placed on the governor systems and therefore, the governor or frequency response control are only deployed during larger contingency events.

0.2.2 Load-following Reserve

Load-following reserve is similar to regulation but on a slower time scale. It is used to correct anticipated imbalances as it addresses uncertainty caused by erroneous load forecasts. Load-following reserve requirement does not depend heavily on the duration of the scheduling interval; it depends mostly on the factors that affect the forecast error. Humans are creatures of habit. They tend to load dishwashers, turn on televisions and boil kettles at roughly the same time each day, making the rise and fall in demand easy enough for the SO to predict. Therefore, the load generally follows a similar path every day. The ramping and energy needed to follow this load can thus usually be supplied. Unlike regulation which is autonomous in activation, load-following reserve is manually activated by the SO and can be supplied by both online and offline units as shown in Figure 0.2.

0.2.3 Contingency Reserve

Contingency reserve is called upon during major and steep energy imbalances that occur after a contingency. Contingencies occur quickly and much of the reserve must act immediately. It should be noted that contingency reserve can be primary, secondary or tertiary.

0.2.3.1 Primary Reserve

When a severe and steep energy imbalance occurs, it is initially substituted by the kinetic energy of the rotating machines of the grid. This type of response is called inertial response. For example, a sudden supply loss would cause the frequency to decline and the rotating machines to slow down to provide inertial energy. This inertial response that comes from synchronous generators and motors help slow down frequency decline. The more the rotating of the synchronous machines, the higher the inertia and the slower the rate of change in the frequency deviation. Soon after the imbalance and frequency deviation occurs, conventional generators will sense the change of frequency and adjust mechanical input to provide an opposing response through their governor systems. This response is called primary response. When the primary response has been fully activated, frequency is stabilized at a level below its nominal value. A certain amount of primary reserve must be constantly available, to ensure that the system frequency deviation is arrested and the load balance is maintained soon after the event. The full response deployment time for the primary reserve is usually some tenths of seconds. Primary reserve is only provided by online units equipped with a governor. The governor usually has a deadband so that primary control is activated only for large frequency deviations, and not during normal conditions.

0.2.3.2 Secondary Reserve

Secondary reserve is deployed to drive the frequency back to its nominal value and nullify the Area Control Error (ACE). The secondary reserve must be fully deployed within several minutes (i.e. 10 mins or 15 mins) after the imbalance occurs. They are usually supplied by online units operating under AGC control but they can also be supplied by offline units that can be dispatched within several minutes. Secondary reserve can therefore be automatically

or manually activated.

0.2.3.3 Tertiary Reserve

Tertiary reserve aims to replenish the primary and secondary reserve that were deployed so that the generating system has enough flexibility to respond to a new major event. Tertiary reserve is unique in the way it is deployed to cover a reserve imbalance instead of an energy imbalance. Tertiary reserve is manually deployed by proper recommitment and redispatch of the generation fleet.

0.3 Setting Reserve Requirements in Evolving Power Grids

In practice, scheduling reserve means operating the grid at less than its full capacity, while the deployment of reserve usually translates into the redispatch of units previously committed, the voluntary curtailment of specific loads and/or even the quick start-up of extra generating units to palliate unexpected shortages of energy supply. However, an important question is how to determine the amount of reserve to be scheduled.

0.3.1 Deterministic versus Probabilistic

Most utilities have adopted the deterministic method for their reserve requirements. This method is based on rules of thumb type criteria such as the scheduling of enough reserve to cover the loss of the largest generating unit (known as the N-1 criterion), or the supply of a portion of the hourly demand, or a combination of both (Billinton and Allan, 1996; Wood et al., 2013). Though it is easy to implement, these criteria are insensitive to factors that significantly influence system reliability, such as the failure rates of components in the grid. Moreover, deterministic reserve conveys the misguiding idea that all the risk can be removed, keeping a fixed amount of reserve. The probabilistic approach provides an analytical basis to consistently define system risk for different configurations. However, it normally requires on the one hand, the evaluation of a huge number of possible disturbances which may result in computational intractability, and on the other hand, the acquisition of the statistical failure data necessary to compute outage probabilities. This data is usually exposed to great

uncertainties. For these reasons, there is a considerable reluctance to apply probabilistic techniques and despite the obvious disadvantages of the deterministic criteria, they are still widely used by many utility companies. Indeed, if this quantity-constrained method that sets security constraints for a single forecasted set of grid conditions without an explicit inclusion of economic criteria has largely resulted in satisfactory levels of reliability, it is because traditional grids were thermal-dominated[4] and operated under cost-of-service model of pricing: utilities did not have incentives to reduce costs since the pricing model allowed them to recover all their expenditure. Costs were passed to consumers, who did not realize which portion of their bills went to cover reliability services. The changing nature of today's grid with the introduction of liberalization has brought about competitive electricity markets, coupled with the large penetration of WEGs that has introduced increased levels of variability and uncertainty into power grid operation, raising the importance of reserve as well as the methods for establishing the amounts needed.

0.3.2 Impacts of Large-Scale WEGs on Reserve Requirements

The acceptance that anthropogenic greenhouse gas (GHG) emissions have resulted in climate change has sparked discussions on the benefits of limiting industrial emissions of these gases in comparison with the cost that such alterations would entail. Actually, from the environmental perspective, there is a need to lessen dependence on carbon-intensive fossil fuels and move towards low-carbon energy supplies as a means of improving the security of supply and reducing exposure to fossil fuel price volatility.

In the last decade, a significant part of these actions that drastically curb air pollution has been heightened in the electricity generation sector (Denny and O'Malley, 2006; Gil and Joos, 2007) where renewable energy has become a meaningful part of the generation mix. Among all renewable energy forms, wind power generation has seen an ever-increasing development and its sheer amount coming online is definitely due to its technological maturity, widespread availability and speed of deployment among others.

[4]Electric parks in the past included almost solely deterministic production facilities, such as coal-fired units, gas-fired units, or nuclear power plants. If a unit of this type is not out of order, its functioning depends only on the will of its owner.

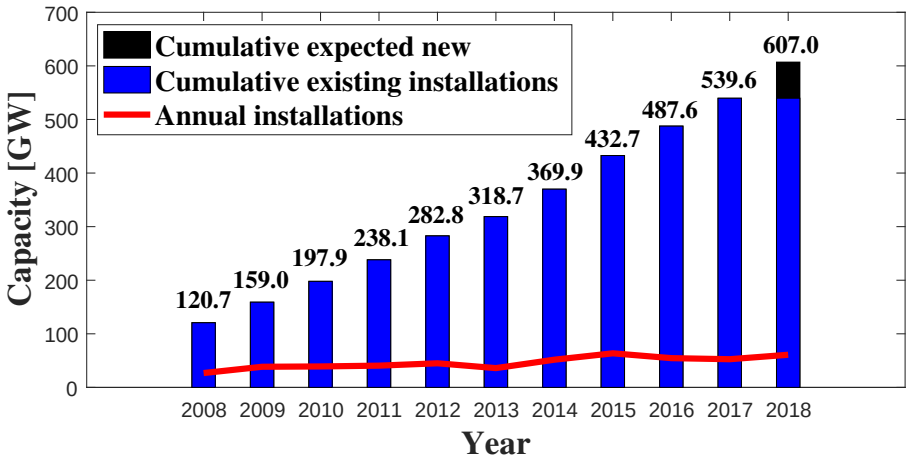

Figure 0.3: Projected annual and cumulative installed capacity worldwide (GWEC, 2018).

According to the Global Wind Energy Council (GWEC), about 539.6 GW of wind power was spinning around the globe by the end of 2017, 52.6 GW of which had been newly brought online. This represents a 10.66% growth in cumulative capacity and 3.79% down from a year earlier, with China continuing to lead the world as outlined in Figures 0.3 and 0.4. If we can believe (GWEC, 2018), by the end of 2018, global wind power cumulative installed capacities could reach 607 GW.

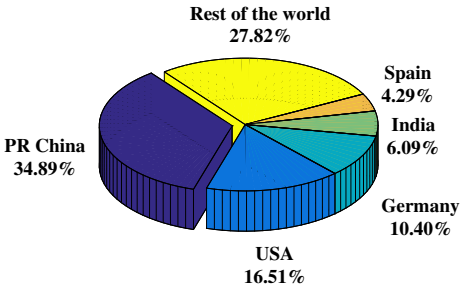

Figure 0.4: Top 5 cumulative installed capacity December 2017 (GWEC, 2018).

Despite the benefit of low operating cost and low pollution, the harnessing of large-scale WEGs, however, poses many technical problems apart from the costly economics because of their intrinsic intermittent and fluctuant output characteristics. Particularly, due to their poor predictability, the power grid operational reliability cannot be guaranteed with the conventional deterministic reserve methods, and extra generation reserve is needed to accommodate WEGs integration Ummels et al. (2007); Chen et al. (2013). Moreover, WEGs being an inertia-less resource, they do not contribute to maintaining grid balance, hence expected or unexpected reductions in the system's net load[5], which can arise due to declining WEGs output, will force conventional plants to ramp up their output, or if sufficient ramping capability is not available, fast-starting units will need to come online. Also, periods of low demand

[5]Net load is the output the grid requires from non-WEGs to balance supply and demand.

coinciding with high WEG output can lead to conventional plants being shut down, resulting in revenue reductions for these units to recover their variable and capital costs. However, if sufficient downward reserve from conventional resources are not present, wind power may have to be curtailed, leading to a waste of available resources. Given the temporal operating restrictions (ramp rates and minimum downtimes, among others) that limit the rate at which these units can be brought on line and that alter their output, the competitive functioning of the electricity market can be altered as the energy transactions agreed on in these markets may not be implemented in real-time, exactly as agreed, for security reasons. Large-scale WEGs do not only increase the amount of reserve scheduled, they also adversely impact the way the scheduled reserve is deployed, calling for sophisticated methods based on more-complex characteristics of variability and uncertainty.

It emerges from serious research in the literature that the variable output and imperfect predictability of WEGs face stochastic approaches to strategically accommodate WEGs in the short-term operation of power grids. However, stochastic programming and/or robust optimization are still not used in practical systems yet (Chen, 2016). SOs and practitioners are concerned with the complexity and transparency of these methods as their efficacy and high computational requirements still need to be further addressed before their full practical implementation. For these reasons, all market clearing tools are based on the deterministic method which assumes a fixed knowledge of system conditions for the next day. The sole use of the deterministic criteria may not be economical or reliable in limiting the risk of uncertainty. A hybrid of the deterministic methods and the prevalent stochastic techniques may be an alternative way that is more applicable and acceptable.

0.4 Thesis Objectives

The main objective of this research has been to propose viable and sound solutions to the increasing variability and uncertainty in the short-term power grid operations, emanating from increasing the share of WEGs in the electricity generation mix and competition from electricity markets. The deterministic method for the settlement of reserve requirements in particular is examined, as having been developed for a single forecasted set of system conditions and with a centrally operated nature of generation, transmission and distribution in

mind (Allan and Billinton, 2000), this method tends to have higher levels of conservativeness than required by the actual conditions, which therefore can alter the competitive operation of electricity markets as the energy transactions settled in these markets may not be implemented in real-time, exactly as agreed for security reasons. The performance of this method has been improved on with an adjustable extra generation reserve that accounts for the stochastic feature of WEGs. The potential benefits and impacts of this hybrid approach are investigated in this research.

Having identified that the operation of conventional units will be significantly impacted as WEGs penetrations increase, the incorporation of some inherent flexibility–design that could reduce the onus placed on them to balance the system can be advantageous. This research considers such flexibility in investigating how it could mitigate the jerkings around these units while responding to large and fast variations in the system net load. Base load units in particular are examined, as these units, having been designed to operate under creep conditions, tend to have limited operational flexibility. As such, when subjected to cycling operation, these units can accrue large levels of damage to plant components that could potentially leave them permanently out of operation prior to their expected lifetimes.

While this physical flexibility can be gained from those generators, it can impose significant costs too and revenue reductions to recover their variable and capital costs (Maggio, 2012) as their output levels must be turned to a lower level with WEGs in the system. If incentives are not provided to encourage these resources, it is unlikely for the system to get the efficient balance of generation resources as potential reliability degradation or costly out-of-market actions can occur. Most current markets do not reward these flexible resources for their positive environmental attributes as they are frequently moved on the dispatch stack to a new loading point. In this research, adequate market policies that address the financial implications of these requirements have been crafted.

0.5 Summary of Thesis Contributions

The innovative ideas emanating from this dissertation can be summarized as follows (i) the development of a hybrid of deterministic and stochastic reserve requirement method that accounts for risks of generation shortfalls from both conventional units and WEGs, (ii) the

identification and investigation of adequate market policies that will incentivize the availability of generation reserve capacity in a high wind power scenario, (iii) the formulation of a loosely multi-period stochastic optimization framework that co-optimizes energy and reserve and that is efficient in terms of computational time.

The consideration of the shortfall of supply of the WEGs in the reserve constraints revealed that the need for reserve increases as the hourly Expected Energy Not Served (EENS) increases, necessitating the use of quick start units, or short-term market purchases that will lead to higher variable costs through increased fuel consumption hence, increased operation costs. However, the displacement of conventional plants by WEGs will make the transaction profitable in terms of total operating costs despite the increase in reserve. Furthermore, scaling the wind power uncertainty has been proven to be advantageous as at RTM operation, the operator system can maintain adequate defensive system posture likely to wind events, while dialing in system reliability.

Adopting ramping charge and spreading variability across more units has been found as a promising measure that can spur the widespread deployment of WEGs into power grids. Indeed, by receiving compensation for costs incurred based on the decisions of others, generators will have greater incentives to both make their units available with higher ramp rates and follow dispatch signals. A large pool of generation substantially decreases the jerkings around conventional units and lessens costs that are imposed on the power system for accommodating WEGs.

The formulation of a combined SCUC and OPF that improves the conventional deterministic spinning reserve method, and that rewards load-following units when they are moved on the dispatch stack to a new loading point has particular implications for wind integration studies, as it can reverse the hidden cost of integrating WEGs to grid, it is time-saving thus can be recommended for production grade programs.

0.6 Thesis Overview

The remainder of this dissertation is organized as follows:

Chapter 1 presents a synthesis and analysis of the relevant published works linked to this

research. A critical evaluation of different methodologies used in the available literature helps to identify the appropriate approach to investigate the research question of the thesis outlined in section 0.3. This chapter also provides the basic framework required to understand the context of electricity markets in which the decision-making problems addressed in this dissertation take place. Through an illustrative example, the author shows how under the coordination of the Independent System Operator (ISOs), market participants, by responding to price signals, help to achieve operation objectives including the delicate task of balancing the grid, a feature which fundamentally drives electricity price formation.

Chapter 2 gives the model for WEGs as used throughout this dissertation. The specificities of the wind power generation process are exposed as well as the method of estimating the EENS due to the uncertainty of supply from WEGs. The main features of the published work presented in chapters 3 and 4 as well as the information on the implementation of the methodology used are also presented here.

Chapter 3 presents the improved deterministic tool used to schedule reserve requirements in the context of large WEGs penetration. Case studies are used to investigate various effects of grid integration on reducing the overall operation costs associated with more wind power in the system.

Chapter 4 provides the model used to validate the improved tool presented in Chapter 3. The uncertainty of component failures are represented with discrete probability and reserve requirement is endogenously determined. A comparative study of contingencies analysis makes it possible to adjust the scaling factors from the exogenous requirements and closes the gap of operating cost between DAM and RTM.

The conclusion of this dissertation and the topics for future research are provided in the last part of the thesis.

Appendix A provides the mathematical background material relevant to this dissertation. It includes i) the DC load flow used throughout the thesis, ii) the fitting methods of the Weibull distribution used to model wind speed in Chapter 2.

Appendix B lists the technical and economic data pertaining to the 6-bus two-area, the modified IEEE 118-bus and the IEEE-RTS three-area systems used to examine the market-

clearing procedure presented in Chapters 1, 3 and 4.

Appendix C describes the Matlab code sources used to implement the short-term decision-making problems formulated in chapters 3 and 4.

Chapter 1

Literature Review

1.1 Introduction

After this introductory paragraph, the second part of this chapter constitutes a review of the literature pertaining to this research. By systematically breaking down the relevant literature into its constituent parts, and by making connections between those parts, we figure out an appropriate approach to investigate the research question of the thesis. This approach is outlined in Chapter two. Section three presents a description of the wholesale electricity market where decisions on the problems addressed in this thesis are taken. The author uses an example to illustrate how by responding to price signals under the coordination of the ISO, market participants help to achieve operation objectives including the delicate task of balancing the grid, a feature which is fundamental to electricity price formation. A brief history of the liberalization of the power industry as well as the impact of WEGs on electricity markets will also be provided in this chapter.

1.2 Managing Uncertainties in Short-Term Scheduling Problems

To face increased WEGs penetration to grid, both academia and industry seek new efficient tools for effectively managing uncertainties and enhancing economy and the security of power grid operations. This section attempts to review certain current trends pertaining to short-

term power grid scheduling and operation, namely:

- Advanced forecasting methods.
- Efficient mathematical modeling of uncertainty.
- Improvement of the grid flexibility.

1.2.1 Advanced Forecasting Methods

Reliable prediction of wind power reduces the need for operating reserve leading to more economic power system operations. An extensive literature review on wind power forecasting methods are presented in (Monteiro et al., 2009), where state-of-art tools are categorized as physical or statistical, with modern forecasting systems employing a combination of both. Physical approaches namely weather prediction models, which are typically used for horizons of 6 to 72 hours utilize data such as land and sea surface temperatures to physically model atmospheric dynamics. Statistical approaches transform meteorological predictions into wind generation and are found to give better accuracy for horizons up to 6 hours. The SOs desire for information regarding the reliability of forecast has led to ensemble or probabilistic forecasts becoming popular. Ensemble forecasting produces multiple forecasts by varying the input parameters or by using multiple weather prediction models to generate a probability density function of the most likely outcome (Möhrlen et al., 2007).

1.2.2 Efficient Mathematical Modeling of Uncertainty

Researchers had been investigating optimal operating reserve requirements for some time before large penetrations of WEGs could change these requirement methods. As discussed earlier, the unit commitment (UC) problem had traditionally been formed within a deterministic framework in the sense that generation is scheduled over a single expected value of system conditions. In this framework, reserve to hedge operation risks caused by uncertainties was predefined, based on statistical analysis of historical system data. Deterministic security measures, however, do not account for the probability of occurrence of the contingencies they are supposed to cover. Most times, the level of conservativeness is more than what the actual

conditions require, thereby impacting its economic efficiency. Occasionally, it may adversely affect reliability.

Probabilistic method (Guy, 1971; Dillon et al., 1978; Gooi et al., 1999; Wang et al., 2005) seem to be far superior to the deterministic methods. Reserve needs are set by considering both the probability of the occurrence of every possible failure event and the damage caused to the grid by each of them, unlike in the deterministic approach which is pre-specified. But, for the reasons outlined in the previous chapter, deterministic reserve requirements are still widely used. Table 1.1 summarizes some of these rules that are currently utilized by ISOs (CAISO, 2005; IESO, 2004; UCTE, 2004; REE, 1998).

Table 1.1: Operating reserve requirements in different countries and ISOs.

Country or ISO	**Operating reserve criterion**
Australia & New Zealand	$\max_g u^{gt} \cdot P^{gt}$
BC Hydro	$\max_g u^{gt} \cdot P^{gt}$
Belgium	ENTSO-E rules. Currently at least 460 MW.
CAISO	$50\% \max\left(5\% P_{hydro} + 7\% P_{other}; P_{largest\ contingency}\right) + P_{non-firm\ import}$
ENTSO-E	$\left(10 \cdot D^{\max} - 150^2 - 150\right)^{\frac{1}{2}}$
France	ENTSO-E rules. Currently at least 500 MW.
Southern PJM	$\max_g u^{gt} \cdot P^{gt}$
Western PJM	$1.5\% \cdot D^{max}$
PJM(other)	$1.1\% \times$(peak load)+ probabilistic calculation on typical days & hours.
Spain	Between $3 \times (D^{\max})^{\frac{1}{2}}$ and $6 \times (D^{\max})^{\frac{1}{2}}$
Yukon Electrical	$\max_g u^{gt} \cdot P^{gt} + 10\% \cdot D^{\max}$

With the fast pace of integration of WEGs into the grid, the nature of uncertainty and variability that come from these resources are different from that of conventional generation outages, therefore the methodologies in place may change significantly in order to determine the optimal reserve requirements and maintain a reliable, yet cost-effective grid. In order to strategically accommodate the uncertainty of wind power in the short-term scheduling of power grids, significant work has been done through stochastic optimization techniques. Various UC models have been proposed and can generally be divided into four categories based on the manner

in which they address uncertainty, namely, scenario-based stochastic programming, robust optimization, chance-constrained optimization and risk-based optimization. Additional information is provided in (Birge and Louveaux, 2011; Ben-Tal et al., 2009).

1.2.2.1 Scenario-Based Stochastic Programming

In the stochastic UC, wind power uncertainty is represented by a set of scenarios which are generated via presumed probability distribution functions learned from historical data. Intuitively, the quality of solutions increases with a larger number of scenarios with the capture of a full spectrum of uncertainty. Equally, the computational requirements also increase with the number of scenarios. Thus, a trade-off usually needs to be made between the desired accuracy and the computational performance of the algorithm. Correspondingly, scenario reduction techniques (Dupacová et al., 2003; Conejo et al., 2010) have been proposed to bundle similar scenarios. The goal is to reduce the number of scenarios to a large extent without sacrificing their accuracy. Also known as the two-stage UC model, the objective of the stochastic programming is to optimize the decisions on both stages and thus to guarantee that the scheduling of conventional generation is sufficiently flexible for the uncertainties. Proposed stochastic models vary in the scenarios considered, e.g., equipment failure, wind power and load uncertainty.

(Bouffard and Galiana, 2008) propose a stochastic market-clearing model to address load and wind power uncertainty in which tertiary reserve levels are explicitly calculated. Load and wind power forecast errors are assumed to follow a normal distribution and net load scenarios are generated by slicing the net load normal distribution into a finite number of slices, taking the probabilities in the middle of the slices. In this model the reserve levels and UC decisions are first-stage decisions, while generation levels, responsive demand, involuntary load shedding and wind energy curtailment are second-stage decisions. The principal benefit of this stochastic operation planning approach is that, when compared to a deterministic worst-case scenario planning philosophy, the proposed model allows higher wind power penetration without sacrificing security.

A stochastic UC with wind uncertainty for the day-ahead scheduling, in which the commitment of the slow units is considered as first-stage decision while the commitment of fast units

and dispatch are taken as second stage decisions is studied in (Papavasiliou et al., 2011). To enhance computational tractability, a decomposition method based on Lagrangian relaxation of the non-anticipativity constraints (the constraints that enforce the commitment of slow units to be the same for all scenarios) is employed. The proposed model is compared with two variants of its deterministic counterpart: the first variant schedules load-following reserves as a percent of peak load and the second variant with the 3+5 rule. Results show that for wind penetration levels of 14%, the proposed stochastic model yields approximately 1% less cost. However, reserve bids are not considered although reserve quantities are explicitly calculated.

(Wang and Hobbs, 2016) compare a deterministic UC having flexible ramping constraints with a stochastic UC in the framework of CAISO real-time UC. Transmission constraints and outages are not taken into consideration. Flexible ramp constraints reserve committed capacity to meet unexpected net load ramps. Their results indicate that the deterministic UC incorporating flexible ramp constraints can be inefficient compared to the stochastic counterpart.

1.2.2.2 Robust Optimization

In contrast to stochastic programming models, robust UC models try to incorporate uncertainty without informing the underlying probability distributions, and instead with only a range of the uncertainty. Instead of minimizing the total expected cost as in the stochastic UC, robust UC minimizes the worst-case cost regarding all possible outcomes of uncertain parameters. Certainly this type of models produce very conservative solutions, but computationally it can avoid incorporating a large number of scenarios. There are numerous research devoted to robust optimization that address wind power uncertainty in the UC.

(Wang et al., 2016) have formulated a robust risk-constrained UC in which the wind generation uncertainty set is adjustable via choosing diverse levels of operational risks, which include expected operational loss for wind generation curtailment as well as load shedding. By optimizing the uncertainty set, the model can allocate an optimal operational flexibility of the power systems over spatial and temporal domains, thereby reducing operational cost in a risk-constrained manner. Moreover, since the impact of wind generation realization out

of the prescribed uncertainty set on operational risk is taken into account, the model can outperform in the case of rare events.

(Lorca and Sun, 2015) present a robust multi-period economic dispatch formulation to be used to address increasing wind penetration by presenting the concept of dynamic uncertainty sets. Dynamic uncertainty sets explicitly model the temporal and spatial correlation of variable sources. Results show the superiority of using dynamic uncertainty sets to using static uncertainty sets or deterministic multi-period economic dispatch.

1.2.2.3 Chance-Constrained Optimization

Chance-constrained optimization is another viable approach to be used in handling uncertainties in the UC problems. By setting the constraints with stochastic variables based on a certain probability, the scheduling is optimized while guaranteeing that the violations of the real operation constraints, e.g., the generation deficiency and branch overload due to uncertainty are limited within a small probability. Only certain forms of the chance-constrained UC model can be transformed to an equivalent deterministic UC problem (He et al., 2012). In general, such chance constraints lead to non-convex problems, and the model is solved using a sample-average approximation approach (Wang et al., 2012; Vrakopoulou et al., 2013; Pozo and Contreras, 2012). In (Wang et al., 2012), the hourly UC problem is formulated as a chance-constrained two-stage stochastic programming problem and solved by a combined sample average approximation algorithm which guarantees that a large portion of the uncertain hourly wind power generation will be utilized with a high probability. (Pozo and Contreras, 2012) present a chance-constrained two-stage stochastic UC model that encompasses a n-K security criterion. Load and wind power uncertainties are modeled as zero mean normal distributions while the probability of simultaneous conventional unit outages is modeled using the unit forced outage rates. The model is solved as Mixed-Integer Linear Programming (MILP) considering a linear approach for the probabilistic constraint based on conditional value-at-risk definition (Rockafellar and Uryasev, 2000) and a dual formulation of the second-stage problem leading to a recast of the problem as a linear set of constraints for the K worst contingencies.

1.2.2.4 Risk-Based Optimization

In the risk-based UC model additional constraints are added to restrict risk exposures of a particular set of UC decisions. Several different risk measures have been used in the literature, such as Expected Load Not Served (ELNS) in (Venkatesh et al., 2008), Loss of Load Probability (LOLP) in (Gooi et al., 1999), and Conditional Value at Risk (CVaR) in (Pozo and Contreras, 2012). The risk UC model allows for a tradeoff between generating costs and underlying costs of uncertainties. It often requires the integration of probability density functions and is usually solved using nonlinear optimization techniques (Venkatesh et al., 2008). In (Zhi and Botterud, 2014) the risks of load shedding is considered by introducing the demand curve of the operating reserve. It is quantified by the cost of unserved energy and the expected loss of load. The operating reserve demand curve is modeled by a stepwise function. Such modeling of risks maintains the UC model to be a MILP problem.

1.2.3 Improvement of the Grid Flexibility

If we can define the flexibility of a power system as its ability to respond rapidly to large fluctuations in supply or demand, a flexible power system, therefore, is inherently capable of supporting a larger penetration of WEGs. As wind generation continues to grow, the operating flexibility of conventional plants may prove insufficient to meet an increasingly variable net demand. In addition, increased cycling of these plants can lead to extensive damage of the plant components, particularly for base-load plants, as stated before. Thus, considerable interest surrounds the idea of incorporating sources of flexibility into power systems to support a higher penetration of wind power. Energy storage facilities, interconnection to neighbouring power systems and demand side management schemes (DSM) are well cited sources of flexibility in power systems. (He et al., 2012) propose the superconducting magnetic energy storage (SMES) as a novel technology to provide up and down regulation reserve, owing to its fast response to charge and discharge. The authors have formulated a chance-constrained stochastic UC model in which SMES technology allows more freedom to ISOs in order to balance the system dispatch cost and reliability. It was found in (Brown et al., 2008) that pumped storage on isolated systems can allow a greater penetration of renewables and improve the dynamic security of the system however, (Tuohy et al., 2009) also show that,

although pumped storage can reduce wind curtailment, the increased use of base-load units can actually lead to increased emissions. (Hamidi and Robinson, 2008) found that responsive demand on a system with a high wind penetration makes greater use of the wind resource and reduces emissions, whilst (Keane et al., 2011) finds DSM substitutes production from peaking units and can provide a valuable source of reserve. The net benefits of wind generation can be increased significantly by increasing the level of interconnection on the power system, as shown in (Denny and O'Malley, 2007). Ahmadi-Khatir et al. (2014) developed a decentralized UC algorithm for multi-area power systems using an augmented Lagrangian relaxation and auxiliary problem principle. Reference Li et al. (2016) proposed a coordination framework for tie-line scheduling and power dispatch of multi-area systems in which a two-stage adaptive robust optimization model was applied to account for uncertainties in the available wind power. In Doostizadeh et al. (2016), an adjustable interval robust scheduling of wind power for day-ahead multi-area energy and reserve market clearing was proposed.

1.3 Overview of the Wholesale Electricity Markets

Up until recently, the electricity industry was monopolized by state-owned utilities which were in charge of the whole chain of activities. Liberalization which has brought in competition, has led to improvement in economic efficiency. However, risk mitigation remains the main focus of power grid operations; requiring that grid operations and market operations be coupled tightly to ensure a steady supply.

1.3.1 History and Main Features

Electricity generation is capital intensive, and like many high fixed cost industries, its market has traditionally been organized as a natural monopoly with the public sector taking a lead in the maintenance of its critical infrastructure. Vertically-integrated companies were in charge of the generation, transmission, distribution, and retail, and were effectively guaranteed the recovery of their operating costs plus a regulated return on capital expenditure. However, generation assets were not used at their optimal operating durations, resulting in a structural overcapacity that led to increasing cost. Hence, the liberalization of the sector was seen

as a great opportunity to reduce the electricity bill of large consumers through their direct participation in the wholesale markets. Conceptually, the generation and retail activities have to be isolated and the physical control of the transmission system is invariably assigned to ISOs who are non-commercial organizations. Generators therefore live or die due to their cost of production and the price they get for their output.

The first steps towards the creation of the electricity markets were taken in 1982 by the Chicago Boys in Chile (Sioshansi, 2013), during the Pinochet dictatorship by the separation of generation and distribution activities, the introduction of competition between producers, as well as the adoption of the production cost model of pricing. Since then, competitive electricity markets and unbundling of utilities have been progressively spreading out in an increasing number of countries in Europe and America. In the resulting markets, large amounts of generation capacity were converted from utility status to Independent Power Producers (IPPs) status. For instance, the grid that powers mainland North America in Figure 1.1 now relies on both public and private ownerships, and is divided into regional markets or ISOs. These markets are organized differently in various jurisdictions, and procedural rules tend to differ markedly even between systems that are decentralized at the same degree. Currently one of the most pertinent questions for liberalization programs in the light of key objectives as stated above is how to arrange electricity trading between generators (sellers) and retailers (buyers) in the wholesale electricity market. It is possible to identify two main market arrangements from the several models implemented around the world, bilateral contracts and electricity pools (Onaiwu, 2010) as depicted in Figure 1.2.

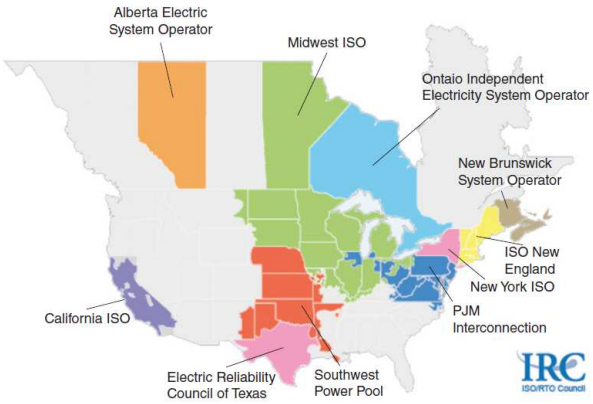

Figure 1.1: The North America electricity markets (NYISO, 2017).

1.3.1.1 Bilateral Trading

In the bilateral or decentralized trading model, buyers and sellers pair up and reach an agreement on the price and quantity of electricity to trade, as well as other master terms and conditions that form the basis of their trade. They may both be generators and/or

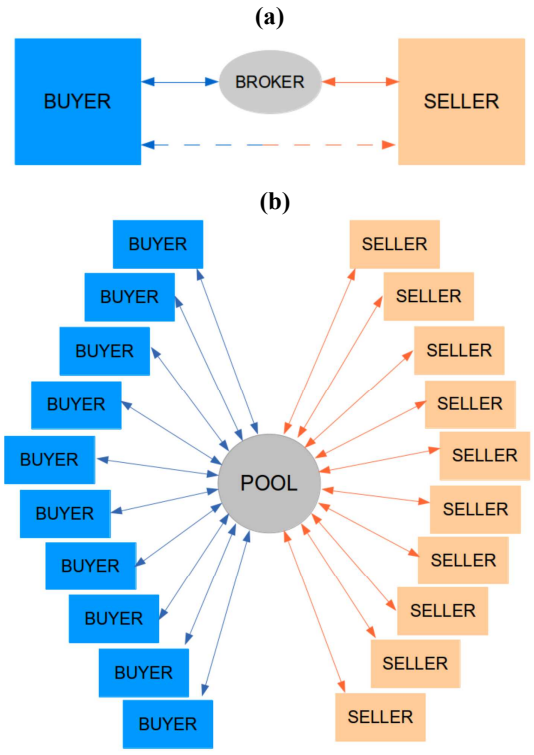

Figure 1.2: Trading forms in wholesale electricity markets.

- (a) Bilateral contract.
- (b) Electricity pool.

retailers. Most likely intermediaries (brokers) are involved in the transactions; though not strictly necessary. At the gate closure[1], participants disclose their net contract sales and purchases to the ISO. Each generator decides on when to dispatch and the ISO is required to manage the imbalances that occur by buying or selling the reserve in order to guarantee the security of transactions and also by limiting the amount of power that sellers can inject at some nodes, if security cannot be ensured by other means. Since the ISO does not get involved directly in the bilateral trading, the price from the spot market is used to settle imbalances. The ISO auctions tradable transmission rights to manage congestion. The auction resolves the problem of who the users of the transmission system will be and the price they will pay.

[1]The point in time when submission or update of a balancing energy bid for a standard product on a common merit order list is no longer permitted.

1.3.1.2 Electricity Pooling

Electricity pool[2] represents the cornerstone of the liberalized electricity market philosophy. The absence of any negotiation between market participants and the embedment of the grid security management into the process of electricity price formation have turned the pool into a well established platform for trading in electricity systems. Despite some differences in the manner in which the market is organized (single-sided or double-sided auction), the rules guiding the operations of the market (pay-as-bid or uniform pricing settlement) and the action of market participants (price-based or cost-based bidding), electricity pools operate on similar basic principles:

• sellers submit offers to the ISO. An offer is specified as a set of price–quantity pair indicating the amount of energy the producer is willing to sell at a given price.

• Similarly, buyers submit their bids, specifying both the quantity and price they are willing to pay for each energy unit.

• The ISO typically relies on an auction to efficiently obtain the quantity of electricity socially accepted and the price consumers are willing to pay in a short-term market. This is done by ranking offers according to increasing price and bids in the inverse order. A supply curve (in blue) and a demand curve (in red) are obtained as shown in Figure 1.3 and this defines the merit order.

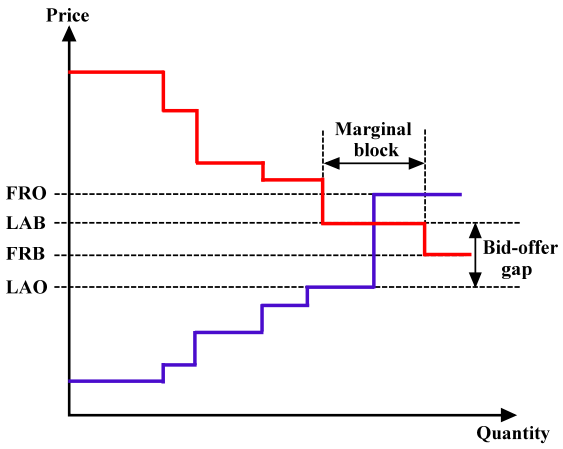

Figure 1.3: Double-sided auctions.

• The intersection point of the two curves sets the Market Clearing Point (MCP) whose coordinates represent the Market Marginal Price (MMP) and the total tradable energy volume. Offers inferior to the MMP and bids above this price are in merit and are accepted to participate in the short-term market. The out of merit offers and bids, i.e., market participants whose offerings are on the right side of the MMP are excluded for the respective market spanning period.

The most preferred marketplace for short-term transactions is a DAM (often referred to as

[2] What is the Electricity pool? http://www.elecpool.com/about/about_f.html, (last visited on 30 November 2018).

forward market in the USA and as spot market in Europe), a market that allows participants to buy or sell wholesale electricity a day in advance. This market usually operates on an hourly basis. This means that market participants must submit 24 selling offers/purchasing bids in total, corresponding to the 24 different pool markets of the day, i.e., one for each hour of the following day. Later adjustments of day-ahead contracts are possible in intra-day

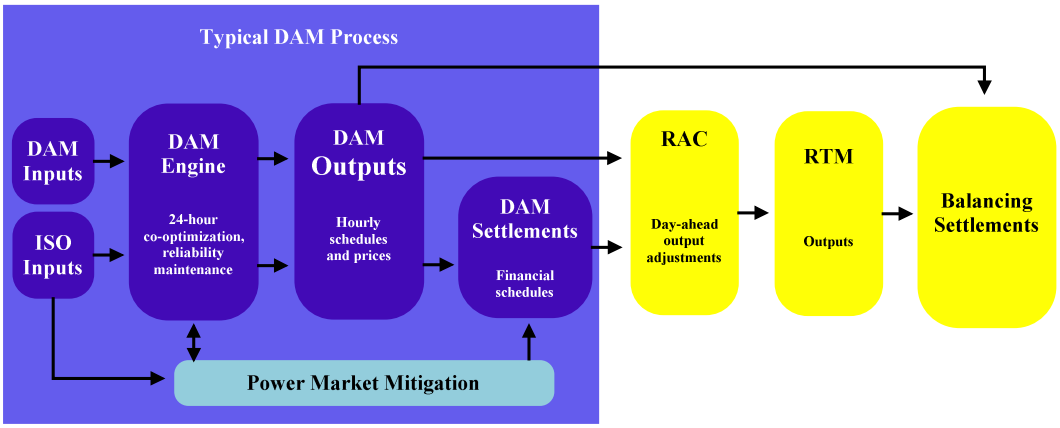

Figure 1.4: Wholesale electricity market time line: DAM to settlements after RTM.

markets known under the more generic name of adjustment markets. Indeed, right after the DAM clearing, there is a re-bid period for in merit participants to adjust their bids. The ISO in this case runs a Reliability Assessment Commitment (RAC) to commit additional units that will cover the difference between forecasted load and bid-in load, as well as the difference in corresponding operating reserve requirements. Finally, the RTM (also known as balancing market or regulation market) is the last-resort market that ensures the balancing of the grid at any point in time. The balancing settlements, i.e., the payment to or from the ISO is proportional to the amount of energy actually delivered to or withdrawn from the grid by sellers and buyers, respectively. A schematic diagram of the wholesale electricity market operation can be seen in Figure 1.4 where the different timeframes from DAM to RTM settlements, including the adjustment and real-time markets are highlighted. A more detailed history and description of electricity markets can be found in (Shahidehpour et al., 2002; Borenstein and Bushnell, 2015; Stoft, 2002).

1.3.2 Understanding the Locational Margin Pricing

The market-based auction set up above must consider network constraints to ensure the delivery of the commodity cleared does not leave the system vulnerable. To overcome this drawback, OPF can be accommodated in an auction as an externality. When using the DC form to solve an active power market with block offers/bids, it produces a set of Lagrange multipliers λ_p^k at each bus. These Lagrange multipliers are prices for active power since they come from an auction where sellers/buyers are offered/bid at a price to the auction participants. In the jargon of power systems LMP is the most frequently heard term in the discussion of bus prices or bus costs today. LMPs λ_p^k correspond to the incremental cost of additional supply (demand) at each bus. In an uncongested transmission network, there are no incremental losses and the λ_p^k for the system are uniform and they will all be equal to the price of the marginal or last accepted unit. Depending on the type of auction, λ_p^k can be set to the LAO or the FRO if the market is a single-sided auction with inelastic demand. Similarly, the uniform λ_p^k in a double-sided auction market can be set to the LAO, LAB or anything else within the bid-offer gap will also be satisfactory for all buyers and sellers since it is less than or equal to all accepted bids and greater than or equal to all accepted offers. The total amount collected from the buyers equals exactly the amount paid out to the sellers.

With binding line and contingency constraints[3], however the bus λ_p^k are different. The difference between these nodal prices represents the cost of transmission between locations. Although λ_p^k are non-uniform, the prices are still determined by the marginal offer(s)/bid(s), but since they differ based on location, finding the equivalent of a first rejected price or of a bid-offer gap at each node is no longer straightforward. However it is possible to compute exchange rates for normalizing location specific prices, offers or bids to a reference location r, using λ_p^k as they represent the marginal value of power at a location.

Knowing that the marginal value of a single unit at node k is λ_p^k, the same unit has a value λ_p^r at node r. Therefore any price offer or bid at node k can be converted to the equivalent at node r by multiplying by an exchange rate λ_p^r/λ_p^k. Given the OPF solution which specifies the nodal prices along with which offers/bids are accepted or rejected, these offers and bids are normalized to a reference location r as above, then rank ordered as in a standard auction

[3]Even without binding line and congestion, the AC OPF typically produces non-uniform nodal prices due to losses. Congestion in the form of binding line flow or voltage limits increases the nodal price differences.

and the normalized uniform price can be chosen directly according to the desired pricing rule , i.e, LAO, LAB, FRO,..., FRB. For example, if the normalized uniform price at node r is x_p^r, then the uniform price at each node k is simply

$$x_p^k = \left(\frac{x_p^r}{\lambda_p^r}\right)\lambda_p^k = \mathscr{X}\lambda_p^k, \tag{1.1}$$

which is a simple scaling of all nodal prices λ_p^k by some factor $\mathscr{X}$ termed exchange rate. It is shown in (Zimmerman, 2010) that the exchange rate corresponding to the LAO is

$$\mathscr{X}^{LAO} = \max_g \frac{o_p^{g,LA}}{\lambda_p^{k(g)}}. \tag{1.2}$$

The author refers the reader to (Zimmerman, 2010) for the relationships between the OPF results and other pricing rules of the various uniform price auctions listed above.

In the next section, a sample OPF based auction will be used to demonstrate the LAO model of pricing, which is typically used in actual markets. In Chapters 3 and 4 however, an OPF based on generator cost functions and inelastic demand will be used instead. The shadow prices on the nodal power balance constraints represent the same Lagrange multipliers that can be used directly as the market clearing prices.

1.3.3 A Sample Auction Setup with OPF

We assume that producers and retailers owing the assets as presented below are participating in the DAM over a planning horizon of one hour.

1- on the supply side,

- a set of offers: $\mathscr{G} = \{G_g,\ g = 1,...,N_G\}$
- minimum and maximum capacity for offer G_g: $P^g_{G_{\min}}$ and $P^g_{G_{\max}}$, respectively,
- price for offer G_g: λ_p^k,
- generation level: $\left\{P_G^g,\ g = 1,...,N_G\right\}$, $P^g_{G_{\min}} \le P_G^g \le P^g_{G_{\max}}$

2- on the demand side,

- a set of bids: $\mathscr{D} = \{D_g,\ g = 1,...,N_D\}$
- minimum and maximum quantity for bid D_g: $P^g_{D_{\min}}$ and $P^g_{D_{\max}}$, respectively,
- price for bid D_g: λ_p^k,
- consumption level: $\left\{P_D^g,\ g = 1,...,N_D\right\}$, $P^g_{D_{\min}} \le P_D^g \le P^g_{D_{\max}}$.

An OPF based auction in which network constraints are considered through a DC load flow representation is set up to clear the market. The resulting optimization problem whose output are the optimal allocations and prices can be approached as a minimization problem and formulated as follows:

$$\min_{P_G^g,\, P_D^g} \quad \sum_g \lambda_p^k P_G^g - \sum_g \lambda_p^k P_D^g \tag{1.3a}$$

$$\text{subject to} \quad \sum_g P_G^{gk(g)} - \sum_g P_D^{gk(g)} = \sum_{n \in \mathscr{B}} Flow_{nk} \;\forall k \;:\; \lambda_p^k, \tag{1.3b}$$

$$Flow_{nk} = \frac{1}{x_{nk}} (\theta_n - \theta_k) \;\forall (n,k) \in \mathscr{L}, \tag{1.3c}$$

$$\theta_r = 0, \tag{1.3d}$$

$$P_{G_{\min}}^g \leq P_G^g \leq P_{G_{\max}}^g \;\forall g, \tag{1.3e}$$

$$P_{D_{\min}}^g \leq P_D^g \leq P_{D_{\max}}^g \;\forall g, \tag{1.3f}$$

$$\left| \frac{1}{x_{nk}} (\theta_n - \theta_k) \right| \leq f_{nk}^{\max} \;\forall (n,k) \in \mathscr{L}, \tag{1.3g}$$

where P_G^g, P_D^g, λ_p^k, θ_n, $Flow_{nk}$ are the optimization variables.

One recognizes the so-called Linear Programming problem (LP) here in a compact form:

$$\min_{\mathbf{y}} \quad \mathbf{c}^\top \mathbf{y} \tag{1.4a}$$

$$\text{subject to} \quad \mathbf{A}_{eq}\mathbf{y} = \mathbf{b}_{eq}, \tag{1.4b}$$

$$\mathbf{A}\mathbf{y} \geq \mathbf{b}. \tag{1.4c}$$

Note that the objective function and constraints (1.3a)-(1.3g) are replaced by affine expressions involving the following vectors and matrices:

- $\mathbf{c} \in \mathbb{R}^{(N_G+N_D)}$ is the cost coefficient of the decision vector $\mathbf{y} \in \mathbb{R}^{(N_G+N_D)}$.
- $\mathbf{A}_{eq} \in \mathbb{R}^{(\mathbf{N_G}+\mathbf{N_D})\times(\mathbf{N_G}+\mathbf{N_D})}$, $\mathbf{b}_{eq} \in \mathbb{R}^{(N_G+N_D)}$ define the (N_G+N_D) equality constraints (1.4b).
- $\mathbf{A} \in \mathbb{R}^{(\mathbf{N_G}+\mathbf{N_D})\times(\mathbf{N_G}+\mathbf{N_D})}$, $\mathbf{b} \in \mathbb{R}^{(N_G+N_D)}$ define the (N_G+N_D) linear inequality constraints (1.4c).

In (1.4c) the sign of the constraints is changed with respect to (1.3e)-(1.3g). This is to simplify the representation of the dual problem. Let us associate the vector $\lambda \in \mathbb{R}^{(N_G+N_D)}$ to the equalities (1.4b) and the vector $\mu \in \mathbb{R}^{(N_G+N_D)}$ to the inequalities (1.4c). The following LP problem is the dual of the LP (1.4) which is referred to as the primal problem:

$$\max_{\lambda,\mu} \quad \mathbf{b}_{eq}^\top \lambda + \mathbf{b}^\top \mu \tag{1.5a}$$

$$\text{subject to} \quad \mathbf{A}_{eq}^{\top}\lambda + \mathbf{A}^{\top}\mu = \mathbf{c}, \tag{1.5b}$$

$$\mu \geq 0. \tag{1.5c}$$

The dual LP (1.5) can be considered as a transposed version of the primal problem (1.4). Both LPs can be solved using commercial solver. The solutions of the primal LP problem provide the cleared offers/bids quantities whereas the dual LP solutions are the Lagrange multipliers λ and μ and represent the system prices and the unitary benefits on the demand and supply sides.

Table 1.2: Load bids

	Block 1 MW @ $/MWh	Block 2 MW @ $/MWh	Block 3 MW @ $/MWh
D2	20 @ 110	20 @ 90	20 @ 80
D5	20 @ 110	20 @ 90	20 @ 60

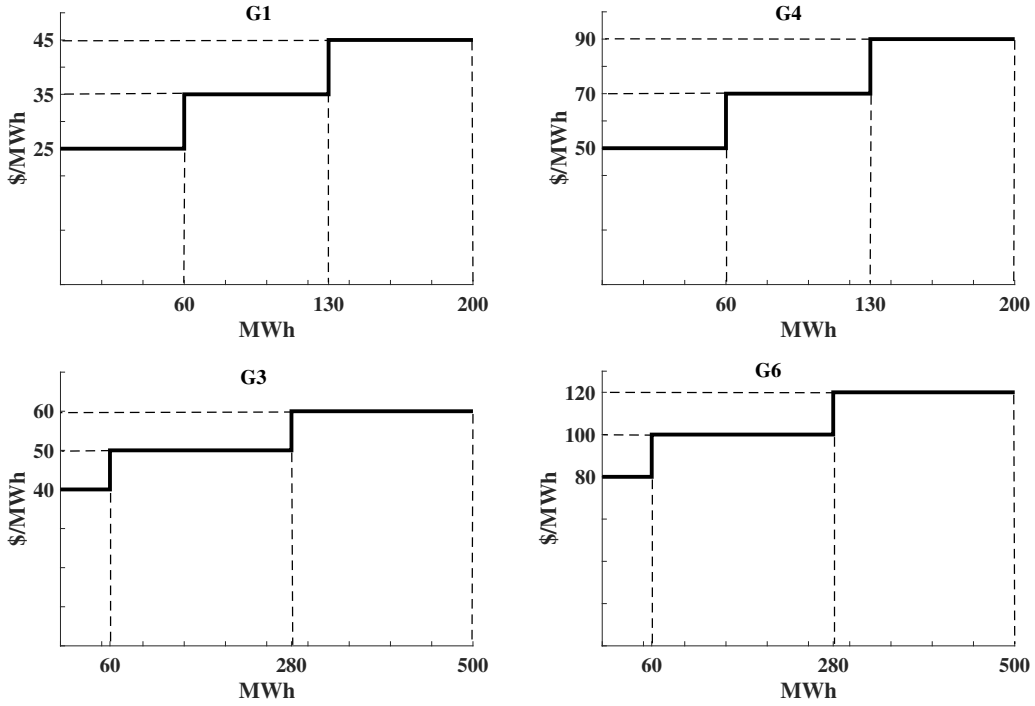

Figure 1.5: Sample auction supply curves for the DAM.

The test system in Figure B.1 which data are given in Table 1.2 and Figure 1.5 is used to analyze the proposed formulation. The following changes have been made to the system:

- generators have piecewise linear costs to ease the calculation of the economic dispatch while

start-up costs and shot-down costs are not considered;

- the WEG is shut-down;

- generators G2 and G5 have negative $P^{g}_{D_{\min}}$ to model the dispatchable loads. In doing so, we mimic the withdrawal of energy from the grid as a result of purchase. Thus, the two buyers's bidding with three blocks each in Table 1.2 are submitted to the market. However, a fixed load totalling 880 MW as distributed in the first period of Table B.1 is also considered for allocation;

- similarly, the four supplier's offering curves comprising three blocks of capacity each, are considered from the supply side as shown in Figure 1.5;

- the other system data are unchanged.

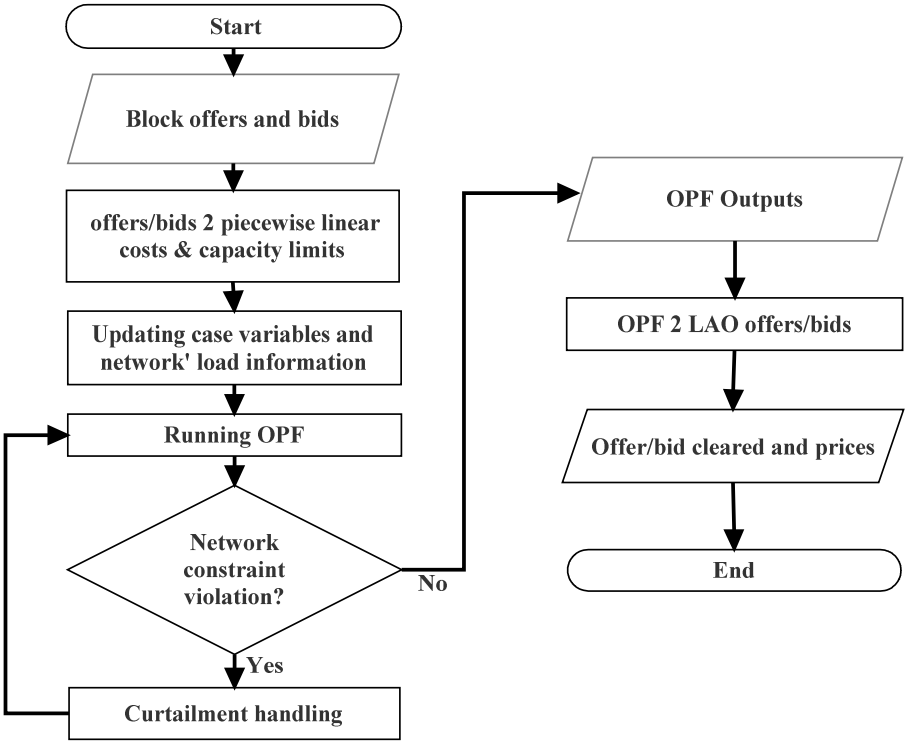

Figure 1.6: Flowchart of the market clearing algorithm.

The algorithm used to solve the market clearing model is implemented in MATPOWER (Zimmermann et al., 2011). The flowchart can be seen in Figure 1.6. Conceptually it consists of the following basic steps:

1- the conversion of market participants' block offers and bids into corresponding generating unit capacities and costs of operation.

2- To run an OPF in order to find generating unit allocations and nodal prices.

3- The conversion of generating unit allocation and nodal prices into a set of cleared offers and bids based on the LAO pricing rule.

The results of the market clearing are hereby presented. In the case of an infinite transmission capacity, the location of suppliers and buyers in the power grid has no influence on the optimal scheduling dispatch and on the resulting prices, leading to cheaper in merit suppliers G1 and G3 committing at the maximum capacity of each of their offer block.

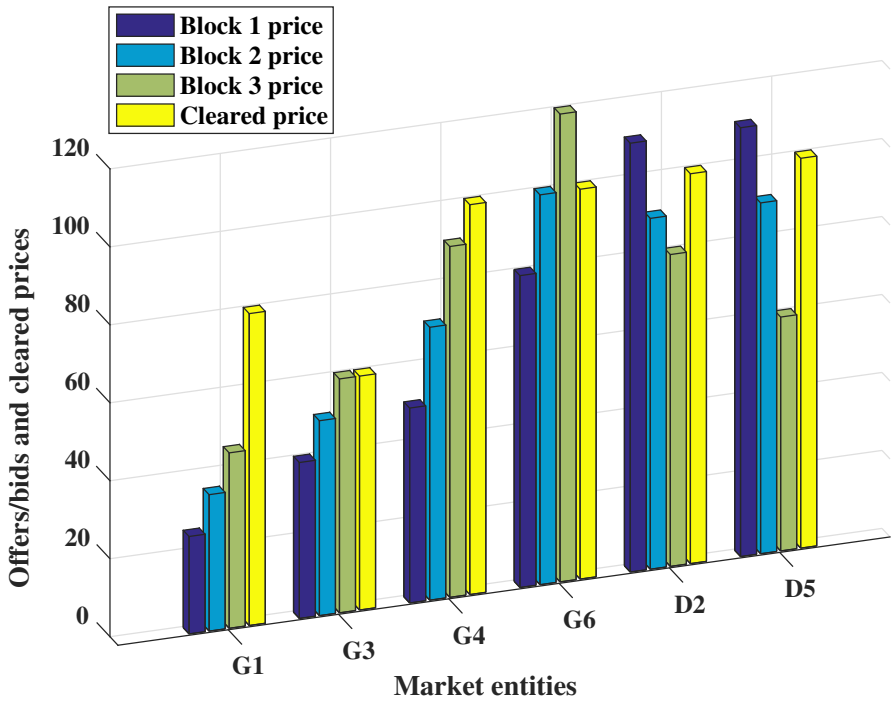

Figure 1.7: Market participants' offers/bids and cleared prices.

Table 1.3: Offers and bids quantity cleared

	Block 1 MW	Block 2 MW	Block 3 MW
G1	60	70	70
G3	60	220	100
G4	60	70	70
G6	60	120	0
D2	20	20	20
D5	20	0	0

As a result, the uniform MMP is set at \$90/MWh. However, with line limit checking, the optimal flow on line L3 occurs at its limit as shown in Figure 1.8, leading to LMPs across

the grid. An analysis of the quantity of offers and bids cleared as well as a comparison of the offers/bids prices and cleared prices presented in Table 1.3 and Figure 1.7 show that, congestion on line L3 has forced the ISO to reduce the last block of supplier G3 by 120 MW compared to the unconstrained schedule. This has benefited supplier G6 where block 2 previously out of merit is now committed as bus B5 price equals the offer price.

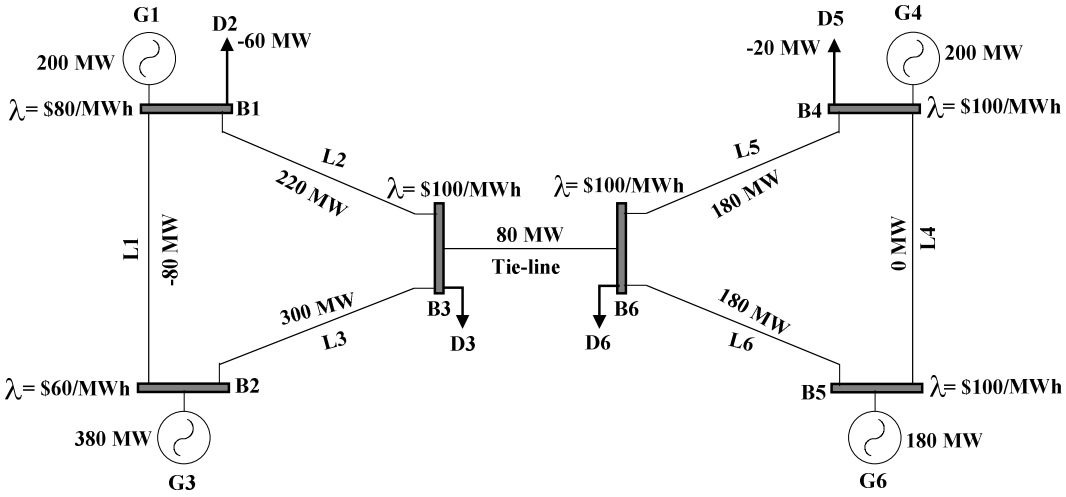

Figure 1.8: Result of the market dispatch.

Although actual flow on many lines lie away from their boundary and despite the fact that some suppliers' offer blocks are not yet exhausted as reported in Figure 1.8, buyer D5 could not afford the $100/MWh price for a MW of its location since its biding price is low for its blocks 2 and 3. As a result, only 80 MW of the demand of 120 MW requested is sold. Accordingly, the latter does not make any profit in this transaction as shown in Table 1.4. Indeed its revenue equals its total cost. As for the supplier G6, he does not sell a MW of his block 3 because the cost of operation is higher than the selling price at its location.

On the overall, the market summary in Table 1.4 shows that suppliers with offer prices below the LMPs are paid more than their offer and thus make more profit. This situation is also true for buyers if their willingness-to-pay associated with their bids is sufficient. It is important to emphasize, however, that the consideration of elastic demand in a competitive market is fundamental to the argument of efficient capital formation. When supply does not meet all of the desired bid demand, then market prices will provide incentives for levels of investment that will maximize overall benefits of consumption minus the capital and operating costs of production.

Table 1.4: Market summary

	Quantity sold/purchase MW	Selling/purchase price $/MWh	Revenue $	Total cost $	Earnings $
G1	200	80	16000.04	8900.03	7100.01
G3	380	60	22799.99	21399.98	1400.00
G4	200	100	20000.05	6450.02	13550.03
G6	180	100	17999.93	9599.95	8399.98
D2	-60	80	-4800.00	-6000.00	1200.00
D5	-20	100	-2000.00	-2000.00	0.00
Total	880		70000.00	38349.98	31650.02

1.3.4 Trading Reserve in Electricity Markets

DAM, intra-day market, and RTM are energy markets, in the sense that the payment to or from the ISO is proportional to the amount of energy actually delivered to or withdrawn from the grid. In addition to energy markets, reserve capacity markets exist in some countries to guarantee the availability of sufficient balancing power during the real-time operation of the power grid. However, as in the determination of reserve requirement for reliable grid operation, there are two schools of thought on how reserve should be traded in electricity markets. The sequential approach procures reserve capacity in a series of auctions run once the day-ahead energy dispatch has been determined. The advantage of this approach is that, by procuring reserve with different activation times, the free capacity that has not been successfully placed in one market can then be offered in the following auctions where the required activation time for the traded reserve is not as demanding. Consequently, reserve capacity offers that are successful in one market are not considered in the subsequent ones. Such practice is effective in some European markets e.g. the markets of Spain and Portugal (Omie, 2014).

Alternatively, energy and reserve may be simultaneously procured in the same auction using a co-optimization algorithm that captures the strong coupling between the supply of energy and the provision of reserve capacity. In this way the most efficient outcome for the market is ensured. This is the case in most electricity markets in North America.

In Ontario for example, to offer operating reserve, dispatchable generators or loads must be able to provide energy within the time frame specified and be able to sustain the supply of operating reserve energy for up to one hour. Even if their offer is selected but not activated,

they will receive stand-by payments for all megawatts for which they were selected, without having to make changes to their production schedule.

A price for this reserve energy is determined every five minutes through auctions. All accepted offers are paid the market clearing price for that class. When the operating reserve is activated, the suppliers are paid for the energy provided. Supplier G3 in the sample auction has 380 MW capacity committed to the DAM. Given the quantity of remaining power 120 MW the supplier can submit an offering curve to the regulation market with the following supply curve.

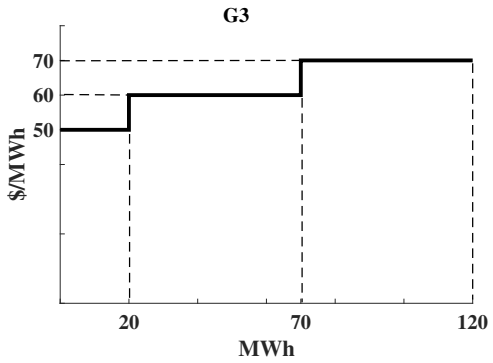

Figure 1.9: Sample auction supply curve for operating reserve market.

In this thesis a co-optimization of energy and reserve is adopted to study the impact of WEGs penetration to grid.

1.3.5 Impacts of WEGs on the Electricity Markets

Because WEGs have essentially zero and even negative variable costs when production-based subsidies are considered, they enter the aggregate supply curve at the bottom of the stack. In other words, WEGs are scheduled before conventional power producers and as a result their output directly influences the market price. This phenomenon is known as merit-order effect.

With WEGs output being variable, the system's aggregate supply curve is shifted to the left in case of low production from WEGs, and to the right in case of high wind power outturn. This has an effect on the intersection between the supply and demand curves. In periods with high WEGs production, the amount of scheduled production and consumption increases, and the market price is low. On the contrary, periods with low WEGs production are characterized by higher prices and lower production and consumption schedules.

Therefore, regions with high WEGs output forecast tend to have lower and more volatile prices than regions with lower WEGs output forecast. A typical example is illustrated in Figure 1.10 where the 24-hourly day-ahead prices had been recorded in the Electricity Market of the Iberian Peninsula in March 12, 2013. On that day, zero prices occurred for hours in which the renewable and hydro production exceeded energy demand.

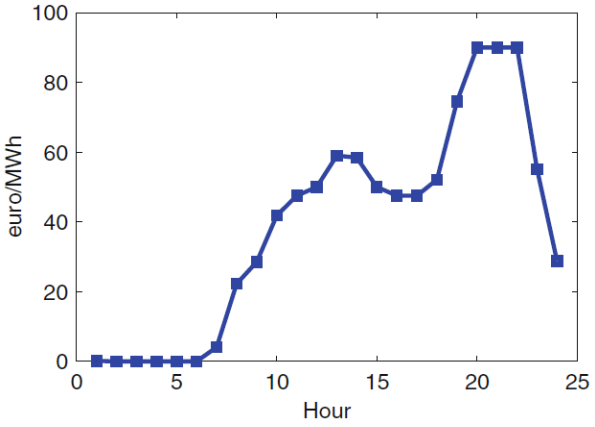

Figure 1.10: DAM prices registered in the Spanish area of the Iberian Electricity Market in March 12, 2013 (Morales et al., 2014).

Besides, the inherent uncertainty of WEGs increases the need for reserve to deal with the unexpected fluctuations of power production as stated in the introduction. This results in an increasing need for liquidity in markets whose gate closure approaches real-time, as well as for an efficient use of the resources participating in these markets. The balancing market is of particular importance to renewable power producers, as it allows them to adjust their contracts so that they match their actual output. Consequently, as the penetration of WEGs production in the electricity market grows, the share of balancing costs in the total system operation costs increases. This increase may become critical if the balancing market is not provided with enough flexible and competitive generation capacity to cope with uncertainties during the real-time operation of the power system economically.

1.4 Conclusion

This chapter has provided the literature review pertaining to this research work as well as the basic framework to understand the context of electricity markets. The principle of electricity price formation necessary for a market participant to strategically prepare his offer has been analyzed. It has been demonstrated that electricity markets as currently designed are being challenged by the growth in the share of WEGs as these resources tend to impact conventional behavior and incomes especially when system security is involved.

Chapter 2

Wind Electric Generator Modeling and Research Methodology

2.1 Introduction

WEGs are weather-driven resources whose power output depends on local meteorological conditions. Thus, wind power increases the risk of power shortages and failure to supply a contracted load, hence, cannot be managed like conventional generating units while solving the day-ahead UC problem. This risk can be quantified as EENS, i.e., the amount of output that may not become online from WEGs at any given hour. Being able to compute EENS in a timely manner can help smooth the inclusion of WEGs as they become a larger part of the power grid. However, a forecast for WEGs output as well as an error distribution of the forecast are both required.

This chapter develops an accurate method to calculate the EENS suitable for computing optimal bids necessary to participate in the day-ahead UC process and for real-time OPF calculation. The method considers that a forecast for WEGs output is available. We also attempt in this chapter to show how the amount of energy produced by a WEG is calculated based on the characteristics of both wind speed at the site and the turbine power performance curve. The main features of the market clearing models as formulated in the chapters 3 and 4 as well as the platform and solver used to tackle these scheduling problems are also presented in this chapter.

2.2 Distribution of the Wind Speed Measurement Sample

When considering a location for the harnessing of wind energy, the potential power output of a wind turbine subjected to the wind present at that location must be determined from historical wind data recorded there. Wind data generally provides the speed and direction in which the wind is blowing at a given period of time. This data is influenced by the geographical environment, be it natural or man-made, as well as the height at which it is measured. For the purpose of this research, the data sets used were obtained from a weather station in Belfort-France, as shown in Table 2.1.

Table 2.1: Geographical coordinates of the weather station at Belfort in France.

Location	Variable	Value
Belfort	Latitude	47°38.40' N
	Longitude	06°51.00' E
	Anemometer height	10 meters
	Altitude	358 meters above the sea level

2.2.1 Data Acquisition and Processing

The data were recorded at a height of 10 m, from 2011-06 to 2012-05, with a time resolution of 10 minutes and is made available to academic researchers through the website of the FCLAB (FCLab). The data contained many variables of no relevance to this research, which were deleted to leave only the wind speed and the timeline. Table 2.2 gives an example of a short segment from the series. However, a total number of 11493 raw measurements were recorded and plotted in Figure 2.1. The first visual impression confirms that most intra-hourly changes are small, but the wind can change a great deal in a few hours, and that pattern displays a degree of self-similarity on different timelines. This is confirmed by plots of the time series when compacted into daily averages.

2.2.2 Cleaning-up and Frequency Representation of Data

The wind speed data in the raw form of Figure 2.1, is merely an estimate of what the average wind speed was during the measuring period. This in itself is not enough to quantize the

Table 2.2: Example of a short segment from the series

Timeline		Wind speed [m/s]
15/02/12	1:30	0
15/02/12	1:40	0
15/02/12	1:50	0
15/02/12	2:00	0.1
15/02/12	2:10	0.2
15/02/12	2:20	0.3
15/02/12	2:30	0.3
15/02/12	2:40	0.3
15/02/12	2:50	0.2
15/02/12	3:00	0.2
15/02/12	3:10	0.2
15/02/12	3:20	0.3

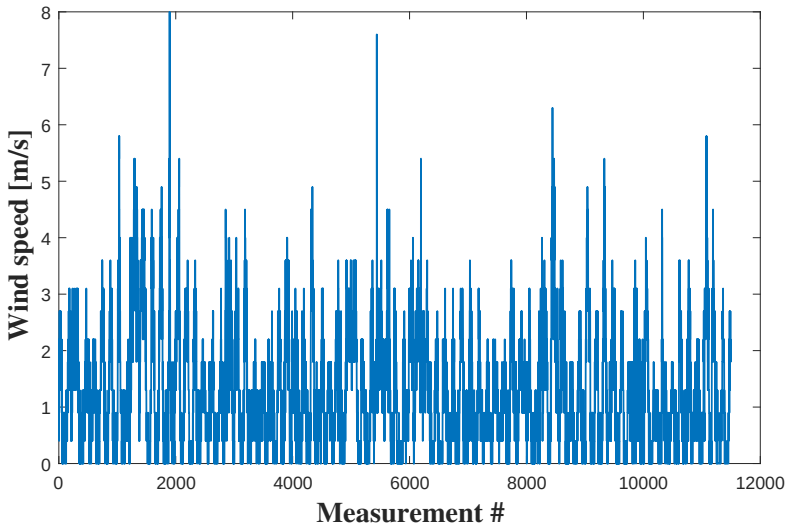

Figure 2.1: Wind speed time series.

availability of the wind, which is further complicated by the variable nature thereof. In order to overcome this quantizing problem, statistical techniques can be employed for data distribution and in doing so, make the data more intelligible and easier to work with. Accordingly the histogram has been chosen to represent the measured wind speed with all nil values ignored. The most common form of the histogram is obtained by splitting the range of data into equal sized bins called classes. Each class is represented by the middle value of the bin. Therefore, each bin j with Δ_v width has an associated relative frequency:

$$fr_j = \frac{n_j}{n}, \tag{2.1}$$

where n is the number of data points, n_j is the number of data points that falls inside the bin represented by the wind speed v_j, and fr_j is the relative frequency associated with bin j. With this definition, the following relationships are fulfilled:

$$\sum_{j=1}^{N} n_j = n, \tag{2.2}$$

$$\sum_{j=1}^{N} fr_j = 1, \tag{2.3}$$

where N is the number of bins.

When drawing a histogram of the wind speed data using an adequate bin width Δ_v, one is left with a distribution showing how many observations fall within each bin essentially providing an estimation of the probability distribution of the data (Lysen, 1983; Chang, 2011; Carta et al., 2008). The typical values used for wind energy analysis are $0.5m/s$ or $1m/s$ (Chang, 2011; Carta et al., 2008). In this research, following the international standards, the value of $\Delta_v = 0.5m/s$ was selected to compute the density and cumulative density of the distribution extracted from the recorded wind speed time series as shown in Figures 2.2 and 2.3, respectively. This mathematical representation of the wind speed distribution i.e., the distribution of the proportion of time spent by the wind within narrow bands of wind speed, will speed up calculations and free up memory, no matter how large the data was initially.

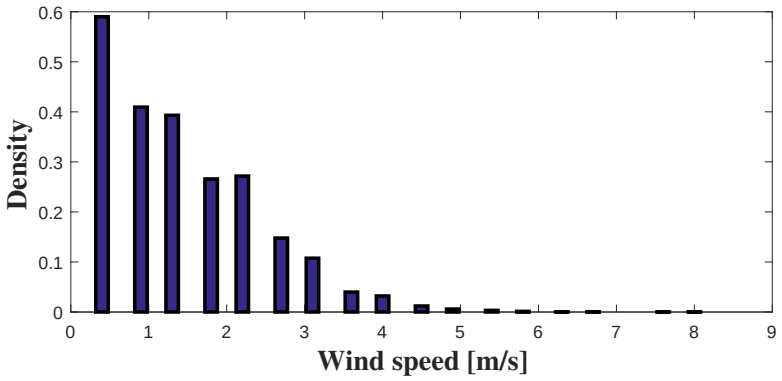

Figure 2.2: Distribution extracted from the time series.

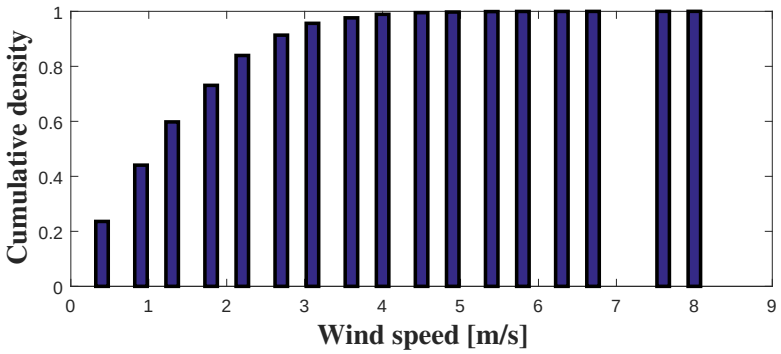

Figure 2.3: Cumulative distribution extracted from the time series.

2.3 Wind Speed Modeling

In order to calculate the mean power from a wind turbine over a range of mean wind speeds, a generalized expression is needed for the probability density distribution. An expression which gives a good fit to wind data is known as the Weibull distribution. Accordingly, the wind data from the Belfort test site has been approximated by means of the Weibull distribution. This distribution performs a task similar to a histogram, but surpasses it by smoothing and allowing the data to be easily represented by means of a simple equation. The Weibull Probability Density Function (PDF) and Cumulative Density Function (CDF) can be expressed by the following equations:

$$f(v) = \frac{k}{c}\left(\frac{v}{c}\right)^{k-1} \cdot e^{-\left(\frac{v}{c}\right)^{k}}, \tag{2.4}$$

$$F(v) = 1 - e^{-\left(\frac{v}{c}\right)^{k}}, \tag{2.5}$$

where $k > 0$ is the dimensionless shape parameter and $c > 0$ is the scale parameter in units of wind speed, m/s in our study. This kind of distribution is widely used for product lifetime analysis and reliability engineering (Lun and Lam, 2000; Billinton and Allan, 1996). Its shape and properties have made it the most appropriate description of the wind speed behavior when studying potential sites for wind park installations (Dukpa et al., 2010; Vallee et al., 2007; Camilo et al., 2007; Petkovic et al., 2014; Costa et al., 2012). It is clear from Figures 2.4 and 2.5 that the Weibull probability function provides a good representation of the raw wind data. Notice how the histograms in Figures 2.2 and 2.3 are right-skewed, reflecting the fact that strong winds are rare while moderate and fresh winds are more common: a display of an almost perfect Weibull function plots. However, the accuracy of a Weibull function

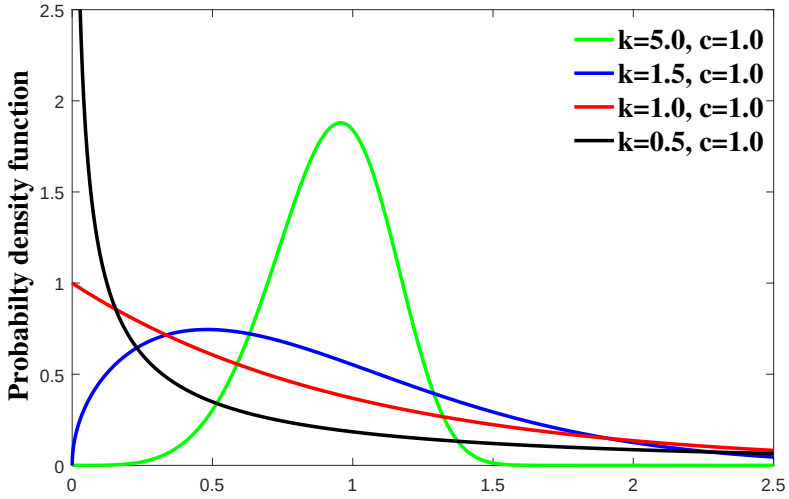

Figure 2.4: Examples of the Weibull density curve with various values of k.

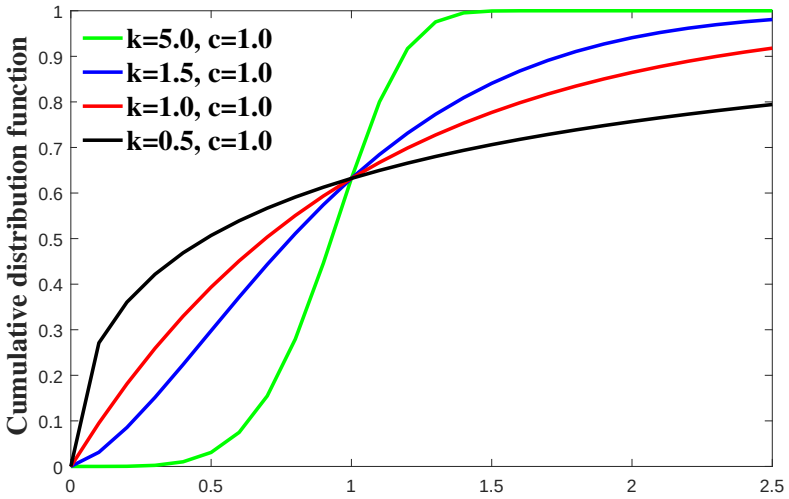

Figure 2.5: Examples of the Weibull cumulative curve with various values of k.

depends on the shape and scale parameters used. To examine the situation more precisely, the best fit Weibull parameters for the recorded data were approximated.

Several methods have been proposed to estimate Weibull parameters (Chang, 2011; Costa et al., 2012; Justus et al., 1978; Mathew, 2006; Seguro and Lambert, 2000; Al-Hasan and Nigmatullin, 2003) as described in appendix A.2. However, the wind speed data recorded been skewed, the LSQM, also known as the graphical method (Chang, 2011; Costa et al., 2012; Akdağ and Dinler, 2009; Mathew, 2006), have been chosen since the logarithmic transformations applied to the

Weibull CDF can decrease the variability of data and make the wind speed model conform more closely to the extracted distribution. Taking twice logarithm of (2.5), we obtain:

$$y = ax + b, \tag{2.6}$$

derived from

$$\ln\left[-\ln\left[1-F\left(v\right)\right]\right] = k\ln v - k\ln c, \tag{2.7}$$

where

$$x = \ln v, \tag{2.8}$$

and

$$y = \ln\left[-\ln\left[1-F\left(v\right)\right]\right], \tag{2.9}$$

which means that we are interested in fitting a straight line (2.6) with gradient k and intercept $-k\ln c$, to the given data $(x_j = \ln v_j, \quad y_j = \ln\left[-\ln\left[1-F\left(v_j\right)\right]\right])$.

Letting $\bar{x}$ and $\bar{y}$ the mean values of x and y respectively, computing the values of x_j and y_j respectively from (2.8) and (3.9), then, (2.6) parameters a and b can be derived as follows:

$$a = \frac{\sum_{j=1}^{N}\left(x_j-\bar{x}\right)\left(y_j-\bar{y}\right)}{\sum_{j=1}^{N}\left(x_j-\bar{x}\right)^2}, \tag{2.10}$$

$$b = \bar{y} - a\bar{x}. \tag{2.11}$$

Hence,

$$k = a, \tag{2.12}$$

$$c = \exp(-\frac{b}{a}). \tag{2.13}$$

It was found that the weather station under study produced a graph that was very nearly a straight line. As shown in Figure 2.6, the fitted line with parameters $k = 1.298$ and $c = 1.2903m/s$, makes the residuals (the signed vertical distance between the points and the line) small.

Having established the best fit parameters, corresponding Weibull density and distribution functions were plotted along with the histograms extracted from the time series. The results

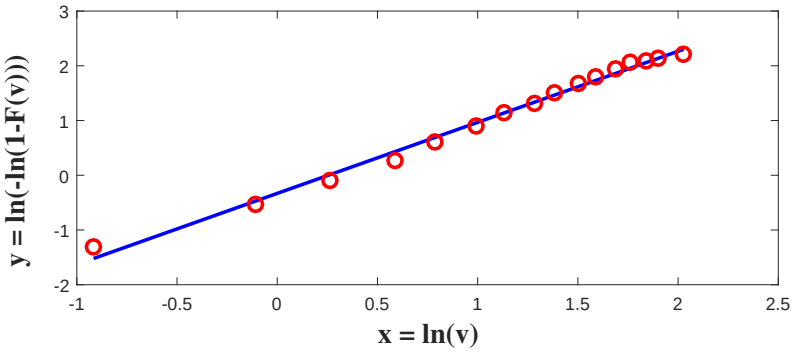

Figure 2.6: $\ln[-\ln[1-F(v)]]$ versus $\ln v$. Straight line implies Weibull distribution.

shown in Figures 2.7 and 2.8 was found to be typically a good fit. With an accurate model of wind speed distribution achieved, accurate wind energy production simulation can be expected. Indeed, the Weibull PDF does not provide only the average wind speed, but also the probability of encountering each wind speed. This wind speed probability will later be used to determine the probable power output of WEGs.

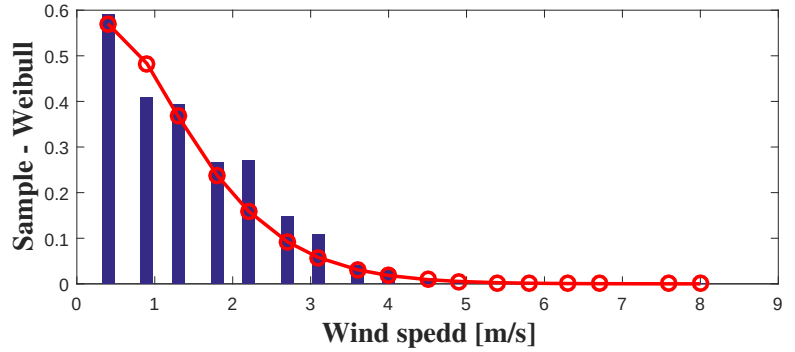

Figure 2.7: Time series histograms & Weibull density with best fit parameters.

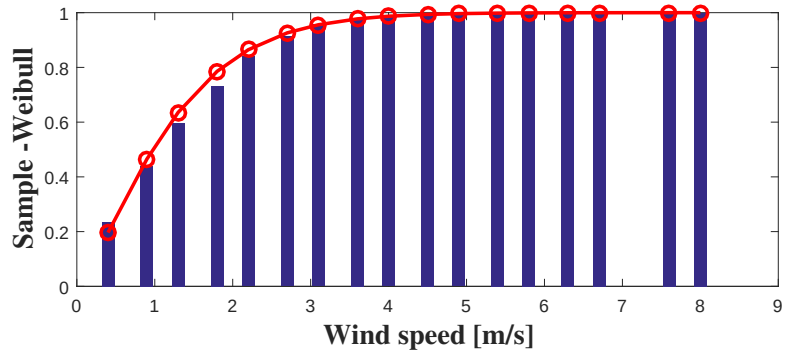

Figure 2.8: Time series histograms & Weibull distribution with best fit parameters.

2.4 Physical Modeling of WEG output

Wind turbines are devices that convert the kinetic energy of the wind into mechanical energy, which in turn generates electricity with the help of an electric generator. The theoretical power available in the wind can be given by (Heier, 2014; Tai-Her and Li, 2008):

$$P(v) = \frac{1}{2}\rho_{air} A_r v^3, \tag{2.14}$$

where $P(v)$ is the power in watts, A_r in m^2 is the rotor swept area exposed to the wind and ρ_{air} in kg/m^3 is the air density. In practice, due to a number of factors like the Betz limit[1], the generator and gearbox efficiencies as well as other losses, it is only possible to extract $20-30\%$ of the original energy available in the wind:

$$P(v) = \frac{1}{2}\rho_{air} C_p \eta_g \eta_b A_r v^3, \tag{2.15}$$

η_g being the generator efficiency (up to 0.8), η_b the gearbox/bearings efficiency (could be as high as 0.95 for good design) and C_p, the turbine coefficient of performance is bounded by the Betz limit. This coefficient is a function of both the turbine and wind speeds. Variable-speed wind turbines have the capability to track the maximum as wind speed varies by adjusting the turbine speed.

Since the overall efficiency of the turbine, $C_p \eta_g \eta_b$, is practically not constant (Pallabazzer, 1995), the output of a certain turbine is obtained from the power performance curve. This curve is available from the manufacturer and is characterized by the operational parameters of the turbine. The three commonly used parameters are the cut-in, rated, and cut-out wind speeds as shown in a schematic example of such a curve in Figure 2.9.

- **Cut-in speed.** At very low wind speeds, there is insufficient torque exerted by the wind on the turbine blades to make them rotate. However, as the speed increases, the wind turbine will begin to rotate and generate electrical power. The speed at which the turbine first starts to rotate and generate power is called the cut-in speed v_{cut-in}.

- **Rated speed.** As the wind speed rises above the cut-in speed, the level of electrical power output rises rapidly and reaches the limit that the electrical generator is capable

[1] The Lanchester-Betz limit states that the maximum theoretical amount of energy that can be extracted from the wind is approximately 59%.

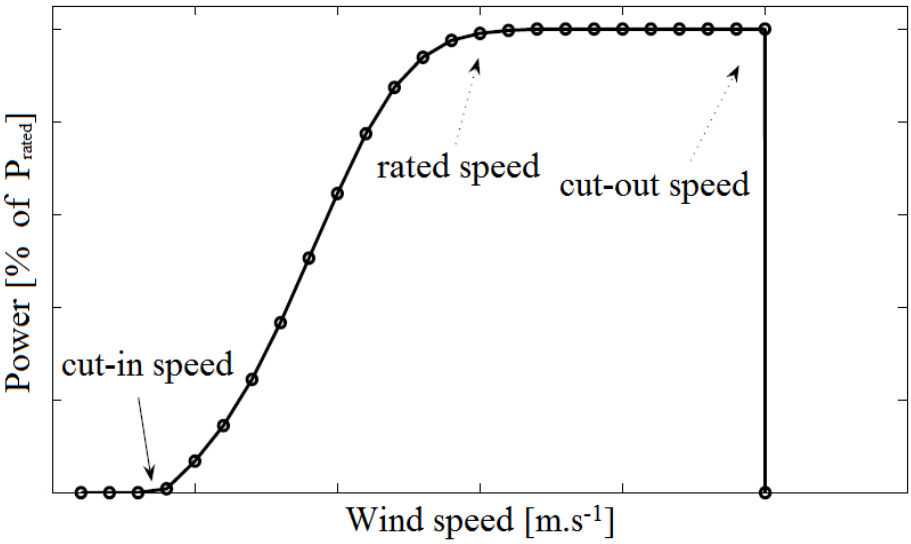

Figure 2.9: Example of a typical wind turbine power curve.

of. This limit to the generator output is called the rated power output P_{rated} and the wind speed at which it is reached is called the rated output wind speed v_{rated}. At higher wind speeds, the design of the turbine is arranged to limit the power to this maximum level and there is no further rise in the output power. How this is done varies from design to design but typically, with large turbines, it is done by adjusting the blade angles so as to keep the power at a constant level.

- **Cut-out speed.** As the speed increases above the rated output wind speed, the forces on the turbine structure continue to rise. To avoid any risk of damage to the rotor and prevent over-powering of the infrastructure, a braking system is employed to bring the rotor to a standstill. As a result, the turbine ceases to produce power. The wind speed at which this happens is called the cut-out speed $v_{cut-out}$.

Rewriting (2.15) into the form $P = C_v v^3$ with C_v a combined coefficient, allows us to approximate the generation output from a WEG as follows:

$$P(v) = \begin{cases} 0, & v < v_{cut-in} \\ C_v v^3, & v_{cut-in} \leq v \leq v_{rated} \\ P_{rated}, & v_{rated} < v \leq v_{cut-out} \\ 0, & v > v_{cut-out} \end{cases} \tag{2.16}$$

By making use of the Weibull PDF $f(v)$, which provides the probability of each wind speed being present as shown in Figure 2.7, and the power curve $P(v)$ which displays the power that will be available at each wind speed shown in Figure 2.9, these two graphs can be multiplied to obtain a WEG power probability graph (Bradbury, 2008). The average power produced by a WEG can then be calculated by integration in terms of (2.17). However, the knowledge of the average output of a WEG may not suffice for our study. Sequential WEG output over

$$P_{wbl} = \int_{v_{cut-in}}^{v_{cut-out}} f(v) \cdot P(v) dv \tag{2.17}$$

the horizon of study is required instead. To this end, WEGs output scenarios was achieved by means of Monte-Carlo simulation (Billinton and Wangdee, 2007; Vallee et al., 2007). Sampling methods (Kamalinia and Shahidehpur, 2010) and the Latin Hypercube simulation techniques (Wang et al., 2011) can also be utilized for this purpose.

In this research, it is assumed that, for each time interval of the horizon of study, three samples of wind availability serve as the base scenarios representing low, average and high wind realizations. Each scenario samples a possible wind power output with its associated probability as shown in Table 2.3, made available by the WEG to the ISO in this form.

Table 2.3: Forecasted cumulative probability and associated power output.

Hour	Cumulative Probability		
	$F = .6$	$F = .7$	$F = .8$
1	44.51	37.84	30.46
2	86.00	18.97	1.96
3	68.13	46.60	19.34
4	59.36	41.86	37.95
...	...	...	...
24	67.21	64.49	42.89

2.5 Wind Power Data

Three test systems have been used throughout this dissertation to show the effectiveness of our models. An illustrative 6-bus test system comprising a WEG with a rated power output of 200MW, the IEEE Reliability Test System (RTS) and the IEEE 118-bus test system in which 03 three WEGs, namely, WEGs #1, #2 and #3 which capacity in the same order are 300 MW, 300 MW and 200 MW have been added. As stated above, the forecasted power

outputs of a WEG is approximated by a set of probability-weighted scenarios for low, average and high wind realizations. In the deterministic model, transitions between these scenarios are not allowed from period to period. That is, if the system is in the high wind state in the first period, it will stay in the high wind state in the subsequent period, the same with the average and low wind states. However, for the probabilistic counterpart, all transitions are possible. Figure 2.10 displays the sequential output of the WEG considered in the 6-bus test system for both individual trajectories and full transition probabilities. For RTS and the 118-bus test system, the expected profiles can be seen in Figures 2.11 and Figure 2.12, respectively.

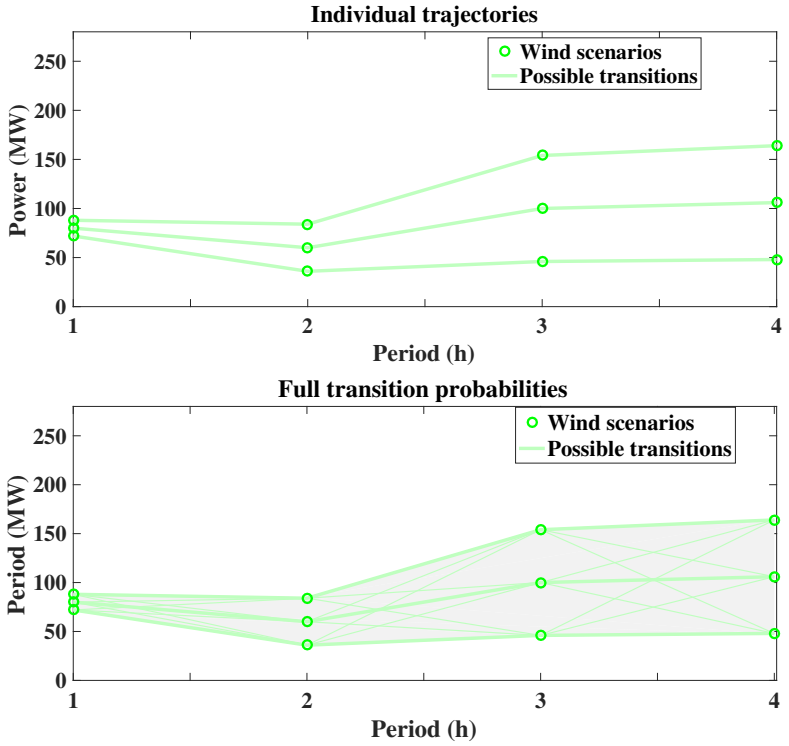

Figure 2.10: 4-hour period wind profile.

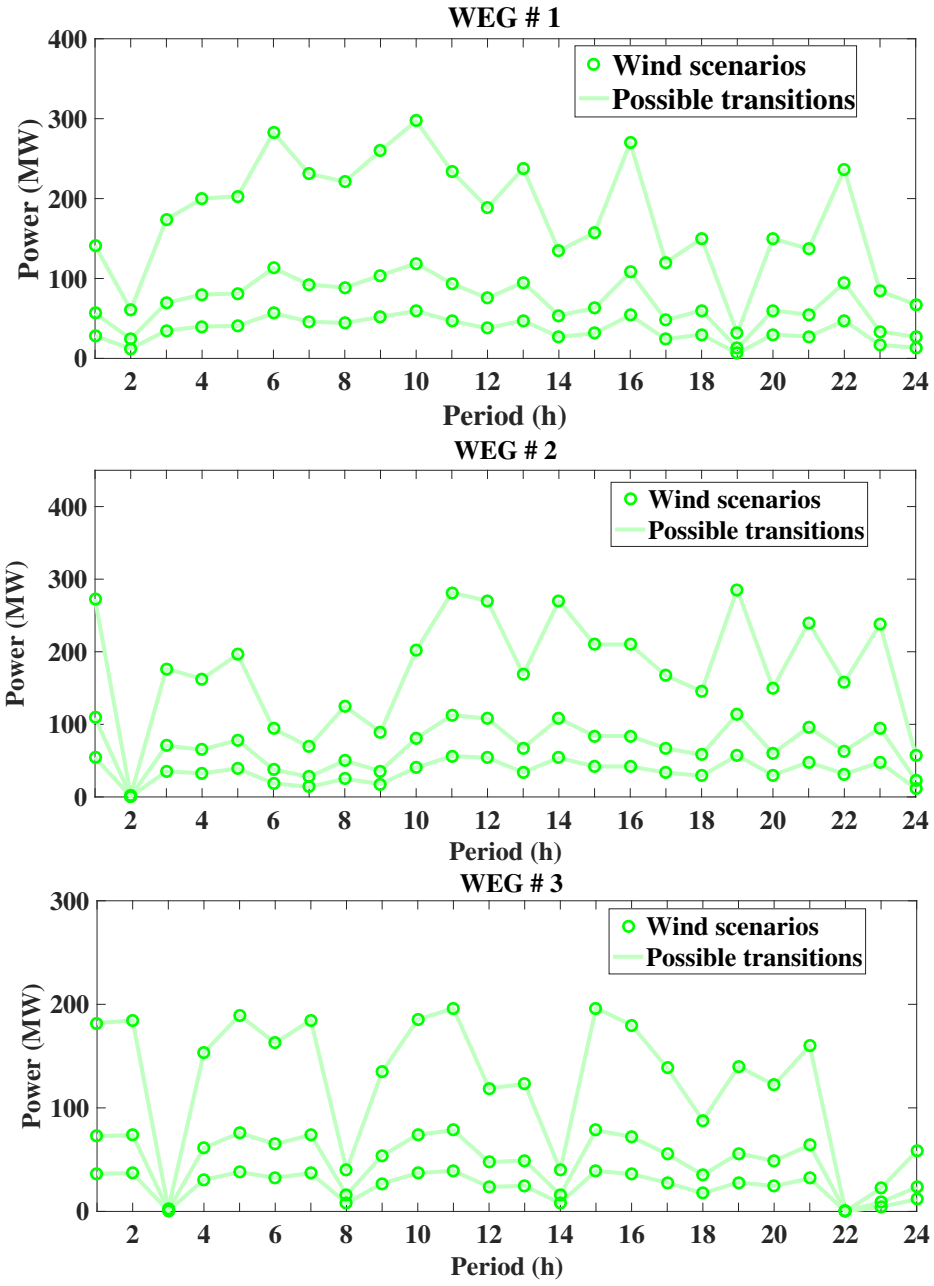

Figure 2.11: 24-hour period wind profile, individual trajectories.

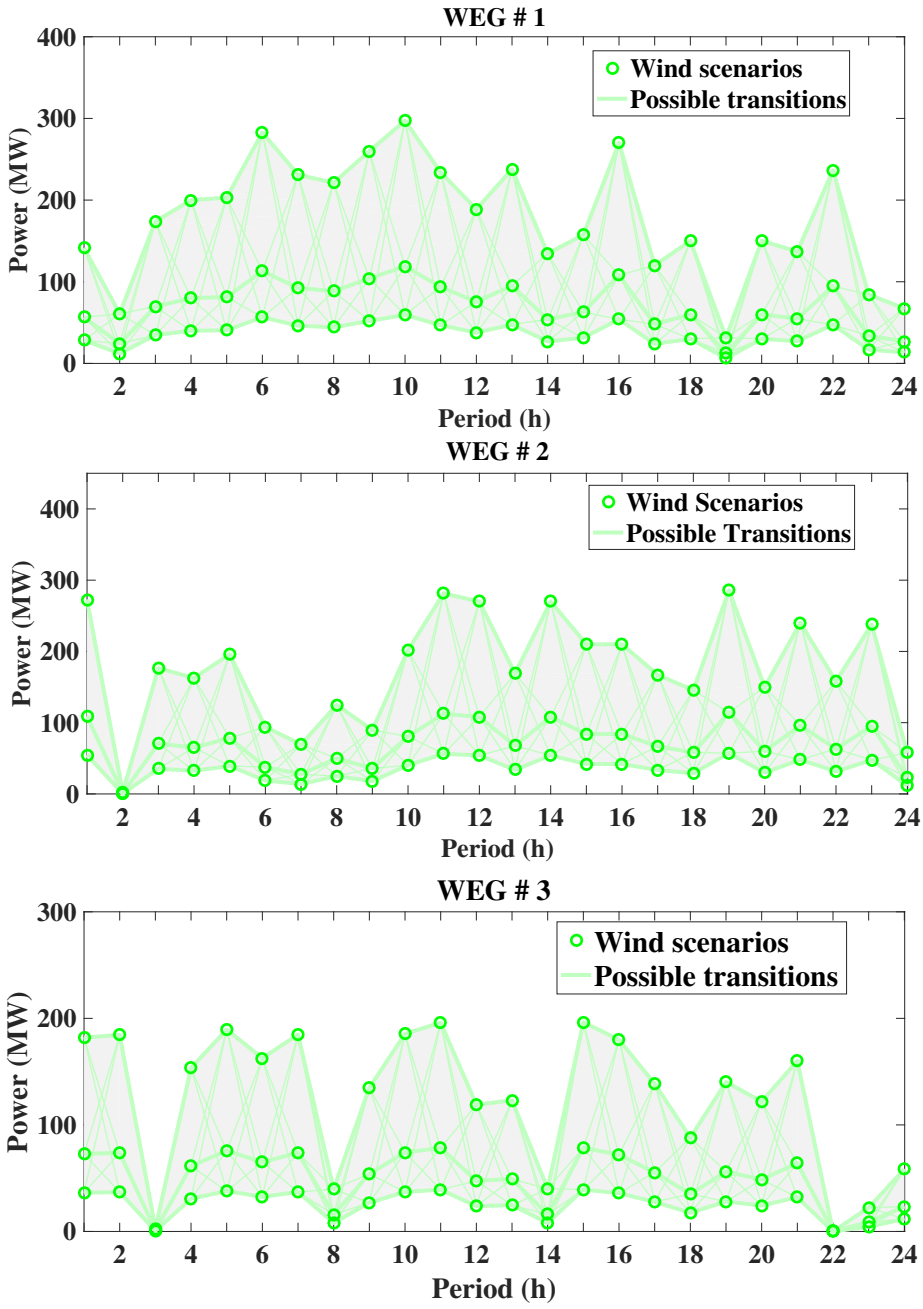

Figure 2.12: 24-hour period wind profile, full transition probabilities.

2.6 Estimation of the EENS

A WEG is considered dispatchable around the forecasted power output. This Means that there may be a shortfall between observed and scheduled power. Risk borne by the system through inclusion of WEGs is quantified as EENS computed using stochastic feature of wind power. Let F_m^{gt} be the cumulative probability associated with a WEG output, then, the probability that power output of P^{gt} may not appear is equal to: $1-F_m^{gt}$. Hence, the EENS in this case considering a block of one hour equals: $(1-F_m^{gt})\cdot P^{gt}$. Summing this term for all generators and segments for an hour, one gets the total EENS for that hour of optimal schedule as follows:

$$E_t(\mathbf{X}) = \sum_{R}\sum_{g\in RG^R}\sum_{m}(1-F_m^{gt})\cdot\left(\prod_{\substack{y\in RG^R\\ y\neq g}} F_{\max}^{gt}\right)\cdot P^{gt} \tag{2.18}$$

where $F_{\max}^{gt} = \max(F_m^{gt}),\ \forall m.$

(2.18) is an average risk and represents the amount of shortfall energy from WEGs that must be compensated through reserve provision. In Figures 2.13 and 2.14, EENS profiles corresponding to the single WEG of the 6-bus test system and the 03 WEGs of the IEEE test systems have been drawn.

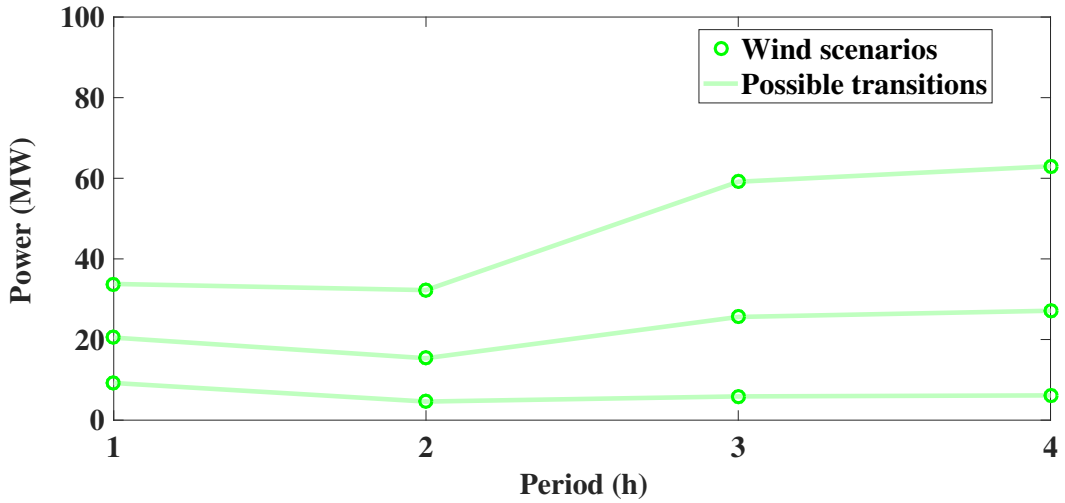

Figure 2.13: 4-hour period EENS profile.

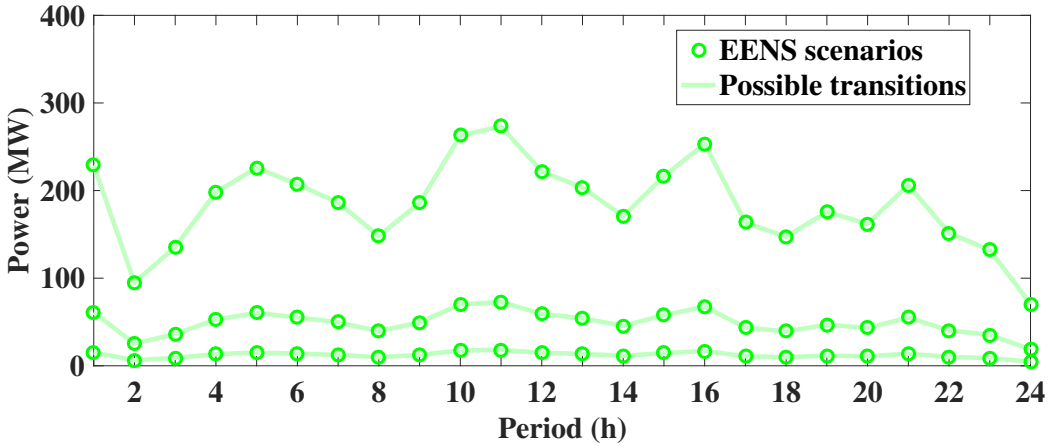

Figure 2.14: 24-hour period EENS profile.

2.7 Research Methodology

A critical evaluation of the different methodologies used in the literature review has helped to build an appropriate optimization framework to investigate the issues of scheduling, allocation and deployment of reserves in a power grid with large share of WEGs, as managed by an ISO or a plant owner. The procedure embeds the advantages of the co-optimization of energy and reserve to reconcile economic efficiency and system security for the clearing of electricity markets, while making use of the modeling capabilities of the deterministic and stochastic programming methods.

2.7.1 Overview of the Proposed Approach

The overall framework can be characterized as a hybrid of deterministic/stochastic, combined UC and DC-OPF problem. The objective is to maximize the social welfare over the planning horizon, while taking into account costs and benefits, including those arising from eventual demand deviation originating from redispatch, contingency and shedding.

2.7.1.1 Types of Uncertainty

Two types of uncertainty are considered in the proposed optimization framework. The first is related to low probability discrete events such as line, generator or other equipment failures,

in other words, contingencies. The second category has to do with limited knowledge about the values of future model parameters, such as nodal demand or WEGs production. This type of uncertainty can be described as a set of probability distributions[2] of the uncertain parameters. In this case, the distributions can be approximated by a set of system states and associated probabilities, each with specific realizations for the uncertain parameters. The selection of the set of system states and probabilities that best represent the underlying probability distributions is clearly an important consideration as all possible selected trajectories should be feasible in order to ensure that an optimal operating plan is reached. Putting these two types of uncertainty together, with the second providing a set of base states or scenarios, and the first adding a set of corresponding contingency states to each of the base states, results in a tree-like structure of system states and corresponding probabilities that approximate the uncertainty faced in any given period in the planning horizon. For a problem with multiple N_w states per period, N_c contingencies associated to each state over N_t periods of study, the set of all possible trajectories grows combinatorically, making the problem intractable. Selecting a specific set of representative trajectories (Papavasiliou et al., 2011) has the benefit of allowing the enforcement of strict feasibility, but it requires a very large number of trajectories to capture the full range of possibilities. The approach used in this thesis, thanks to (Murillo-Sánchez et al., 2013a), attempts to take into account a larger number of trajectories without sacrificing strict feasibility within a high-probability 'operating point envelope': the base states (no contingency occurring) in each period and the corresponding transitions between periods define an operating point envelope in which all transitions must be feasible and a Markovian transition probability matrix governs the propagation from period to period.

2.7.1.2 Security Management

Two type of security are also considered. In Chapter 3, the author quantifies the overall possible risks of generation shortfall by considering the spinning reserve generation as an exogenous parameter (listed in Table 1.1) comprising a fraction of the hourly demand due to equipment unreliability, and a fraction of the EENS due to the uncertainty of supply from WEGs computed using the stochastic feature of WEGs. A formula is established in

[2] In this thesis, the Weibull distribution which models wind speed, and the power curve which displays the power that will be available at each wind speed are used to estimate the average power produce by a WEG. The reader is referred to chapter 2 where the specificities of the wind power generation process are exposed.

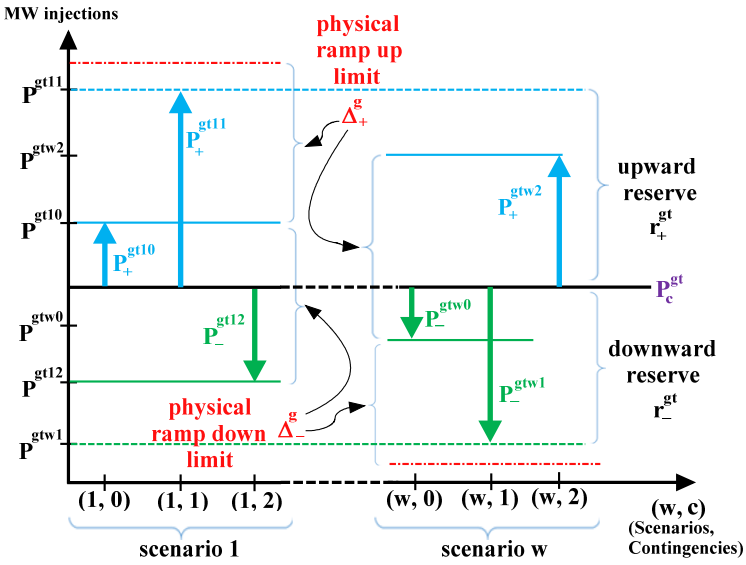

Figure 2.15: Reserve structure for generator g at time t. Adapted from (Murillo-Sánchez et al., 2013b).

this Chapter for the calculation of the EENS. However, the spinning reserve constraints as formulated in chapter 3 are typically used only for cases with a single base scenario with no contingencies, that is, when $\mathscr{W}^t = \{1\}$ and $\mathscr{C}^{tw} = \{0\}$.

In chapter 4 however, upward and downward contingency reserves are defined by the maximum deviations from a contracted reference output that are required to cover each of the system states, including the contingencies. In this way, the reserve is determined endogenously as a function of uncertainty in the system conditions, not pre-specified as in chapter 3. Within each scenario, physical ramp limits are imposed on each unit to ensure feasible transitions from the base to contingent states. Costs are imposed on reserves, and probability-weighted costs on both the injections and deviations from the contract in each state. Figure 2.15 illustrates the structure of reserve for unit g at time t. In this Figure, P^{gtwc} represents the active power injection for unit g in post-contingency state c of scenario w at time t. P_c^{gt} is the active power contract quantity for unit g at time t. P_+^{gtwc} and P_-^{gtwc} are the upward and downward deviations from the active power contract quantity for unit g in post-contingency state c of scenario w at time t, respectively.

2.7.1.3 Load-Following Ramping

The feasibility of the operating point envelope is ensured by applying a number of intertemporal constraints between adjacent time periods. The first of these are the critical load-

following ramping constraints needed to guarantee sufficient ramping capability and follow rapidly changing system conditions, such as those encountered during morning load ramp-up or a sudden change in wind generation. At each hour, this capability is determined by two types of decisions: the type, number, capacity, location, and ramp capability of the units that are online, and the actual scheduling of the pool of committed units. Load-following ramping limits are applied for each unit, constraining the corresponding change in dispatch for all transitions, that is, from each scenario w_1 in period t to each scenario w_2 in period $t+1$. Ramping costs representing market offers for a potential ramping reserve product are imposed on the maximum up and down ramp capacities procured in the optimal schedule.

2.7.1.4 Post-Contingency Constraint modeling

Survival of a contingency implies a state trajectory that does not exceed system ratings or operating limits and which reaches an equilibrium that does not violate any limits. Then, the system can be steered towards a more economical and secure operating point with the resources available. By modeling all post-contingency situations with load flows that join the overall problem formulation, the variables defining those flows are incorporated and thus available to impose coupling constraints such as ramp rates on them, generator capability and transmission capacity limits for the post-contingency solution. This is different from continuation load flow such as (Lavaei and Low, 2012).

2.7.1.5 Load Shedding Specification

Post-contingency load shedding is considered as a possibility to reach a secure operating point with the resources available if it is economical to do so. Such loads are modeled as fictitious generators at the VOLL which is nominally set to \$10,000/MWh. Minimizing the expected cost, including load shedding as a cost, corresponds to maximizing the expected sum of consumer and producer surplus.

2.7.1.6 Unit Commitment

Unit commitment decisions also have an intertemporal dependency in the form of minimum up- and down-times. In addition, these decisions introduce binary variables with associated startup and shutdown costs for each unit in each time period. This structure results in a single commitment schedule for the planning horizon that applies to all of the scenarios under consideration. As with other post-contingency actions, updates of this commitment schedule following a contingency event come from the solution of a new OPF problem.

2.7.2 General Formulation and Model Assumptions

Considering the main features of the model as exposed above, the optimization model can be expressed as a minimization problem over variables $\mathbf{X}$, defined as follows:

$$\min_{\mathbf{X}} \quad f(\mathbf{X}) \tag{2.19a}$$

$$\text{subject to} \quad g(\mathbf{X}) = 0, \tag{2.19b}$$

$$h(\mathbf{X}) \leq 0, \tag{2.19c}$$

$$\mathbf{X}_{min} \leq \mathbf{X} \leq \mathbf{X}_{max}. \tag{2.19d}$$

Where The different components of the objective function $f(\mathbf{X})$ include:
1) The cost of energy delivered
2) The cost of re-dispatching the system (e.g. deviations from contracts)
3) The benefit that consumers receive, having all their load serviced (no load shedding cost)
4) The cost of reserves (fixed/up and down) for low probability events (e.g. contingency reserve)
5) The cost of ancillary services, for high probability events (e.g. load-following reserve).

All of this is subject to:
1) the active power flow constraints (2.19b) in the base case flow, all scenarios and contingencies,
2) the transmission capacity and generation capability curve (2.19c) for all flows,
3) and new additional constraints that couple the base case and the post-contingency flows,

defining the deviation variables and the reserve variables as well as unit commitment constraints.

Pursuing clarity and simplicity, the main modeling assumptions formulated as the optimization problems as far as chapters 3 and 4 are concerned are listed below:
1) Loads are assumed to be inelastic and a single load profile is applied to all scenarios.
2) The transmission grid is modeled through a linear DC power flow model, thus the Lagrangian function for the defined problem assumes an active power-only.
3) The supply cost functions of thermal generating units are described by quadratic functions of the form $C_g\left(P^{gtwc}\right) = c_g \cdot \left(P^{gtwc}\right)^2 + b_g \cdot P^{gtwc} + a_g$. In this function, c_g, b_g and a_g are the cost coefficients for unit g which output at time t is P^{gtwc}.
4) WEGs do not supply operating reserve, they are not considered competitive and offer their forecast generation at zero price.

2.7.3 Model Implementation

With assumption made on the transmission network which is represented by a lossless DC model, while ensuring that none of the additional constraints are nonlinear, the full framework can be posed as a large MIQP and solved by one of the commercially available state-of-the-art MIQP solvers. To this end, (2.19) along with the additional constraints have been converted to the quadratic constrained optimization problem as follows:

$$\min_{\mathbf{s}} \quad f(\mathbf{s}) = \frac{1}{2}\mathbf{s}^\top Q\ \mathbf{s} + q^\top \mathbf{s} \tag{2.20a}$$

$$\text{subject to} \quad A\ \mathbf{s} \leq b, \tag{2.20b}$$

$$A_{eq}\ \mathbf{s} \leq b_{eq}, \tag{2.20c}$$

$$l_b \leq \mathbf{s} \leq u_b, \tag{2.20d}$$

where

$f(\mathbf{s})$: a general quadratic cost on the optimization vector $\mathbf{s}$.

q: the linear coefficient vector.

Q: the quadratic coefficient matrix.

A: the coefficient matrix of the linear inequality constraints.

b: the right-hand-side of the linear inequality constraints.

A_{eq}: the coefficient matrix of the equality constraints.

b_{eq}: the right-hand-side of the equality constraints.

l_b: the variable lower bounds.

u_b: the variable upper bounds.

The model has been implemented on an Intel(R) Core(TM) i7-3770 cpu @ 3.40 GHz with 32.0 GB of RAM, and programs have been developed using MATLAB R2016a. Relevant MIQP problems were solved by Gurobi 8.0.1 (Gurobi, 2017) under MOST (Murillo-Sánchez et al., 2013a) for Matpower (Zimmermann et al., 2011) Optimal Scheduling Tool. The flowchart of assembling the data struct in MOST is depicted in Figure 2.16.

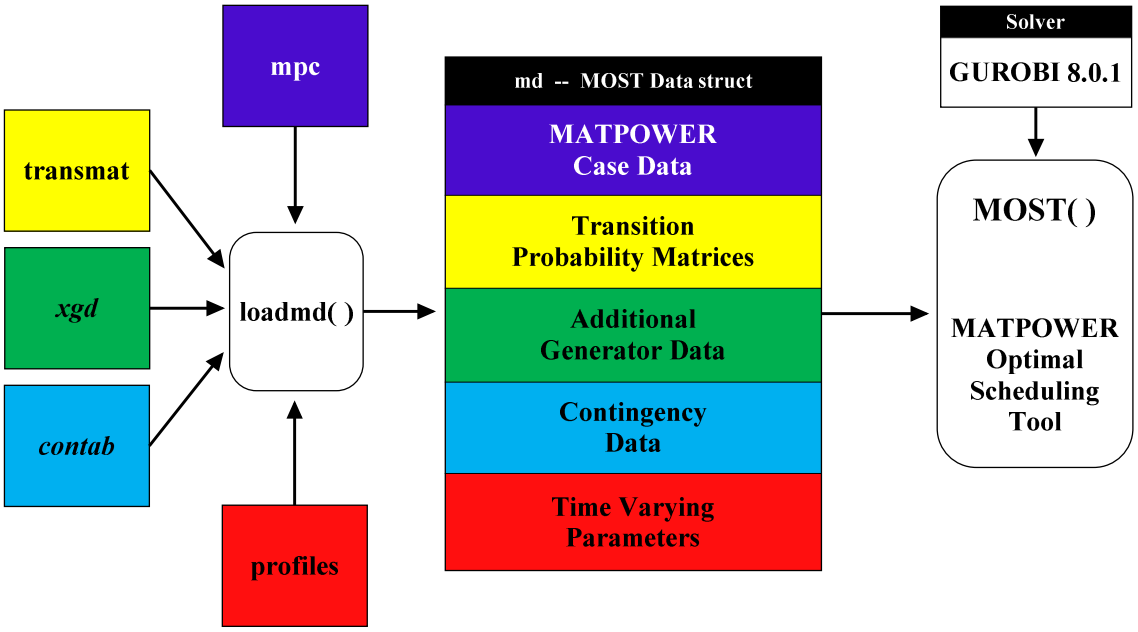

Figure 2.16: Assembling the MOST data struct.

2.8 Conclusion

This chapter has provided the model for WEG to be used throughout this thesis. The specificities of the wind power generation process have been exposed. This has been done by discussing wind characteristics and the way wind is transformed to power. Because low wind speeds are more common than strong breezes, the generation of electricity from wind is most of the time in the low and steep parts of the power curve. This corresponds to a zone where a small wind speed variation induces a large variation of the power generated. The variability

of wind speed leads to a highly dynamic behavior of wind generation. Also, these variations induce a cost for the maintenance of the balance and the supply security of a power system. To counter the risk introduced through the inclusion of WEGs, an accurate forecast of WEGs and an estimation of EENS in a timely manner have been established using Weibull CDF. A general formalism of the market clearing model of chapter 3 and chapter 4 have also been exposed as well as the main features of the methodologies used to solved related problems. The architecture of assembling data for the simulations have also been provided in this chapter.

Chapter 3

An Improved Deterministic Reserve Allocation Method for Multi-area Unit Scheduling and Dispatch under Wind Uncertainty

Résumé

"Un algorithme de programmation des centrales mixtes comprenant des éoliennes à grande échelle a été conçu pour optimiser la participation de celles-ci au marché de l'électricité du jour pour le lendemain. La traditionnelle réserve tournante y est suppléée par un extra qui tient compte de l'incertitude du vent et qui est représentée dans la contrainte de sécurité en terme de scénarios. Traduit en programmation mixte quadratique, l'outil d'optimisation est utilisé pour ordonnancer l'allumage/extinction de chaque centrale, définir sa production ainsi que la réserve d'exploitation à moindre coût. Des études de cas ont été conduites pour investiguer divers effets de la mutualisation des capacités via l'interconnexion sur la réduction des coûts d'exploitations associés à plus d'éoliennes sur le réseau."

Abstract

"A DAM-SCUC suitable for power systems with a large share of wind energy has been devised. The traditional spinning reserve requirement is supplemented by an adjustable fraction of the expected shortfall from the supply of WEGs, computed using the stochastic feature of wind and loosely represented in the security constraint with scenarios. The optimization tool commits and dispatches generating units, while simultaneously determining the geographical procurement of the required spinning reserve as well as load-following ramping reserve, by mixed integer quadratic programming. Case studies are used to investigate various effects of grid integration on reducing the overall operation costs associated with more wind power in the system."

3.1 Introduction

PRIOR to the large-scale penetration of WEGs, uncertainty in power grids was limited to load forecast error and unplanned outages of generating units or transmission lines. Because the characteristics of this uncertainty, i.e., the probability of these facilities being forced offline generally does not change significantly with time, satisfactory levels of reliability was met by the use of the deterministic criteria. WEGs do increase the amount of variability and uncertainty on power systems because they have a maximum available limit that varies with time and that limit is not known with perfect accuracy. Static amounts of pre-specified reserve do not take advantage of this information for more reliable and efficient requirements. As a result, the power system's operational reliability cannot be guaranteed with the conventional deterministic spinning reserve method, and extra generation reserve is needed to accommodate WEGs integration. Moreover, WEGs, being inertia less resources do not maintain system balance. Hence, reductions in the system net load resulting from declining WEGs output will force conventional plants to ramp up their output, or if sufficient ramping capability is not available, fast-starting units will need to come online. These units are thus stressed given the temporal operating restrictions limiting the rate of altering their output or of bringing them online. This makes the grid costly to operate, insecure and

vulnerable.

Additional costs generally occur because the unit commitment is inefficient due to forecast errors and because it is adjusted to provide more flexibility, accommodating the wind's increased variability and uncertainty. Thus, an optimal schedule that takes into account extra spinning reserve generation in order to mitigate WEGs' intermittency can save considerable fuel input and cost. Equally, some inherent level of flexibility–design can relieve the jerkings around these units and prevent them from breaking down. Although physical flexibility can be gained from these units, large penetrations of WEGs on a power plant portfolio may lead to a decrease in energy prices Maggio (2012), resulting in revenue reduction for flexible plants to recover their variable and capital costs since their output may decrease. If incentives are not provided to encourage the needed ramping capability, the system is unlikely to get the efficient balance of generation resources because potential reliability degradation or costly out-of-market actions can occur. To gain the system requirement necessary to support the security and reliability of the power grids, adequate market policies must be crafted that address the required financial implications.

3.2 Chapter Contribution

It emerges from the literature review as presented in Chapter 1 that the variable output and imperfect predictability of WEGs face stochastic approaches to plan and operate the power grids in the short-term. While being good, they are not suitable for production grade programs. Indeed, stochastic programming and/or robust optimization are still not being used in practical systems yet Chen (2016). System operators (SOs) are concerned with the high computational requirements of these methods. For these reasons, all the market clearing tools are based on deterministic methods which assume a fixed knowledge of system conditions for the next day Chen (2016). However, with large amounts of WEGs in power systems, the sole use of the deterministic criteria may not be economical or reliable in limiting the risk of uncertainty: an extra spinning generation reserve is needed to accommodate WEGs integration. Besides, except reference Ahmadi-Khatir et al. (2014) that addresses the market clearing problem with the commitment decision of generators, the majority of these references focus on the economic dispatch or OPF problem and none of them rewards conventional units

for their positive environmental attributes. With this in mind, the contributions of this chapter can be summarized as follows:

- a scheduling algorithm in which the stochastic feature of WEGs is related to an adjustable extra spinning reserve constraint loosely represented by only three scenarios. This makes our model more applicable, more acceptable and computationally efficient. Compared to robust optimization that tackles uncertainties through immunizing against the worst-case scenario, our model delivers the feasible solution by providing sufficient ramp capability to ensure a feasible transition from lower to upper bound.

- The valuation of ramping related costs on fossil-fuelled facilities. Indeed, by receiving compensation for costs they incur based on the decisions of others, these generators will have greater incentives to make their units available with higher ramp rates and to follow dispatch signals.

- The translation of the optimization framework into a MIQP problem. A MIQP solver returns a feasible solution with a known optimality level.

3.3 Chapter Organization

The rest of this chapter is structured as follows. Section 4 provides the formulation of the proposed model. Section 5 reports on the results from the studies on a 6-bus two-area, the modified IEEE 118-bus and the IEEE-RTS three-area systems. Conclusions are drawn in Section 6.

3.4 The Proposed Model Formulation

3.4.1 Cost Definition Function

Considering the optimization variables $\mathbf{X}\left[P^{gt}, u^{gt}, v^{gt}, q^{gt}, r^{gt}, \delta_{+}^{gt}, \delta_{-}^{gt}, LNS_{n}^{Rt}, \theta_{n}^{Rt}, Flow_{nk}, Flow_{nl}, r_{tie}^{t}\right]$, for $\forall t$, $\forall R$, $\forall n$, $\forall g$, the objective of the hybrid tool as stated below is to minimize the net costs

$TC(\mathbf{X})$ to purchase adequate energy and reserve to meet the demands of supply and security:

$$\begin{aligned} TC(\mathbf{X}) = \sum_{R}\sum_{t=1}^{N_T}\Bigg\{ & \sum_{g=1}^{N_g^R}\left[a_g \cdot u^{gt} + S_{on}^{g}\cdot v^{gt} + S_{off}^{g}\cdot q^{gt}\right] \\ & + \sum_{g=1}^{N_g^R}\left[c_g\cdot (P^{gt})^2 + b_g \cdot P^{gt}\right] \\ & + \sum_{g=1}^{N_g^R} d_g \cdot r^{gt} \\ & + \sum_{g=1}^{N_g^R}\left[e_{g_+}\cdot \delta_{+}^{gt} + e_{g_-}\cdot \delta_{-}^{gt}\right] \\ & + \sum_{n=1}^{N_b^R} VOLL\cdot LNS_n^{Rt}\Bigg\} \end{aligned} \tag{3.1}$$

In the first row of the objective function (3.1), $a_g(\$/hr)$ is the cost of maintaining the boiler operating and the generator spinning at synchronous speed, but not generating any output(0 MW). a_g is a fixed cost usually termed no-load cost, i.e., the cost that a generator incurs during any period that the unit is operating. u^{gt} is the commitment state for unit g in period t. It is a binary variable that equals one when the unit is on (and zero otherwise). $S_{on}^{g}(\$)$ is the cost to bring the boiler, turbine and generator from shutdown conditions to a state ready to connect to the system. S_{on}^{g} varies with how long the unit has been down and is only incurred once each time the unit operates regardless of the period of operation. A similar definition can be done for the shutdown cost $S_{off}^{g}(\$)$. v^{gt} (resp. q^{gt}) are binary variables that equal one when the unit is turned on (resp. turned off) and are zeros otherwise. The second row of the objective function represents the expected cost of active power dispatch and redispatch, with P^{gt}, the output power of generator g in time t and, $c_g(\$/\text{MW}^2\text{h})$, $b_g(\$/\text{MWh})$ the quadratic and linear fuel cost coefficients of unit g, respectively. In row three, $d_g(\$/\text{MWh})$ is the cost for unit g to provide spinning reserve $r^{gt}(\text{MWh})$. Generators incur significant costs when changing output, and these costs are expected to rise with WEGs penetration to grid due to the rapid and frequent ramping they impose on conventional units. These costs are reflected in our model in row four where for every MW of ramp, up $\delta_{+}^{gt}(\text{MWh})$ or down $\delta_{-}^{gt}(\text{MWh})$, efficiency costs of $e_{g_+}(\$/\text{MWh})$ and $e_{g_-}(\$/\text{MWh})$ in the same order, are incurred. $VOLL(\$/\text{MWh})$ in row five is the cost incurred in shedding load $LNS_n^{Rt}(\text{MWh})$ at bus n of region R in period t during real-time operation.

3.4.2 Constraints

The minimization of the objective function is subject to the following constraints:

–Power balance equations:

$$\sum_{g\in CG_n^R} P^{gt} + \sum_{g\in RG_n^R} P^{gt} + LNS_n^{Rt} = D_n^{Rt} + \sum_{k\in\Phi_{nk}^R} Flow_{nk} + \sum_{l\in\Gamma_{nl}^R} Flow_{nl},\ \forall n\in R, \forall t,\ \forall R \tag{3.2}$$

Constraints (3.2) ensure that the hybrid tool algorithm can schedule sufficient power to meet all real-time demands at any bus and time under any circumstances.

–Network flow and transmission limits:

$$Flow_{nk} = \frac{1}{x_{nk}}\left(\theta_n^{Rt} - \theta_k^{Rt}\right),\ \forall n\in R, \forall t,\ \forall R \tag{3.3}$$

$$Flow_{nl} = \frac{1}{x_{nl}}\left(\theta_n^{Rt} - \theta_l^{Rt}\right),\ \forall n\in R, \forall t,\ \forall R \tag{3.4}$$

$$\theta_1^{Rt} = 0,\ \forall t \text{ but only for the reference region} \tag{3.5}$$

$$0 \le LNS_n^{Rt} \le D_n^{Rt}, \forall n\in R,\ \forall t, \forall R \tag{3.6}$$

$$\left|\frac{1}{x_{nk}}\left(\theta_n^{Rt} - \theta_k^{Rt}\right)\right| \le f_{nk}^{\max},\ \forall (n,k)\in L^R,\ \forall t, \forall R \tag{3.7}$$

$$\left|\frac{1}{x_{nl}}\left(\theta_n^{Rt} - \theta_l^{Rt}\right)\right| \le f_{nl}^{\max},\ \forall (n,l)\in L_{tie}^R,\ \forall t, \forall R \tag{3.8}$$

Constraints (3.3) and (3.4) compute the power flow on internal lines $Flow_{nk}$ and tie-lines $Flow_{nl}$ as a function of the reactance x_{nk} of line between buses n and k, and $\left(\theta_n^{Rt} - \theta_l^{Rt}\right)$, the phase angle difference between the two end buses of the line. These equations represent a linearized and lossless model of the power flow (Kirchoff's law). (3.5) enforce $n = 1$ to be the reference node. (3.6) set bound on the amount of load involuntarily shed. (3.7) and (3.8) enforce the transmission capacity limits $f_{nk}^{max} \in L^R$ and $f_{nl}^{max} \in L_{tie}^R$ of the internal lines and the tie-lines of each area, respectively.

–Security constraints:

$$0 \le r^{gt} \le \min(R_{\max^+}^g, \Delta_+^g), \forall g\in CG^R,\ \forall t, \forall R \tag{3.9}$$

$$P^{gt} + r^{gt} \leq u^{gt} \cdot P^{g}_{\max}, \forall g \in CG^{R},\ \forall t, \forall R \tag{3.10}$$

$$r^{t}_{tie} = \min \left[f^{\max}_{nl} - Flow_{nl}, \sum_{g \in CG^{RR}} r^{gt} \right],\ \forall t, \forall R \tag{3.11}$$

$$\sum_{g \in CG^{R}} r^{gt} \geq \beta_1 \cdot \sum_{n} D^{Rt}_{n} + \beta_2 \cdot E_t(X) - \sum_{RR} r^{t}_{tie},\ \forall t, \forall R, \tag{3.12}$$

The shortfall in real power from potential failure of any generator is compensated by spinning reserve. (3.9) defines the amount of spinning reserve carried by each conventional generator, with $R^{g}_{max^{+}}$, the upward spinning reserve capacity limit for unit g, Δ^{g}_{+}, the upward physical ramping limit on unit g and CG^{R}, the set of conventional generators of region R. (3.10) enforce that the power plus the spinning reserve scheduled must be below the capacity P^{g}_{max} of the unit. The total cost (3.1) is influenced by the uncertainty of the WEGs in terms of their EENS values. To quantify the overall possible risks of generation shortfall, a fraction β_2 of the EENS value (due to uncertainty of supply from WEGs) computed in (3.18), and a fraction β_1 of hourly area demand $\sum_{n} D^{Rt}_{n}$ (due to equipment unreliability) are accounted for in (3.12). Although the spinning reserve constraints ensure that neighboring units can provide power-capacity reserve, they do not guarantee that there is transmission capacity available to deploy it. However, constraints (3.11) guarantee that this power-capacity reserve can be deployed. In these constraints, RR is the index over adjacent regions to region R, CG^{RR} the set of conventional generators of region RR, r^{t}_{tie} is the contribution of region RR to the reserve requirement of region R in time t. In order to study the effect of WEGs uncertainty, β_2 is altered and β_1 is kept constant.

$$\begin{aligned} 0 \leq \delta^{gt}_{+} \leq \delta^{g}_{\max^{+}},\ \ \forall g \in R, \forall t, \forall R \\ 0 \leq \delta^{gt}_{-} \leq \delta^{g}_{\max^{-}},\ \forall g \in R, \forall t,\ \forall R \end{aligned} \tag{3.13}$$

$$\begin{aligned} P^{gt} - P^{g(t-1)} \leq \delta^{g(t-1)}_{+},\ \ \forall g \in R, \forall t, \forall R \\ P^{g(t-1)} - P^{gt} \leq \delta^{g(t-1)}_{-},\ \forall g \in R, \forall t,\ \forall R \end{aligned} \tag{3.14}$$

The set of (3.13) and (3.14) are the variable limits and load-following ramp reserve definition. $\delta^{g}_{\max^{+}}$ and $\delta^{g}_{\max^{-}}$ are respectively the upward and downward load-following ramping reserve limits for unit g.

–injection limits and commitments:

$$u^{gt} \cdot P^{g}_{\min} \leq P^{gt} \leq u^{gt} \cdot P^{g}_{\max}, \forall g \in CG^{R},\ \forall t, \forall R \tag{3.15}$$

$$P^{gt} = u^{gt} \cdot P(t), \forall g \in RG^{R},\ \forall t, \forall R \tag{3.16}$$

–startup and shutdown events:

$$u^{gt} - u^{g(t-1)} = v^{gt} - q^{gt}, \forall g \in CG^{R},\ \forall t, \forall R \tag{3.17}$$

–minimum up and down times:

$$\sum_{y=t-\tau^{g}_{+}}^{t} v^{yt} \leq u^{gt}, \forall g \in CG^{R},\ \forall t, \forall R \tag{3.18}$$

$$\sum_{y=t-\tau^{g}_{-}}^{t} q^{gt} \leq 1 - u^{gt}, \forall g \in CG^{R},\ \forall t, \forall R \tag{3.19}$$

–integrality constraints:

$$u^{gt}, v^{gt}, q^{gt} \in \{0,1\}, \forall g \in CG^{R}, \forall t, \forall R \tag{3.20}$$

$$u^{gt} = 1, \forall g \in RG^{R}, \forall t, \forall R \tag{3.21}$$

Constraints (3.15)-(3.21) constitute the UC constraints and represent respectively, the injection limits and commitments, startup and shutdown events, minimum up and down times and integrality constraints. Notice that, a WEG is always turned on (3.21) and its power output limits (3.16) is controlled by the choice made by the optimal algorithm to operate it in any one of the segments. In these constraints, RG^{R} is the set of renewable generators of region R, P^{g}_{min} is the limit on the output power of unit g, τ^{g}_{+} and τ^{g}_{-} are in this order, the minimum up and minimum down times for unit g in number of periods.

The above formulation has a quadratic objective function and the majority of constraints except (3.11) are linear constraints of both equality and inequality types as well as variables of a mixed nature, i.e. real and integer. (3.11) is a nonlinear constraint due to the non-smooth *min* function which argument are state variables. This constraint has been transformed into linear constraints as below,

$$\begin{aligned} r^{t}_{tie} &\leq f^{\max}_{nl} - Flow_{nl},\ \ \forall t, \forall R \\ r^{t}_{tie} &\leq \sum_{g \in CG^{RR}} r^{gt},\ \forall t,\ \forall R. \end{aligned} \tag{3.22}$$

Hence, MIQP technique is used to obtain the solutions.

3.5 Case Studies

The effectiveness of our method is tested on a 6-bus interconnected system, chosen to illustrate key features of the method and demonstrate its benefits but also on the modified IEEE 118-bus and the IEEE-RTS three-area systems, to show how the method performs for larger and more complicated systems with multiple WEGs.

3.5.1 The 6-Bus Test System

In Figure B.1 where the illustrative example is depicted, two identical systems are interconnected through a 150 MW capacity of tie, those of internal lines being all set to 300 MW as shown in Table B.2. The reactances of internals and tie-line are all 0.01 p.u. on a 100 MVA base.

Two demands with the hourly load profile detailed in Table B.1 are located at buses 3 and 6. The generation mix comprises a WEG located at bus 2 with a bidding price of \$0/MWh and an available generation capacity of 200 MW. The forecasted power outputs as stated in Chapter 2 is approximated by a set of probability-weighted scenarios for low, average and high wind realizations. However, transitions between these scenarios are not allowed from period to period. That is, if the system is in the high wind state in the first period, it will stay in the high wind state in every subsequent period, and the same with the average and low wind states as shown in Figure 2.10. The corresponding EENS profile is also drawn in Figure 2.13.

Conventional generating unit data are given in Table B.3 where region 2 generator costs for energy, spinning reserve and load-following ramping reserve are twice those of region 1. In doing so, we force imports on this region. The hourly model over a time period of 4 hours duration allows the shedding of load at the value of \$10,000/MWh if it is economically efficient to do so. Furthermore, all generators are on service at the beginning of the horizon of study and their ramping capabilities are at the largest possible. The data provided so far for this illustrative example defines the base case.

3.5.1.1 Impact of β_2 on the System Reliability and Operating Cost

The first part of our analysis is devoted to the optimal outcomes of the base case, but before this, we earlier assessed the impact of wind uncertainty on the system reliability and on the cost of operation when $\beta_1 = 20\%$ and β_2 is altered. For the purpose hereof, the program chooses to commit more power from the WEG. An increasing trend of both decision variables

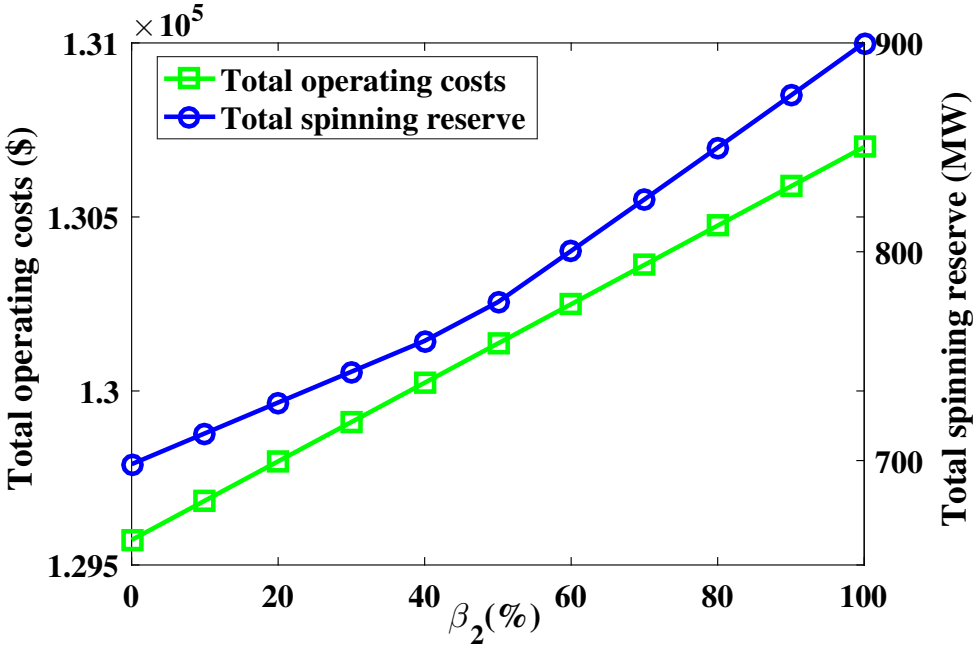

Figure 3.1: Impact of β_2 on system operation cost and spinning reserve.

above are presented in Figure 3.1 as wind power uncertainty increases from 0% to 100% at 10% increments. Indeed, an increased WEG output comes with lower cumulative probability values. This increases the EENS defined in (2.18). From (3.12), system spinning reserve requirement equals a fraction β_1 of hourly area demand to counter any unexpected equipment unreliability, and an additional amount that equals a parameterized value of EENS, in order to account for the uncertainty of supply from WEGs. Hence, as hourly EENS increases, the need for system spinning reserve in (3.12) increases, necessitating the use of quick start units, or short-term market purchases that lead to higher variable costs through increased fuel consumption then, increased operation costs. This is particularly thriving for the values of β_2 above 50% as the rate of change in the total operation cost is faster than the one of the total spinning reserve. If the metric of EENS in risk-averse UC models is easy to calculate and can be included in the bounding constraint, it is based on expected values hence, cannot

tell how risky the scheduled spinning reserve decision may be.

To overcome this limitation, EENS has been factored so that the operator can maintain adequate defensive system posture likely to wind events, while dialing in system reliability. However, in the UC time frame, EENS as defined in our study is a proxy to real time market, so, there is no need to consider its full percentage. For this reason, β_2 has been set to 90% for the rest of this chapter, accordingly with the standards (Robitaille et al., 2012).

3.5.1.2 The 6-bus System Optimal Outcomes

The outcomes related to units scheduling, positive load-following ramping reserve (PLFR), negative load-following ramping reserve (NLFR), spinning reserve allocation and branch power flow of the base case are reported in Tables 3.1 and 3.2, respectively. It is meaningful to point out the effectiveness of our explicit representation and quantification of wind forecast errors into the optimal scheduling program as the model withstands any unforeseen events by deploying spinning reserve and assistance from the other region as defined in (3.11) and (3.12). Indeed, during the entire scheduling horizon and under any scenario, no load shedding or line congestion occurs.

However, the system need for load-following has been found to increase with wind generation. The net load that must be served after accounting for wind has more variability than the load alone. Notice how the output level of conventional generators changes more quickly and turns to a lower level with wind energy in the system. At $t = 2$ when wind generation is typically ramping down, the load is picking up, increasing the need for generating resources to ramp up to meet the increasing electric demand. Conversely, wind production is high at $t = 3$ of minimum load, increasing the need for generating resources that can ramp down. This is due in large part to wind diurnal output, which in many cases may be opposite the peak demand period for electricity. Unfortunately, these changes in the system net load requirements is expected to significantly increase with WEGs penetration to grid and, if incentives are not provided to encourage the needed ramping capabilities, the system is unlikely to get the efficient balance of generation resources as potential reliability degradation or costly out-of-market actions can occur. Therefore, adopting a cycling payment mechanism will not only mitigate the revenue reductions for those conventional generating units (as their output levels

Table 3.1: The 6-bus system optimal scheduling (MWh)

			1st h	2nd h	3rd h	4th h
Area 1	P^{gt}	G1	200	200	196	200
		G2	100	100	100	161
		G3	202	216	0	0
		WEG	88	84	154	164
	δ_{+}^{gt}	G1	0	0	0	4
		G2	0	0	0	61
		G3	0	14	0	0
		WEG	0	0	70	10
	δ_{-}^{gt}	G1	0	0	4	0
		G2	0	0	0	0
		G3	0	0	216	0
		WEG	0	4	0	0
	r^{gt}	G1	0	0	4	0
		G2	100	100	69.22	39
		G3	71.41	145.03	0	0
Area 2	P^{gt}	G4	165	200	85	132.32
		G5	65	200	65	92.68
		G6	60	80	0	0
	δ_{+}^{gt}	G4	0	35	0	47.32
		G5	0	135	0	27.68
		G6	0	20	0	0
	δ_{-}^{gt}	G4	0	0	115	0
		G5	0	0	135	0
		G6	0	0	80	0
	r^{gt}	G4	35	0	100	67.68
		G5	0	0	0	100
		G6	0	0	0	0

Table 3.2: The six-bus test system line power flow (MW)

	L1	L2	L3	L4	L5	L6	Tie-line
1st h	3.33	296.67	293.33	56.67	173.33	116.67	150
2nd h	0	300	300	106.67	293.33	186.67	60
3rd h	47.33	248.67	201.33	50	100	50	150
4th h	65.67	295.33	229.67	75	150	75	150

must be turned to a lower level with WEG in the system), but also compensate the wear and tear costs on these generating equipments resulting from load-following.

Table 3.3: The 6-bus system optimal outcomes comparison

		Area 1	Area 2	System wide
Isolated operation	Total P^{gt}	1,655	1,655	3,310
	Total δ_{+}^{gt}	249	175	424
	Total δ_{-}^{gt}	314	240	554
	Total r^{gt}	500.35	331	831.35
	P^{gt} cost	35,160.26	103,412.50	138,572.76
	δ_{+}^{gt} cost	602	1,560	2,162
	δ_{-}^{gt} cost	1,194	2,160	3,354
	r^{gt} cost	1,391.93	2,210	3,601.93
	Total cost	38,348.19	109,342.50	147,690.69
Interconnected operation	Total P^{gt}	2,165	1,145	3,310
	Total δ_{+}^{gt}	159	265	424
	Total δ_{-}^{gt}	224	330	554
	Total r^{gt}	528.67	302.68	831.35
	P^{gt} cost	52,663.64	69,158.83	121,822.47
	δ_{+}^{gt} cost	336	1,870.72	2,206.72
	δ_{-}^{gt} cost	1,304	2,500	3,804
	r^{gt} cost	2,010.86	1,005.36	3,016.22
	Total cost	56,314.50	74,534.91	130,849.41

The benefits of the interconnection are illustrated in Table 3.3, where we compare the market-clearing results including total generation, total PLFR, total NLFR, total spinning reserve, all in (MW), and total cost of each area in ($), for the isolated (tie-line capacity set to 0 MW) and interconnected (tie-line capacity set to 150 MW) operation cases. The following remarks can be drawn from this table:

- the system's total cost of operation decreases with interconnection.
- The power and spinning reserve requirement of the costly area 2 are partly covered by the green energy and inexpensive generating units in area 1.
- Area 2's contribution to system load-following is more significant.
- Both areas benefit from inter-regional trading: area 2 by buying cheap and area 1 by selling more.
- Though the total operation cost of area 1 has significantly increased between both modes of operation, it is important to underline its contribution to tackling climate change through decarbonization.

3.5.1.3 Impacts of Tie-line Capacity on the System Outcomes

In what follows, we analyze the impact of tie-line capacity on the problem outcomes. For this purpose, the base case is next solved for different tie-line capacities ranging from 0 MW to 375 MW in steps of 75 MW.

Table 3.4: Generating units status versus tie-line capacity

	0*MW*				75*MW*				150*MW*				225*MW*				300*MW*			
t	1	2	3	4	1	2	3	4	1	2	3	4	1	2	3	4	1	2	3	4
G1	●	●	●	●	●	●	●	●	●	●	●	●	●	●	●	●	●	●	●	●
G2	●	●	●	●	●	●	●	●	●	●	●	●	●	●	●	●	●	●	●	●
G3	●	●			●	●			●	●			●	●	●	●	●	●	●	●
G4	●	●	●	●	●	●	●	●	●	●	●	●	●	●	●	●	●	●		●
G5	●	●	●	●	●	●	●	●	●	●	●	●	●	●			●	●		
G6	●	●	●	●	●	●			●	●			●	●			●	●		

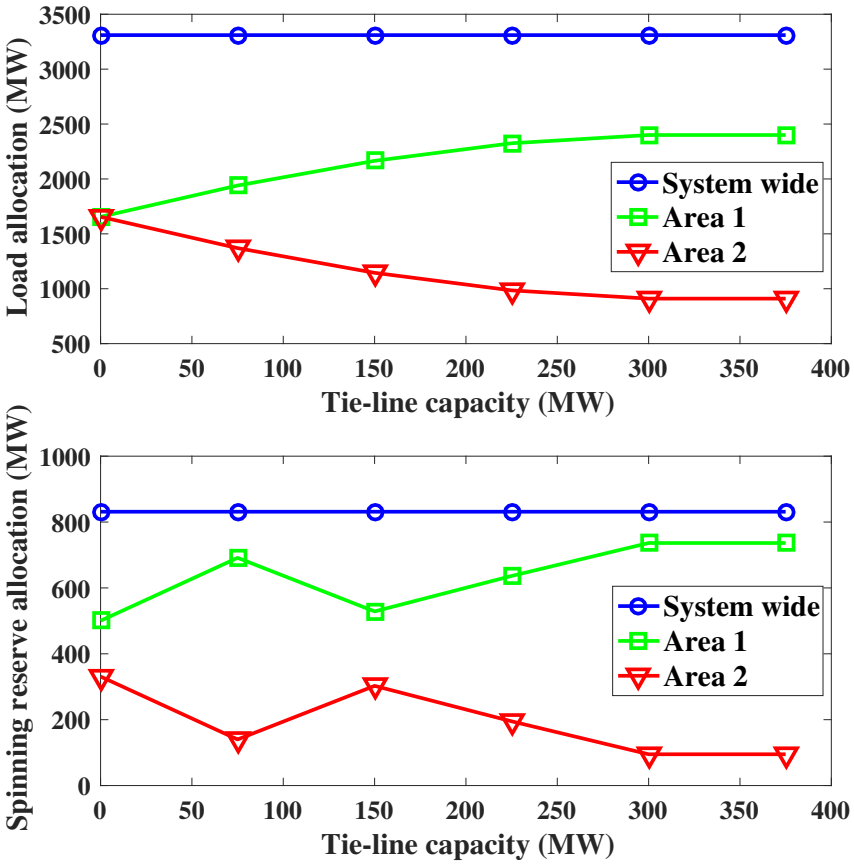

Figure 3.2: Load and spinning reserve allocations versus tie-line capacity.

In Table 3.4 where the black dots indicate the units that are committed, one notices that

increasing the tie-line capacity can have a significant effect on the unit scheduling, as several expensive units will not be scheduled at some time periods.

The evolution of the share of load and spinning reserve allocated for increasing values of the tie-line capacity is depicted in Figure 3.2. By increasing the tie-line capacity, cross border trade of power and spinning reserve rises to more desirable values. Indeed, the portions of imported power and spinning reserve by area 2 increase monotonically as the tie-line capacity increases, making such transactions profitable, as seen in Table 3.3. In Figure 3.3 where the evolution of the sharing of PLFR and NLFR are depicted, contribution of area 1 to load-

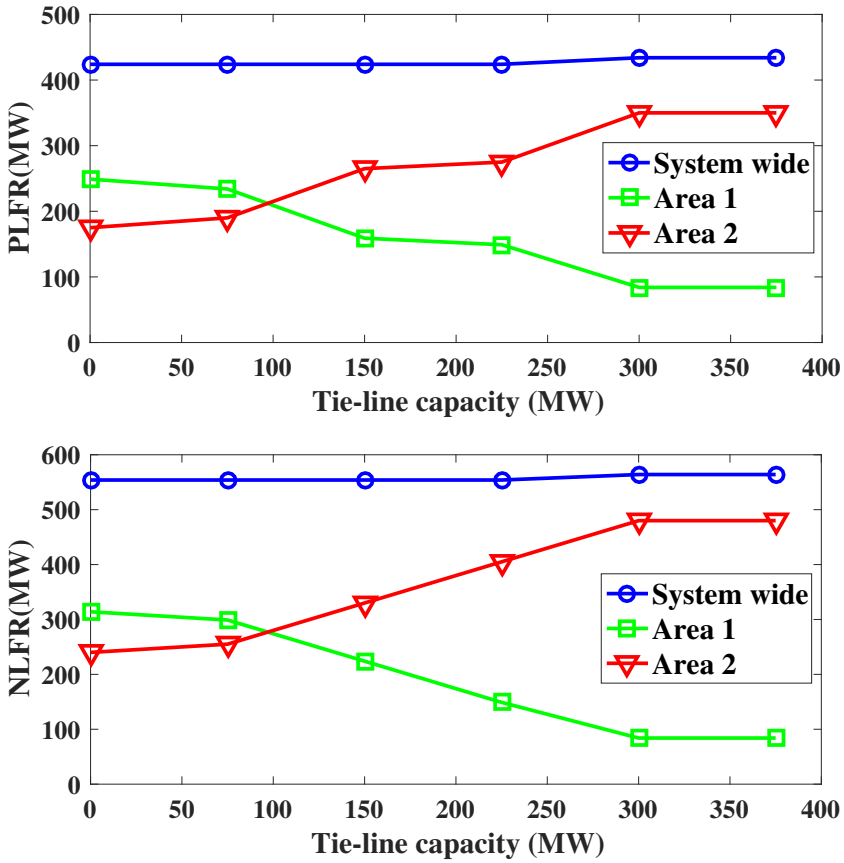

Figure 3.3: PLFR and NLFR allocations versus tie-line capacity.

following is higher for smaller tie-line capacity values, however, for a value of 100 MW and above, area 2 contribution to system frequency restoration is more significant. Quantitatively, it can be inferred from Figures 3.2 and 3.3 that most of the load-following ramping reserve is allocated to area 2 while area 1 covers most of the interconnected system load and spinning reserve as tie-line capacity evolves. Nonetheless, for a tie-line capacity of 300 MW and above,

cross-border exchanges of power and reserve do not change any more.

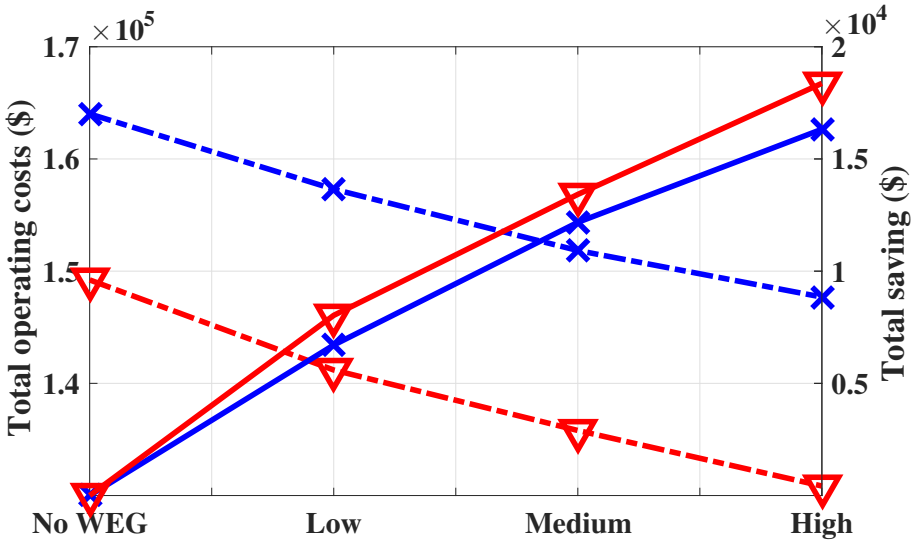

Figure 3.4: Impact of wind scenario on system operating cost and saving.

If the interconnection of electricity grids appear in the above analysis as a promising solution achieving both cost-efficiency and system reliability, it definitely emerges as a good means to spur the widespread deployment of WEGs into power systems. Indeed, in Figure 3.4, we have drawn the system operating cost in dash-dot lines and the system saving (defined as the change in the system's total operating cost compared to its reference value, i.e., when there is no WEG in the system) in solid lines. The comparison of these two quantities with respect to wind power realizations for both isolated and interconnected operations represented by the cross and the downward-pointing triangle markers respectively, reveal that adding wind power to the system has not only considerably lowered the operating cost and increased saving, but also, the system starts to accumulate profit at a lower level of wind penetration when interconnected, while the break-even point for the isolated operation is reached at medium wind realization.

3.5.2 The 118-Bus Test System

To illustrate the effectiveness of the proposed model for practical power systems, a modified IEEE 118 bus system shown in Figure B.5 is considered over a 24 hour study period. This system with 54 conventional generators, 186 transmission lines (174 internal lines and 12 tie-lines), 9 tap-changing transformers, and 91 demand sides is divided into three areas, and here

we take each area as a regional power grid. WEGs #1, #2 and #3 which capacity in the same order are 300 MW, 300 MW and 200 MW, are added to the system, all in area 2 at buses 80, 69 and 59, respectively. Wind power and EENS profiles can be seen in Figures 3.11 and 3.14.

The system data are given at http://www.motor.ece.iit.edu/data/SCUC_118test.xls. The peak load of the interconnected system is 6,000 MW and occurs at hour 21. Each conventional unit offers spinning reserve and load-following ramping reserve at a price equal to 10% of the coefficient b of its cost function. To force cross-border trading, the cost of units in areas 1 and 3 for both energy and reserves are assumed to be twice those of units in area 2. The value of lost load for all demands is assumed to be 10,000 \$/MWh and $\beta_1 = 5\%$. Below are our findings when the program chooses to operate WEGs at lower cumulative probability segments with higher outputs.

Firstly, the solution to the case of isolated operation with a system total cost of \$2,335,694.00 is obtained. The solving time is 280.30 seconds. Economic units of each area are used as base units, some other units are committed accordingly to satisfy hourly load demands while the remaining units are not committed at all as reported in Table 3.5. Interconnecting the 3 power grids has significant effects on the unit scheduling of the whole system. Indeed, from Table 3.6, one can notice that several expensive units of areas 1 and 3 are shutdown throughout the day, while more cheaper units from area 2 are brought online. As a result, the total system cost is driven down to \$1,937,926.08 saving the solving time by 196.37 seconds. Compared to the adjustable interval stochastic model of (Doostizadeh et al., 2016) which CPU time is 878.0 seconds, our approach is less time consuming.

From Table 3.7 where the benefits of interconnection are illustrated, it is observed that areas 1 and 3 being incrementally the expensive, keep less share of their power production (respectively 59.03% and 46.24% of their own load) for the 24 h. Accordingly, area 2 serves part of the loads of these areas. On the other hand, 3.43% of area 1 spinning reserve requirement is allocated to areas 2 and 3. This can be attributed to the facts that - area 3 keeps the lowest share of power production. Therefore, it has more available resources for spinning reserve provision than others, reason why it has kept 9.48% of its load for system reliability, that is 9.48% above its area requirement; - area 2 being the cheapest area, has more available resources to supply spinning reserve at a lower cost even if its requirement is the highest.

Table 3.5: Generating unit status in isolated operation

	t	1	2	3	4	5	6	7	8	9	10	11	12	13	14	15	16	17	18	19	20	21	22	23	24
Area 1 generators	1																					•			
	2,3																								
	4,5	•	•	•	•	•	•	•	•	•	•	•	•	•	•	•	•	•	•	•	•	•	•	•	•
	6																								
	7	•	•						•	•	•	•	•	•	•	•	•	•	•	•	•	•	•	•	•
	8																								
	9										•	•				•	•		•	•	•	•			
	10,11	•	•	•	•	•	•	•	•	•	•	•	•	•	•	•	•	•	•	•	•	•	•	•	•
	12,13																								
	14	•						•	•	•	•	•	•	•	•	•	•	•	•	•	•	•	•	•	•
	30	•	•					•	•	•	•	•	•	•	•	•	•	•	•	•	•	•	•	•	•
	31																				•	•			
	32																			•	•	•	•		
	33																								
	53							•	•	•	•	•	•	•	•	•	•	•	•	•	•	•	•	•	•
Area 2 generators	15-19																								
	20,21	•	•	•	•	•	•	•	•	•	•	•	•	•	•	•	•	•	•	•	•	•	•	•	•
	22,23																								
	24,25	•	•	•	•	•	•	•	•	•	•	•	•	•	•	•	•	•	•	•	•	•	•	•	•
	26																								
	27-29	•	•	•	•	•	•	•	•	•	•	•	•	•	•	•	•	•	•	•	•	•	•	•	•
	34,35																								
	36									•	•	•	•	•	•	•	•	•	•	•	•	•	•	•	•
	44	•	•	•	•	•	•	•	•	•	•	•	•	•	•	•	•	•	•	•	•	•	•	•	•
	54																								
Area 3 generators	37,38																								
	39	•	•	•	•	•	•	•	•	•	•	•	•	•	•	•	•	•	•	•	•	•	•	•	•
	40									•	•	•	•	•	•	•	•	•	•	•	•	•	•	•	•
	41,42																								
	43	•	•	•	•	•	•	•	•	•	•	•	•	•	•	•	•	•	•	•	•	•	•	•	•
	45	•	•	•	•	•	•	•	•	•	•	•	•	•	•	•	•	•	•	•	•	•	•	•	•
	46-52																								

Table 3.6: Generating unit status in interconnected operation

	t	1	2	3	4	5	6	7	8	9	10	11	12	13	14	15	16	17	18	19	20	21	22	23	24
Area 1 generators	1-3																								
	4,5	•	•	•	•	•	•	•	•	•	•	•	•	•	•	•	•	•	•	•	•	•	•	•	•
	6-9																								
	10									•	•	•	•	•	•	•	•	•	•	•	•	•	•	•	•
	11	•	•	•	•	•	•	•	•	•	•	•	•	•	•	•	•	•	•	•	•	•	•	•	•
	12,13																								
	14																•	•	•	•	•	•	•		
	30-33																								
	53																								
Area 2 generators	15																								
	16							•	•	•	•	•	•	•	•	•	•	•	•	•	•	•	•	•	•
	17,18																								
	19	•	•						•	•	•	•	•	•	•	•	•	•	•	•	•	•	•	•	•
	20,21	•	•	•	•	•	•	•	•	•	•	•	•	•	•	•	•	•	•	•	•	•	•	•	•
	22							•	•	•	•	•	•	•	•	•	•	•	•	•	•	•	•	•	•
	23	•	•						•	•	•	•	•	•	•	•	•	•	•	•	•	•	•	•	•
	24,25	•	•	•	•	•	•	•	•	•	•	•	•	•	•	•	•	•	•	•	•	•	•	•	•
	26							•	•	•	•	•	•	•	•	•	•	•	•	•	•	•	•	•	•
	27-29	•	•	•	•	•	•	•	•	•	•	•	•	•	•	•	•	•	•	•	•	•	•	•	•
	34	•	•	•	•	•	•	•	•	•	•	•	•	•	•	•	•	•	•	•	•	•	•	•	•
	35	•	•						•	•	•	•	•	•	•	•	•	•	•	•	•	•	•	•	•
	36	•	•	•	•	•	•	•	•	•	•	•	•	•	•	•	•	•	•	•	•	•	•	•	•
	44	•	•	•	•	•	•	•	•	•	•	•	•	•	•	•	•	•	•	•	•	•	•	•	•
	54																		•	•	•	•			
Area 3 generators	37,38																								
	39	•	•	•	•	•	•	•	•	•	•	•	•	•	•	•	•	•	•	•	•	•	•	•	•
	40-42																								
	43																			•	•	•	•	•	•
	45									•	•	•	•	•	•	•	•	•	•	•	•	•	•	•	•
	46-52																								

Table 3.7: The 118-bus system optimal outcomes comparison

		Area 1	Area 2	Area 3	System wide
Isolated operation	Total P^{gt}	34,949	56,042	22,648	113,640
	Total δ_{+}^{gt}	1,439.30	4,633.80	1,034.90	7,108
	Total δ_{-}^{gt}	1,217.90	4,278.80	891.40	6,388
	Total r^{gt}	1,747.50	6,782	1,132.40	9,661.90
	P^{gt} cost	1,096,867.54	593,338.43	614,408.04	2,304,614.01
	δ_{+}^{gt} cost	4,282.70	2,610.50	2,573.10	9,466.30
	δ_{-}^{gt} cost	3,535.10	1,723.40	2,203.20	7,461.80
	r^{gt} cost	4,767.70	6,947.30	2,436.90	14,152
	Total cost	1,109,453	604,619.69	621,621.30	2,335,694
Interconnected operation	Total P^{gt}	20,632	82,535	10,473	113,640
	Total δ_{+}^{gt}	1,102.30	4,772.40	901.81	6,776.50
	Total δ_{-}^{gt}	907.52	4,517.10	631.85	6,056.50
	Total r^{gt}	550.60	6,964.40	2,146.90	9,661.90
	P^{gt} cost	575,923.43	1,070,028.14	262,458.77	1,908,410.34
	δ_{+}^{gt} cost	2,806.85	3,437.68	2,107.03	8,351.56
	δ_{-}^{gt} cost	2,304.89	2,393.92	1,440.96	6,139.77
	r^{gt} cost	1,419.18	8,985.17	4,620.07	15,024.42
	Total cost	582,454.35	1,084,844.90	270,626.83	1,937,926.08

The effect of load-following on base load units in the presence of wind uncertainty is illustrated in Figure 3.5, where a change in the output of unit 27 from period to period can initially be observed in isolated operations thereafter when expansion access to the resources of areas 1 and 3 is achieved. In the first case, the generating unit ramps frequently in order to coordinate the additional load-following due to wind power variability. Fortunately, by spreading variability across more units, this ramping duty on unit 27 decreases substantially with corresponding price implications. So, having a large pool of generation is advantageous. While it is true that generators have to ramp to provide energy, that does not mean that the cost of ramping must be recovered from energy sales. In the present study, the solution regardless ramping charge with the total operation costs of \$2,318,530.12 and \$1,922,466.19 for both operation modes, do not reflect the marginal cost of producing electricity. So, ignoring ramping costs in the price-setting mechanism inevitably results in pecuniary damage for those generating units suited in supplying the needed function of maintaining the system balance.

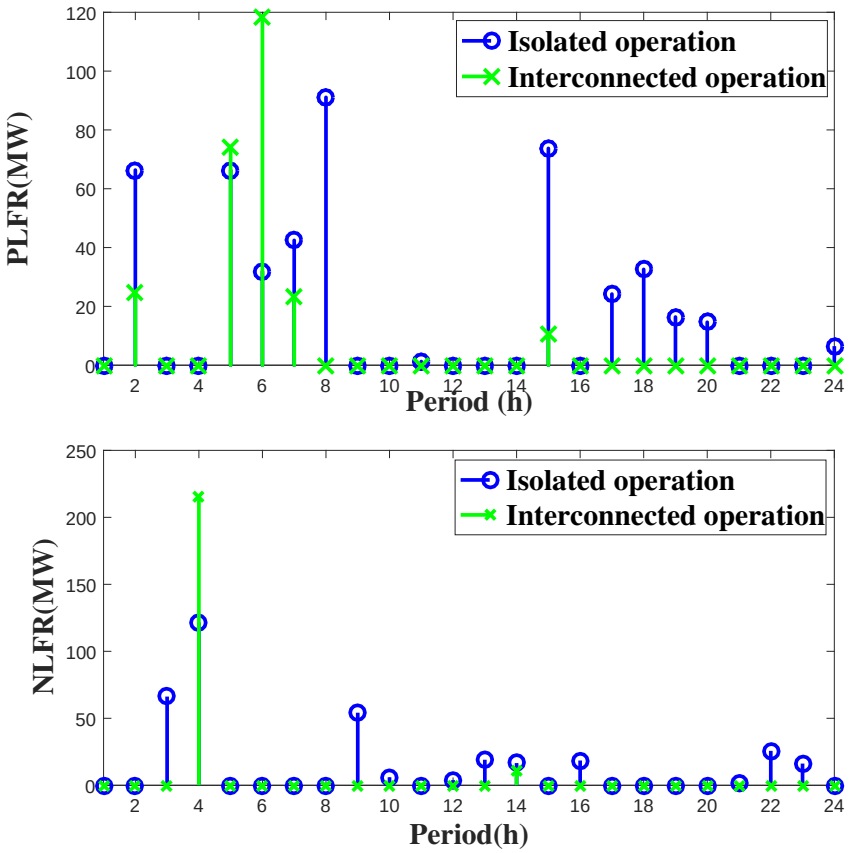

Figure 3.5: Shift in unit 27 output as a result of load-following.

3.5.3 The IEEE-RTS Test System

The results on the 118-bus case study as presented in the previous section show how wind power impacts base load units as well as the benefits of interconnection in reducing the ramping duty on these generating equipments. The IEEE-RTS (Grigg et al., 1999) reliability system is hereby used to analyze the variability that WEGs add to electricity supply in the context of overall system variability. For the purpose hereof, we determine the change in the hourly load-following requirements that are imposed by different penetration rates of WEGs. Three wind plant configurations that represent different penetration levels are considered:

1- no WEG;

2- WEGs #1, #2 and #3 having a 100 MW each and finally the configuration used for the 118-bus system, i.e.;

3- WEGs #1, #2 and #3 which capacity in the same order are 300 MW, 300 MW and 200 MW with corresponding profile Wind power and EENS profiles in Figures 3.11 and 3.14.

The considered test system is presented in Appendix B.2. It comprises 72-bus and 3-area as illustrated in Figure B.4. Unit technical data including units group, number of units, location node, units fuel type, the maximum and minimum power outputs and the coefficients of input-output function of units are given in Table B.6. Note that the unit fuel cost function is derived from multiplying the input-output function by the fuel marginal cost data of generating units as listed in Table B.9. Each generating unit offers the maximum possible up/down reserve at a price equal to the coefficient b of its fuel cost function. The hourly demand data correspond to the Thursday of winter week 45 with a peak load of 2850 MW for each area (8550 MW for the 3-area system) which are indicated in Table B.11. The value of lost load of all demands is assumed to be 1000 \$/MWh and $\beta_1 = 5\%$. WEGs #1, #2 and #3 are added to the system, all in area 2 at buses 25, 33 and 37, respectively.

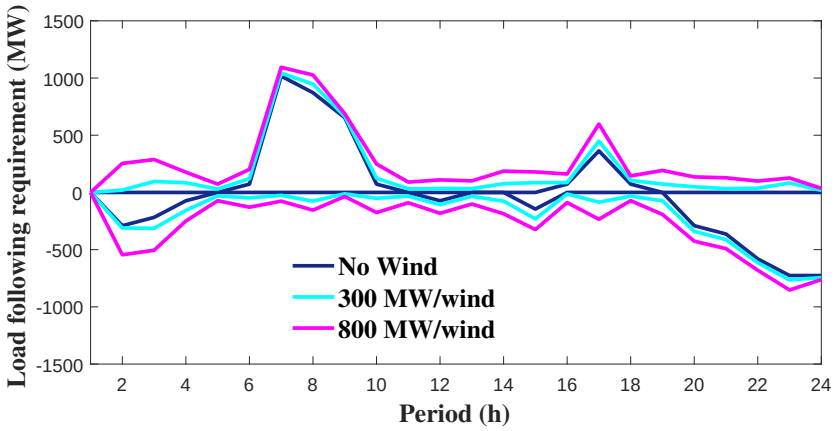

Figure 3.6: Comparison of system load following with/without wind.

The analysis is done over a 24-hour scheduling period and the results show that although load forecasts are generally more accurate than wind forecasts, they are also imperfect. In Figure 3.6 where the overall system load-following requirements are represented for different penetration levels, one can notice that the magnitude of load-following requirements increases nonlinearly with wind penetration. However, there can be relatively large differences in load-following requirements between the wind and no-wind cases. At other times, there is a small difference.

To get a better idea of the load-following impact, a statistical distribution of the load-following requirements over the 24-hour horizon of study is represented in Figure 3.7. From this distribution, we can observe that the frequency of small ramps (at or near zero) declines when wind

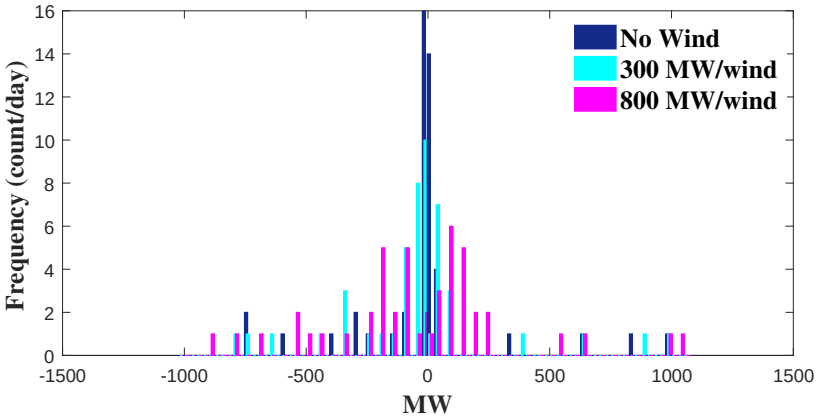

Figure 3.7: Statistical distribution of load following requirements.

is added to the system. Although it is hard to see in the diagram, the tails of the distribution are a little wider as a result.

3.6 Conclusion

This chapter presents a methodology to investigate various effects of grid integration on the reduction of the overall operation costs associated with more wind power in interconnected multi-area power systems. The numerical simulations conducted have led to the following conclusions:

-Although extra spinning reserve need to be borne by a system proportionate to the output power from WEGs, it is always profitable in terms of total operating costs to maximize output from WEGs.

-Spreading variability across more units is advantageous as large pools of generation substantially decrease the jerkings around these units and, lessen the costs imposed on the power system for accommodating WEGs.

-Adopting ramping charge can improve the performance of electricity markets from both the point of views of the plant owner and SOs. This compensation can be used to reverse the ageing effect on a plant over time, and help to maintain profitable operations in the long term.

Chapter 4

Reserve Allocation with Equipment Failure and Wind Uncertainty

Résumé

"La non-inclusion de la défaillance stochastique des composants du réseau dans la formulation du model proposé au chapitre 3 constitue son principal inconvénient. Ce chapitre propose une méthode stochastique pour l'évaluation de notre modèle hybride. Celle-ci incorpore de façon explicite, l'incertitude éolienne et le risque de perte des composants du réseau, en utilisant des probabilités qui reflètent relativement les différents états du système. Les critères de la réserve d'exploitation tels que élaborés en pratique ont été simulés. Une comparaison des résultats provenants des deux approches nous a permis d'ajuster le caractère conservatif de notre modèle hybride, en variant la quantité de réserve nécessaire pour une opération sécuritaire et à coût raisonnable."

Abstract

"The non-inclusion of the failure rate of the grid's components in the model for setting reserve requirement formulated in chapter 3 has been the main drawback. This chapter proposes a stochastic method to benchmark our proposed hybrid model. A combined SCUC and OPF that explicitly includes wind uncertainty

and contingencies by means of probabilities reflecting the relative likelihood of the different states of the system occurring has been devised. We simulate reserve criteria following practices in real-world operations. A comparison of results from both approaches allows us to refine the performance of our hybrid model, by varying its conservativeness with the help of the scaling factor in order to dial in the amount of spinning reserve due to equipment unreliability."

4.1 Introduction

Optimal procurement of reserves can improve reliability and economic efficiency in power systems. With increasing penetration of WEGs, this optimal allocation is becoming even more crucial. Chapter 3 proposes an improved deterministic approach (referred to as hybrid model) that accounts for the stochastic feature of the wind through an extra adjustable amount of the EENS. While being suited to strategically accommodate WEGs in the short-term operation of power grids, this approach is insensitive to factors that significantly influence system reliability, such as the failure rates of components in the grid. Indeed, the spinning reserve constraints as formulated are typically used only for cases with a single base scenario with no contingencies, that is, when $\mathscr{W}^t = \{1\}$ and $\mathscr{C}^{tw} = \{0\}$.

This chapter proposes a model to enable the study of the optimal procurement of energy and reserves which explicitly includes wind uncertainty along with contingencies, using probabilities that reflect the relative likelihood of the different states of the system occurring. In this way, the amounts of operating reserves (e.g., contingency reserve and ramping reserve to mitigate equipment failure and wind variability, respectively) needed to meet the load profiles and maintain the reliability of the delivery system are locational and endogenously determined as a function of the uncertainties in the system conditions. This model is a potential means of improving the economic efficiency of interconnected power systems. However, the aim is to evaluate the effectiveness of the proposed hybrid tool of chapter 3 to withstand disturbances and adjust its price signal and market impact through a comparative cost analysis of the two models.

4.2 Chapter Contribution

Two main contributions are made in this chapter.

• The first is an optimal dispatch of a power system, giving a set of credible contingencies and a characterization of the uncertainty coming from WEGs. We have defined upward and downward contingency reserves as the maximum deviation from a contracted reference output required to cover each of the system states, including the contingencies illustrated in Figure 2.15.

• The second contribution considered the findings of the proposed model (stochastic) as the benchmark to the hybrid model, to refine the outcomes of the latter. Indeed, manually removing a line or generator by setting it's status to zero allows a contingency study of the hybrid model, while dividing the shadow prices on the power balance and flow limits constraints of the stochastic model by the probability of the corresponding scenario (base case or contingency), one obtains the scenario specific price. A comparison of costs incurred, load shed, and commitment schedules of both models can easily be done as the scenario specific price of the stochastic model has a corresponding single hybrid counterpart.

4.3 Chapter Organization

This chapter is structured as follows. Section 4 provides the formulation of the proposed model. Section 5 reports on the simulation results from the comparative studies of the hybrid and stochastic models. Conclusions are drawn in Section 6.

4.4 The Proposed Model Formulation

Considering the following optimization variables P_c^{gt}, P^{gtwc}, P_+^{gtwc}, P_-^{gtwc}, u^{gt}, v^{gt}, q^{gt}, r_+^{gt}, r_-^{gt}, δ_+^{gt}, δ_-^{gt}, LNS_n^{Rtwc}, θ_n^{Rtwc}, for $\forall t$, $\forall w$, $\forall c$, $\forall R$, $\forall n$, $\forall g$, the objective function to minimize is the expected

$$\min_{\mathscr{X}} \quad \sum_{R} \sum_{t \in \mathscr{T}} \left\{ \rho^t \sum_{g \in \mathscr{G}^{Rt}} \left[a_g \cdot u^{gt} + S_{on}^g \cdot v^{gt} + S_{off}^g \cdot q^{gt} \right] \right.$$

$$+\sum_{w\in\mathscr{W}^t}\sum_{c\in\mathscr{C}^{tw}}\pi^{twc}\sum_{g\in\mathscr{G}^{Rtwc}}\left[c_g\cdot(P^{gtwc})^2+b_g\cdot P^{gtwc}+f_{g_+}\cdot P_+^{gtwc}+f_{g_-}\cdot P_-^{gtwc}\right]$$

$$+\rho^t\sum_{g\in\mathscr{G}^{Rt}}\left[d_{g_+}\cdot r_+^{gt}+d_{g_-}\cdot r_-^{gt}\right]$$

$$+\rho^t\sum_{g\in\mathscr{G}^{Rt}}\left[e_{g_+}\cdot \delta_+^{gt}+e_{g_-}\cdot \delta_-^{gt}\right]$$

$$+\sum_{w\in\mathscr{W}^t}\sum_{c\in\mathscr{C}^{tw}}\pi^{twc}\sum_{n\in\mathscr{D}^{Rtwc}}VOLL\cdot LNS_n^{Rtwc}\Bigg\} \tag{4.1a}$$

subject to
$$\sum_{g\in\mathscr{C}\mathscr{G}_n^{Rtwc}}P^{gtwc}+\sum_{g\in\mathscr{R}\mathscr{G}_n^{Rtwc}}P^{gtwc}+LNS_n^{Rtwc}=D_n^{Rtwc}+\sum_{k\in\Phi_{nk}^R}\frac{1}{x_{nk}}\left(\theta_n^{Rtwc}-\theta_k^{Rtwc}\right)$$
$$+\sum_{l\in\Gamma_{nl}^R}\frac{1}{x_{nl}}\left(\theta_n^{Rtwc}-\theta_l^{Rtwc}\right),\ \forall n\in R,\forall t,\ \forall R,\forall c,\forall w, \tag{4.1b}$$

$$\theta_1^{Rtwc}=0,\ \forall t,\forall c,\forall w \text{ but only for the reference region,} \tag{4.1c}$$

$$0\le LNS_n^{Rtwc}\le D_n^{Rtwc},\ \forall n\in R,\ \forall t,\forall R,\forall c,\forall w, \tag{4.1d}$$

$$\left|\frac{1}{x_{nk}}\left(\theta_n^{Rtwc}-\theta_k^{Rtwc}\right)\right|\le f_{nk}^{\max},\ \forall(n,k)\in L^R,\ \forall t,\forall R,\forall c,\forall w, \tag{4.1e}$$

$$\left|\frac{1}{x_{nl}}\left(\theta_n^{Rtwc}-\theta_l^{Rtwc}\right)\right|\le f_{nl}^{\max},\ \forall(n,l)\in L_{tie}^R,\ \forall t,\forall R,\forall c,\forall w, \tag{4.1f}$$

$$0\le P_+^{gtwc}\le r_+^{gt}\le R_{\max^+}^g,\ \forall g\in\mathscr{C}\mathscr{G}^{Rt},\forall t,\forall R,\forall c,\forall w, \tag{4.1g}$$

$$0\le P_-^{gtwc}\le r_-^{gt}\le R_{\max^-}^g,\ \forall g\in\mathscr{C}\mathscr{G}^{Rt},\forall t,\forall R,\forall c,\forall w, \tag{4.1h}$$

$$P^{gtwc}-P_c^{gt}=P_+^{gtwc}-P_-^{gtwc},\ \forall g\in\mathscr{C}\mathscr{G}^{Rt},\forall t,\forall R,\forall c,\forall w, \tag{4.1i}$$

$$-\Delta_-^g\le P^{gtwc}-P^{gtw0}\le\Delta_+^g,\ \forall g\in\mathscr{C}\mathscr{G}^{Rt},\forall t,\forall R,c\ne 0,\forall w, \tag{4.1j}$$

$$0\le\delta_+^{gt}\le\delta_{\max^+}^g,\ \forall g\in R,\forall t,\forall R, \tag{4.1k}$$

$$0\le\delta_-^{gt}\le\delta_{\max^-}^g,\ \forall g\in R,\forall t,\ \forall R, \tag{4.1l}$$

$$P^{gtw_20}-P^{g(t-1)w_10}\le\delta_+^{g(t-1)},\ \forall g\in R,\forall t,w_1\in\mathscr{W}^{t-1},w_2\in\mathscr{W}^t, \tag{4.1m}$$

$$P^{g(t-1)w_10}-P^{gtw_20}\le\delta_-^{g(t-1)},\ \forall g\in R,\forall t,w_1\in\mathscr{W}^{t-1},w_2\in\mathscr{W}^t, \tag{4.1n}$$

$$u^{gt}\cdot P_{\min}^g\le P^{gtwc}\le u^{gt}\cdot P_{\max}^g,\ \forall g\in\mathscr{C}\mathscr{G}^{Rt},\ \forall t,\forall R,\forall c,\forall w, \tag{4.1o}$$

$$P^{gtwc}=u^{gt}\cdot P(t),\ \forall g\in\mathscr{R}\mathscr{G}^{Rt},\ \forall t,\forall R,\forall c,\forall w,\ \forall t,\forall R,\forall c,\forall w, \tag{4.1p}$$

$$u^{gt}-u^{g(t-1)}=v^{gt}-q^{gt},\ \forall g\in\mathscr{C}\mathscr{G}^{Rt},\ \forall t,\forall R, \tag{4.1q}$$

$$\sum_{y=t-\tau_+^g}^{t}v^{yt}\le u^{gt},\ \forall g\in\mathscr{C}\mathscr{G}^{Rt},\ \forall t,\forall R, \tag{4.1r}$$

$$\sum_{y=t-\tau_-^g}^{t}q^{gt}\le 1-u^{gt},\ \forall g\in\mathscr{C}\mathscr{G}^{Rt},\ \forall t,\forall R, \tag{4.1s}$$

$$u^{gt}, v^{gt}, q^{gt} \in \{0,1\},\ \forall g \in \mathscr{CG}^{Rt}, \forall t, \forall R, \tag{4.1t}$$

$$u^{gt} = 1,\ \forall g \in \mathscr{RG}^{Rt}, \forall t, \forall R, \tag{4.1u}$$

cost with five sub-components corresponding to the five rows of (4.1a). Row one includes the no load, startup and shutdown costs, a_g, S^g_{on} and S^g_{off}, respectively, u^{gt}, v^{gt} and q^{gt} are the commitment, startup and shutdown states, in the same order. As stated in chapter 2, while extending the problem to multiple periods, the number of possible states explode due to path dependence. Treating each trajectory as a scenario requires too many trajectories to capture the range of possible outcomes in each period. To avoid an exponential growth of scenarios that could make the problem intractable, the approach is to enforce the feasibility of a central path or operating point envelope the high probability path defined by the set of base scenarios. Therefore, the probabilistic weighting ρ^t in row one of (4.1a), is the probability of reaching period t, i.e., the probability of making it to period t without branching off the operating point envelope in a contingency in periods $1 \cdots t-1$. In doing so, the computational cost is reasonable. Row two is the expected cost of active power dispatch and redispatch, with c_g, b_g the quadratic and linear fuel cost coefficients, respectively; f_{g_+}, f_{g_-} the costs for upward and downward deviations from active power contract quantity for unit g, in the same order; P^{gtwc} the active injection for unit g in post-contingency state c of scenario w at time t and P^{gtwc}_+, P^{gtwc}_- the upward and downward deviation from active contract quantity for unit g in post-contingency state c of scenario w at time t, respectively. The coefficient π^{twc} represents the probability of contingency c occurring in scenario w at time t. d_{g_+}, d_{g_-} in row three are the costs for upward and downward contingency reserve purchase from unit g, respectively. Generators incur significant costs when changing output, and these costs are expected to rise with WEGs penetration to grid due to the rapid and frequent ramping they impose on conventional units. These costs are reflected in our model in row four where for every MW of ramp, up δ^{gt}_+ or down δ^{gt}_-, efficiency costs of e_{g_+} and e_{g_-} in the same order, are incurred. *VOLL* in row five is the cost incurred in shedding load LNS^{Rtwc}_n at bus n of region R in contingency c of scenario w at period t during real-time operation.

In the power balance equations (4.1b) k,l=1 to N^R_b are indices of buses/loads of region R. D^{Rtwc}_n is the demand at bus n of region R in contingency state c of scenario w at time t. $\mathscr{CG}^{Rtwc}_n$ and $\mathscr{RG}^{Rtwc}_n$ are respectively the sets of conventional and renewable generators located at bus n of region R in contingency state c of scenario w at time t. Φ^R_{nk} is the set of buses adjacent to bus

n, all in region R. Γ_{nl}^{R} is the set of buses of adjacent regions to region R, all connected to bus n of region R. $\frac{1}{x_{nk}}\left(\theta_n^{Rtwc}-\theta_k^{Rtwc}\right)$ and $\frac{1}{x_{nl}}\left(\theta_n^{Rtwc}-\theta_l^{Rtwc}\right)$ compute the power flow on internal lines and tie-lines, respectively, as a function of the reactance x_{nk}, x_{nl} of line between buses n, k and n, l. $\left(\theta_n^{Rtwc}-\theta_l^{Rtwc}\right)$ is the phase angle difference between the two end buses n, l of the line in contingency state c of scenario w at time t. (4.1c) enforce $n=1$ to be the reference node. (4.1d) sets bound on the amount of load involuntarily shed at bus n of region R in contingency state c of scenario w at time t. (4.1e) and (4.1f) enforce the transmission capacity limits $f_{nk}^{max} \in L^R$ and $f_{nl}^{max} \in L_{tie}^{R}$ of the internal lines and the tie-lines of each area, respectively.

(4.1g)-(4.1i) and (4.1j) are the reserve, redispatch, contract variables and ramping limits on transitions from the base to contingency case constraints. In these constraints, r_{+}^{gt}, r_{-}^{gt} are the upward and downward active contingency reserve provided by unit g in time t; P_{+}^{gtwc}, P_{-}^{gtwc} the upward and downward deviation from active contract quantity for unit g in post-contingency state c of scenario w at time t; $R_{max^{+}}^{g}$, $R_{max^{-}}^{g}$ and Δ_{+}^{g}, Δ_{-}^{g} the upward and downward spinning reserve capacity limit and physical ramping limit for unit g; $\mathscr{CG}^{Rt}$ is the set of conventional generators of region R in time t.

(4.1k),(4.1l) and (4.1m),(4.1n) are the variable limits and load-following ramp reserve definition. $\delta_{\max^{+}}^{g}$ and $\delta_{\max^{-}}^{g}$ are respectively the upward and downward load-following ramping reserve limits for unit g.

(4.1o)-(4.1u) constitute the UC constraints and represent, the injection limits and commitments respectively, startup and shutdown events, minimum up and down times and integrality constraints. Notice that a WEG is always turned on (4.1u) and its power output limits (4.1p) is controlled by the choice made by the optimal algorithm to operate it in any one of the segments. In these constraints, $\mathscr{RG}^{Rt}$ is the set of renewable generators of region R in time t, P_{min}^{g} is the limit on the output power of unit g, τ_{+}^{g} and τ_{-}^{g} are in this order, the minimum up and minimum down times for unit g in number of periods.

The above formulation has quadratic objective function and linear constraints of both equality and inequality types as well as variables of a mixed nature, i.e. real and integer. Hence, MIQP technique is used to obtain the solutions.

4.5 Simulation Results

Numerical simulations were conducted with a 6-bus interconnected system in Figure B.1 and 118-bus networks in Figure B.5 in order to compare the results of the day-ahead and real-time problems, for both hybrid and stochastic reserves as formulated in Chapter 3 and this chapter, respectively. The metrics for comparison include amount and cost of reserve allocations, overall cost of serving load, and avoidance of load shedding scenarios.

4.5.1 The 6-Bus Test System

4.5.1.1 The DAM Settlement of Chapter 3's Schedules

DAM settlements for energy and operating reserve are both based on day ahead schedules. Several reasons explain the need for the existence of the DAM in the liberalized electricity industry. It is an efficient way of improving operational certainty for SOs as real-time approaches. It contributes the improvement of financial certainty for dispatchable resources and it is used to establish a hedge against price volatility caused by changes in supply and demand in the real-time market.

The settlement of the day-ahead schedule as set up in chapter 3 is hereby presented and analyzed. The market clearing results including the optimal allocation and pricing of the participating assets are reported in Figures 4.1-4.7 as well as Tables 4.1 and 4.2. While no transmission flow violation has occurred at a steady state (see line flow in Table 4.2), congestion on the tie-line at periods 1, 3 and 4 as well as on lines L2 and L3 at the second period have led to LMPs across the grid. These shadow prices reflect the generator cost function used to clear the market, and their variations with respect to the 04 DAMs of the horizon of study follow system load distribution profile as shown in Figure 4.1. Bus B1 cost which decreases continuously then rises towards the end of the last period is an exception to this remark, certainly because the cheapest unit of the system, G1, is located at that bus. Note also that buses 4, 5 and 6 follow the same shadow price path over the horizon of study while this observation is similar for the first three other buses at the last period only.

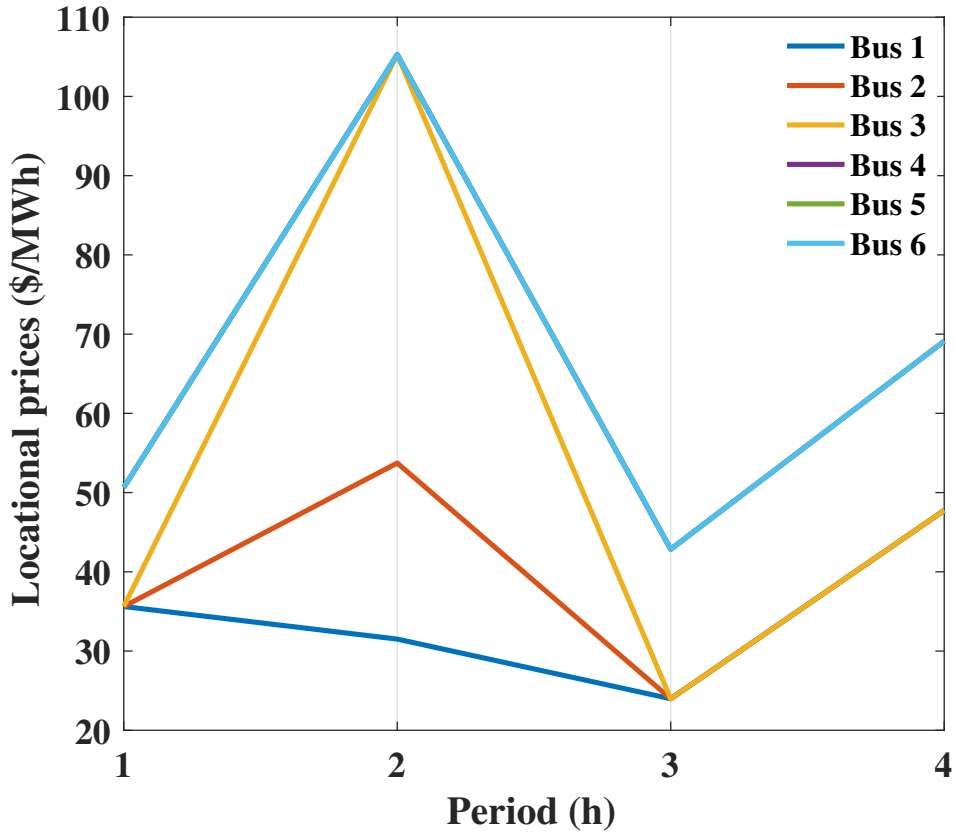

Figure 4.1: DAM clearing prices for the Hybrid approach.

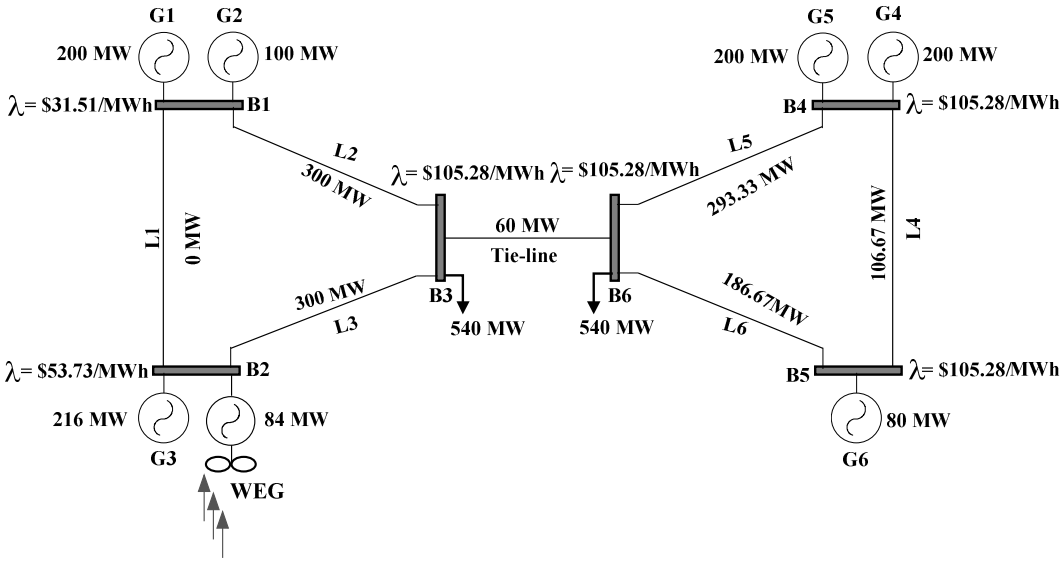

Figure 4.2: Result of the hybrid market dispatch at $t = 2$.

In Figure 4.2 we present a snapshot of the market dispatch at the peak demand period. It is not surprising that the hybrid tool has allocated more load to unit G3 prior to G2 although there is still cheaper power at bus B1 as well as available transport capacity on line L1. Indeed, 100 MW of power reserve is required from unit G2 for system security. This has been scheduled as shown in Figure 4.5 where the expected generation reserve of conventional units is drawn. As a result, line L1 capacity is 0% used and the load is shifted to more expensive units, increasing the resulting operating cost.

Table 4.1: DAM market summary for the hybrid approach

Period h	Quantity sold MW	Revenue $	Total cost $	Earnings $
1	880	32569.74	–	–
2	1080	71593.08	–	–
3	600	13525.58	–	–
4	750	32787.5	–	–
Total	3310	150475.9	130849.25	19626.65

Table 4.2: The six-bus test system line power flow when G2 trips off-line (MW)

	L1	L2	L3	L4	L5	L6	Tie-line
1st h	-50	250	300	70	200	130	110
2nd h	-50	250	300	70	300	230	10
3rd h	-16.67	216.67	233.33	50	100	50	150
4th h	-41.67	241.67	283.33	75	150	75	150

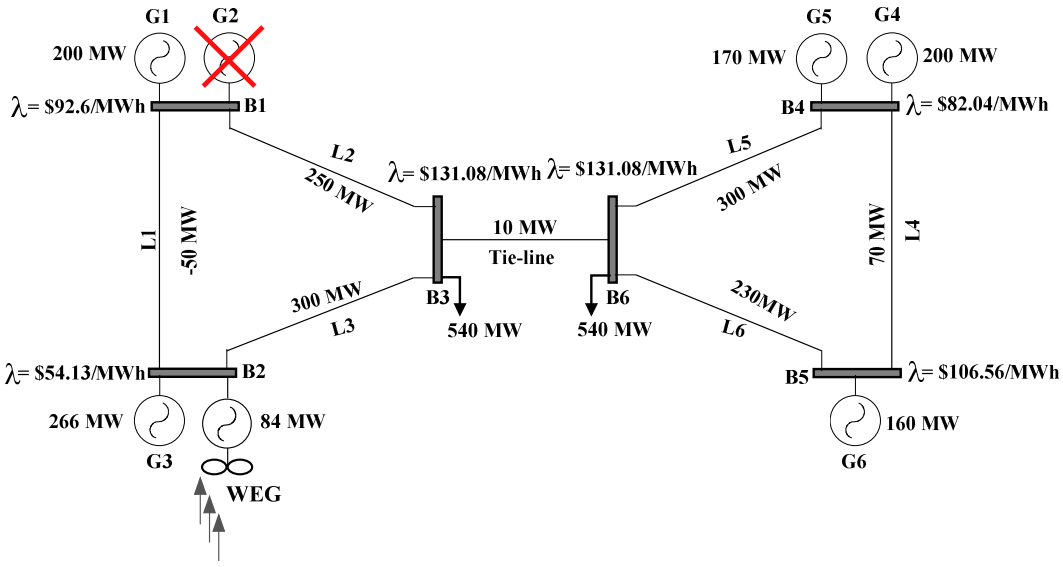

Figure 4.3: Result of the hybrid market dispatch at $t = 2$ following the outage of unit G2

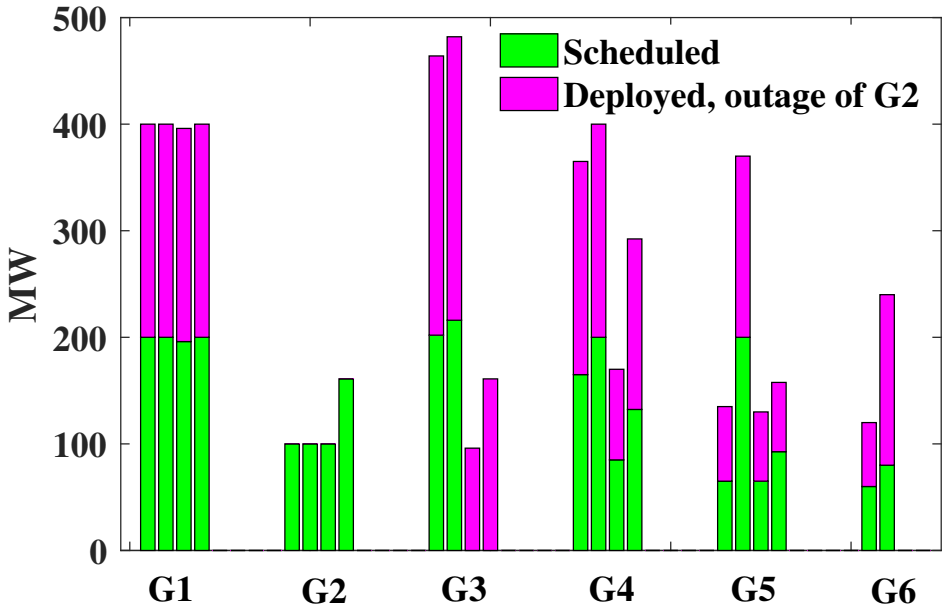

Figure 4.4: Hourly power scheduled and deployed following the outage of unit G2

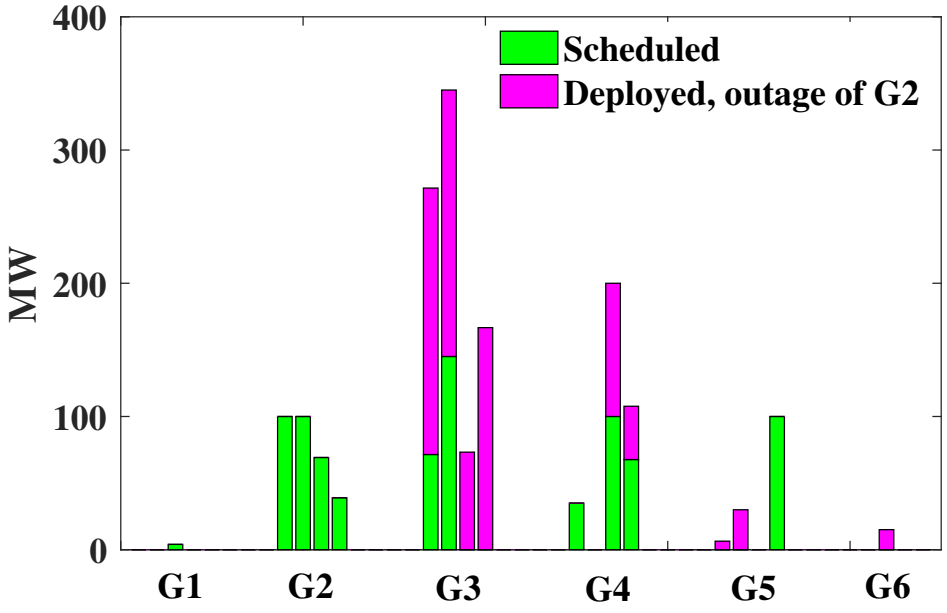

Figure 4.5: Hourly spinning reserve scheduled and deployed following the outage of unit G2

The summary of the market is given in Table 4.1. After supplying 3310 MW of the system demand, the generators's revenue is \$150475.9. Compared to the functional as minimized at the schedule level, the system earns \$19626.65. This substantial profit remains uncertain as long as the redispatching of the available resources on the basis of the steady state of Table 4.1 does not lead the system to a state trajectory that exceeds system ratings or operating limits. Considering, for example, the post-contingency state that follows the outage of generator G2, Table 4.2, Figures 4.4 and 4.5 show that the system has survived the failure of the generating unit without resort to load shedding, as it has reached an equilibrium that does not violate any limits with the resources available. On the one hand, the SCOPF results on Table 4.2 show that there are changes in flows on lines, however, none of them is overloaded. On the other hand, the deficit in generation power as well as generation reserve is made up by redispatching resources as shown in Figures 4.4 and 4.5, thanks to the modeling of all post-contingency situations with load flows: by joining the overall problem formulation, the variables defining those flows are incorporated and thus available to impose coupling constraints such as ramp rates on them, generator capability and transmission capacity limits for the post-contingency solution. One can notice from these Figures that generator G3 was the most solicited during this operation as it was brought online at periods 3 and 4 to supply much of the extra generations.

A direct consequence of such unforeseen events occurring in real time operation is the increase in the total generation cost even with no load shedding. In this particular case, the post-contingency balancing cost is \$139901.45, an increase of \$9052.2 compared to the steady state operation cost. The reason for the increase may be numerous, however, the type of units called on to supply the extra commodities as well as the way the reserve requirement is set are the most important factors. In Figure 4.6, the influence of the scaling factor β_1 to dial in the uncertainty of equipment unreliability on the expected post-contingency operating cost for the case under consideration is drawn. It can be noticed that a smaller value of β_1 increases the operational benefit as a decrease in the total operating cost is observed with decreasing β_1. The question, is to which extent can this be done? Nevertheless, an appropriate choice of β_1 can add value to the system. Similar findings not only show an increase of the different components of the objective function, but also reveals some evidence of system exposure to load shedding as reported in Figure 4.7. Thus, correctly solving the day-ahead schedule problem requires

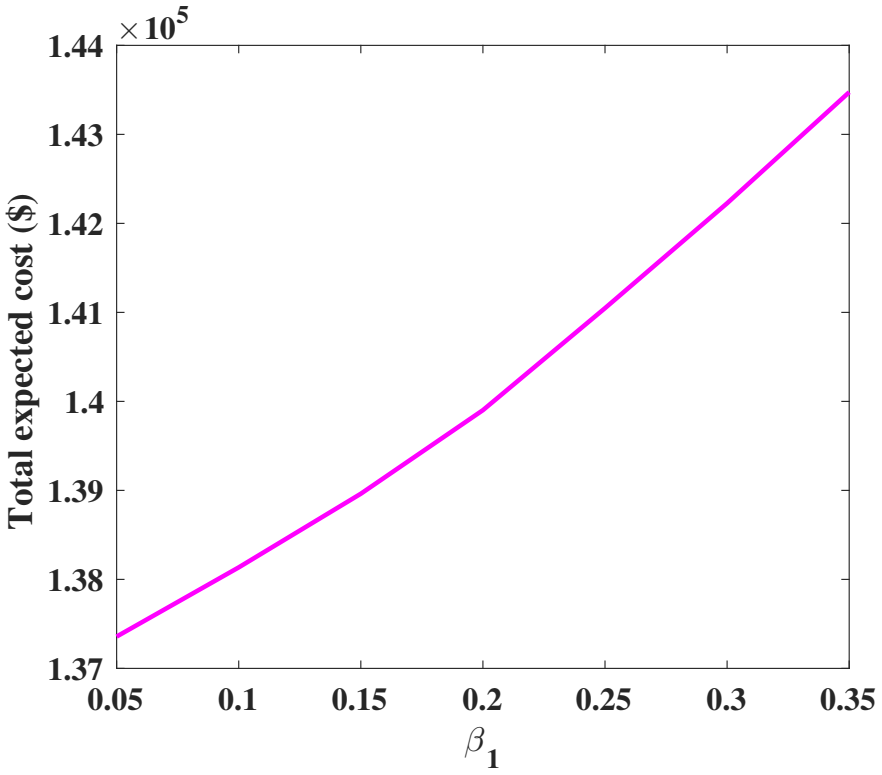

Figure 4.6: Expected cost of serving load following the outage of unit G2

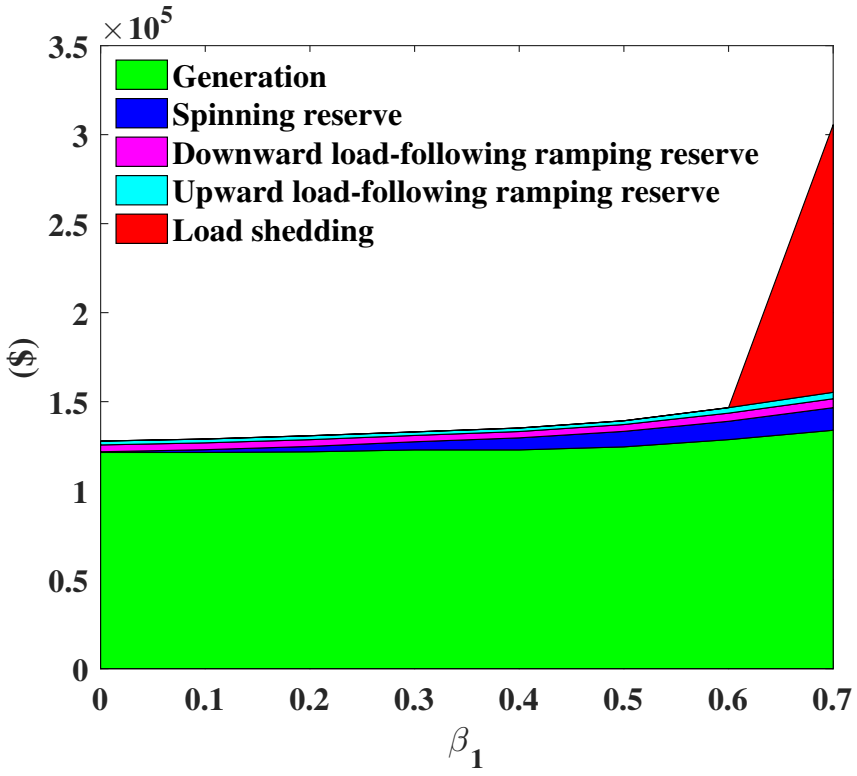

Figure 4.7: Expected cost of serving load for the hybrid approach

addressing the issue of geographically appropriate reserve allocation. Furthermore, correct pricing of this commodity requires that it be explicitly included in the problem formulation. Formulation (4.1a)-(4.1u) does that and is used to benchmark our model by helping to scale the value of β_1. Indeed, our model blindly selects this fraction of the amount of reserve for system security, which is risky to both the reliability and economy of the grid.

4.5.1.2 The Stochastic DAM Outcomes

Secure operation requires planning with respect to credible contingencies in order to position the current state accordingly and plan for corrective rescheduling strategies in the event that one of them does occur (Capitanescu et al., 2011; Liu et al., 2015). We used thirteen contingencies including outages of each generator, as well as each transmission line of the 6-bus test system to illustrate the determination of reserve requirement as an endogenous parameter in power system operation and security. These contingencies are listed in Table 4.3 which includes the label, the probability and the type of contingency. The probabilities defined here correspond to the conditional probabilities π^{twc} of contingency c occurring conditioned on being in base scenario c.

Table 4.3: 6-bus system contingency table

Label	Probability	Type
1	0.04	G1 at B1 trips off-line
2	0.04	G2 at B1 trips off-line
3	0.04	G3 at B2 trips off-line
4	0.04	G4 at B4 trips off-line
5	0.04	G5 at B4 trips off-line
6	0.04	G6 at B6 trips off-line
7	0.06	L1 from bus 1 to bus 2 fails
8	0.06	L2 from bus 1 to bus 3 fails
9	0.06	L3 from bus 2 to bus 3 fails
10	0.06	L4 from bus 4 to bus 5 fails
11	0.06	L5 from bus 4 to bus 6 fails
12	0.06	L6 from bus 5 to bus 6 fails
13	0.06	L7 from bus 3 to bus 6 fails

In Figure 4.8 the outcomes of the stochastic DAM formulated in (4.1a)-(4.1u) and solved as indicated in chapter 2 are presented. These solutions yield optimal day-ahead contract quantities P_c^{gt}, r_+^{gt} and r_-^{gt} as well as generation ranges for all scenarios considered and for each

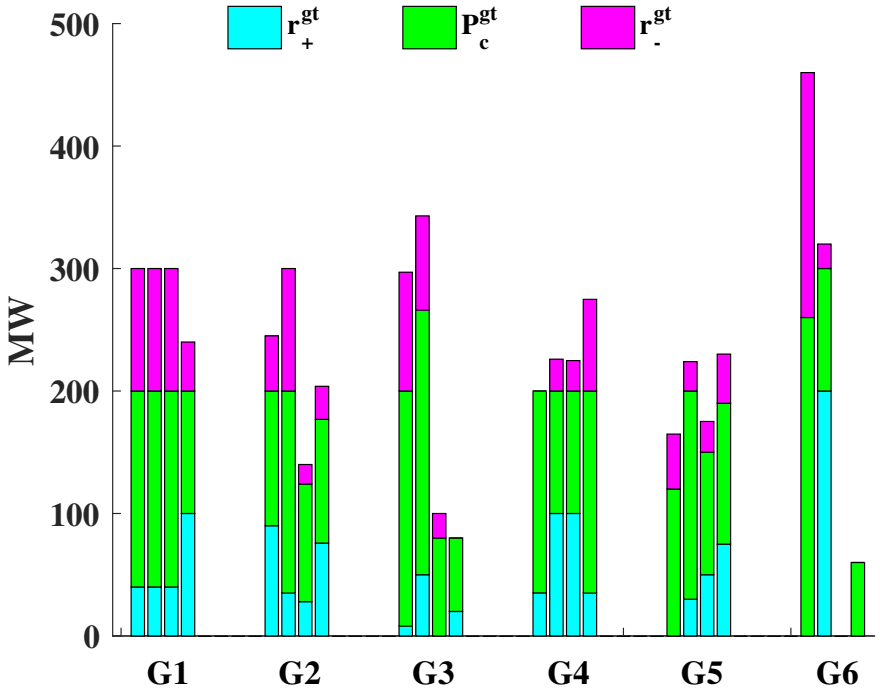

Figure 4.8: Stochastic hourly DAM outcomes and ranges of generation

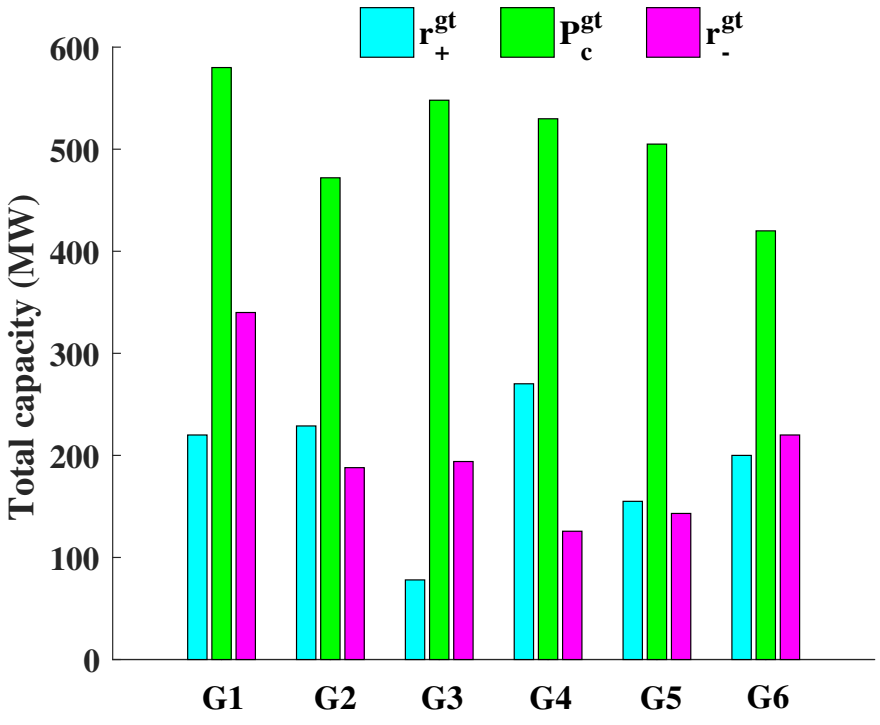

Figure 4.9: Stochastic total capacity cleared at DAM

DAM executed. It can be inferred from this figure that the day ahead schedule results in a contract for the provision of a nominal quantity P_c^{gt} at a price determined by the chosen auction institution and the marginal cost of energy at the generator's location, with the additional obligation of abiding by any redispatch issued by the ISO in real time within the range $[P_c^{gt} - r_-^{gt},\ P_c^{gt} + r_+^{gt}]$. In this way, the reserve requirements are locational and determined endogenously as a function of the uncertainty in the system conditions. In Figure 4.9 the aggregate amount of the same quantities over the horizon of study is presented while Figure 4.10 shows the total amount of reserve as scheduled by the stochastic tool, in comparison to the hybrid approach requirement for various values of the scaling factor β_1.

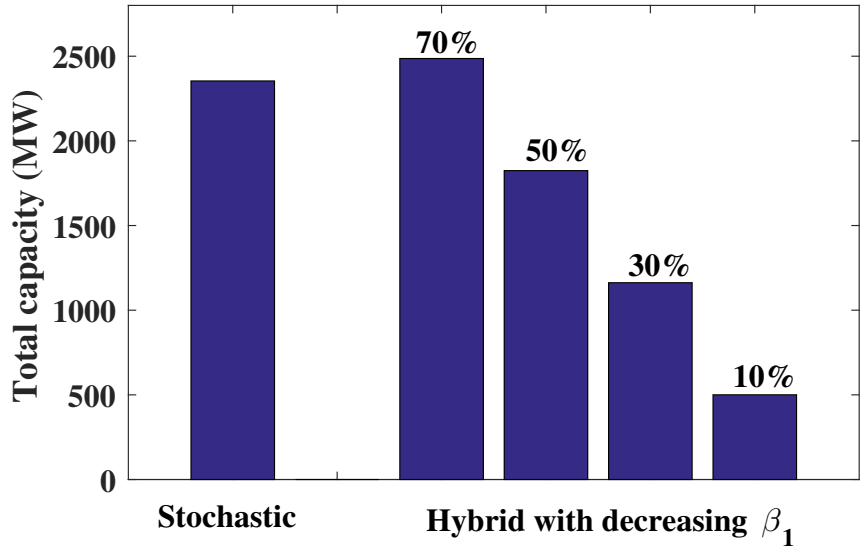

Figure 4.10: Capacity reserve comparison versus scaling factor β_1.

The problem of balancing and pricing the real-time market is now subject to the contract issued the previous day. The results of the real-time operation indicated that the decision on the amount and location of the spinning reserve set aside for use in case of the contingencies 1-5, 7, 10 and 13 were efficiently made by the stochastic approach as these events do not threaten the secure operation of the power system. Indeed, a new system equilibrium was reached following these contingencies, without any violation of the system ratings. Similar observations were made for the blind selection of the reserve using the hybrid method. However, the post-contingency states following the outages of generator G6 at bus 5 as well as the loss of the transmission lines L2, L3, L5 and L6 exhibit a load shedding of 80 MW at bus 6 for the generator G6 outage, and 180 MW for the failure of each transmission line L2, L3, L5

and L6. These load shedding all took place at period 2 for both approaches but the hybrid approach curtailed the 180 MW all at bus 6 while the stochastic method equally shared it between both system's load.

We selected a master set of three contingencies for the comparative study of both approaches in setting the system security, our aim being to vary the conservativeness of the hybrid approach. These include the outages of generators G2 and G6 and the failure of line L5. Note however that, the hybrid approach is compared to scenario 3 of the stochastic approach where individual trajectories of wind power are the path taken for WEGs realizations in our investigations. Figure 4.11 shows the hourly aggregated amount of reserves allocated

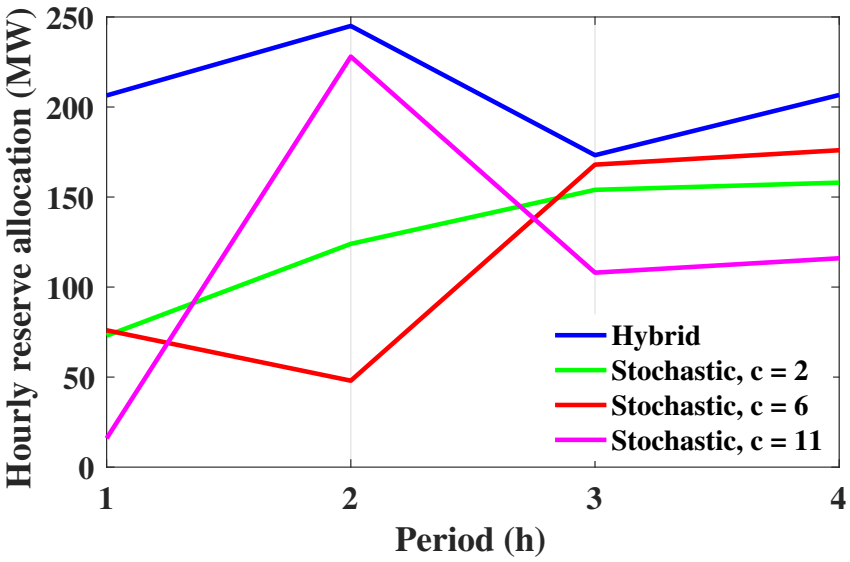

Figure 4.11: Hourly contingency reserve allocation

by the two approaches. It can be noticed that the hybrid approach schedules more reserves than the stochastic approach for each hour of the horizon of study and for each contingency. It should be noted also that the hybrid reserve schedule profile follows the system's hourly load distribution, while the reserves schedule in the stochastic approach in contingency $c = 2$ increases throughout the planning horizon with respect to the uncertainty from WEGs and load. The observation made on the hybrid approach as for as the load profile is concerned is similar to the stochastic approach in contingency $c = 11$ however contingency $c = 6$ exhibits the opposite.

Figures 4.12-4.14 represent on the comparison of each stochastic contingency reserve as al-

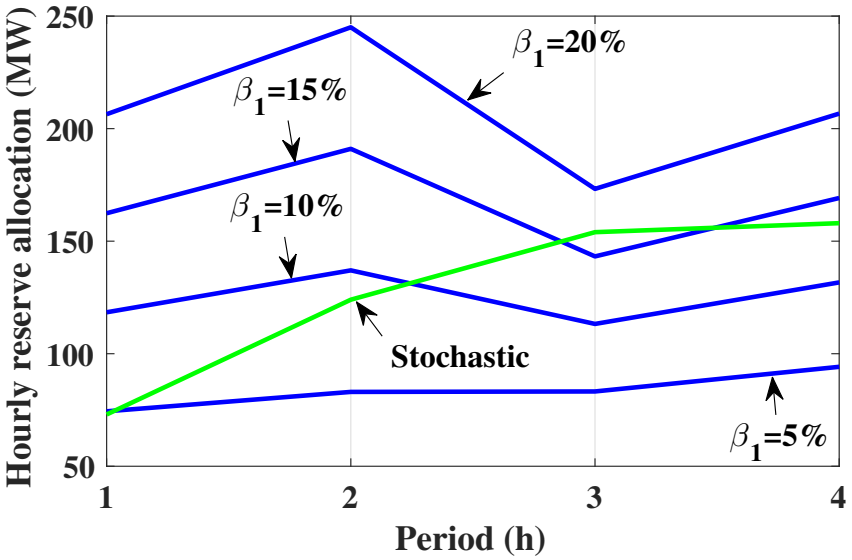

Figure 4.12: Hourly contingency reserve allocation when G2 trips off-line

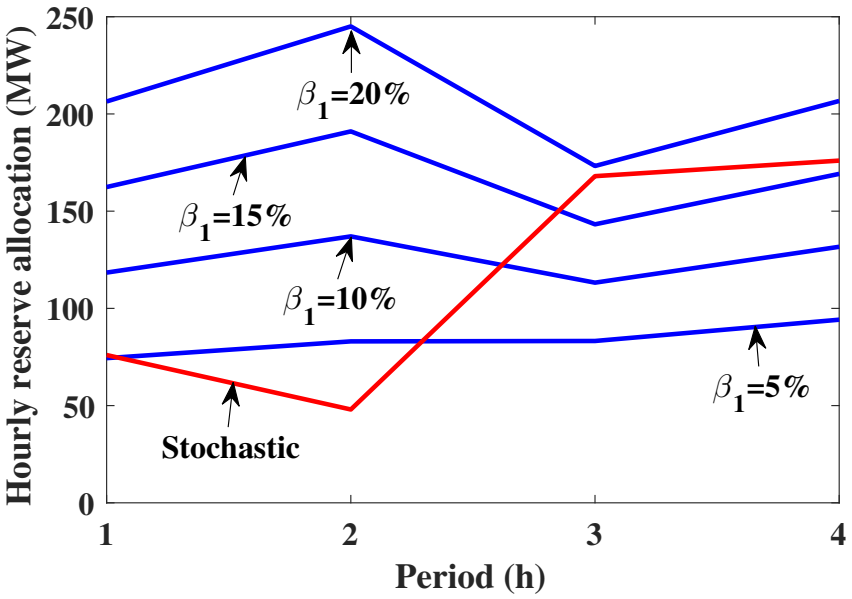

Figure 4.13: Hourly contingency reserve allocation when G6 trips off-line

located in Figure 4.11, to the hybrid counterpart for various values of the scaling factor β_1, assuming the stochastic approach as the reference. Not surprisingly, the scaling factor β_1 controls a trade-off between high costs of *LNS* and high costs of energy, primarily, and reserves to a lesser extent. This observation was made previously as reported in Figures 4.6 and 4.7, however this is because larger reserve requirements (which come with a larger β_1) force less expensive generators to provide more reserves and less energy, shifting that energy to more

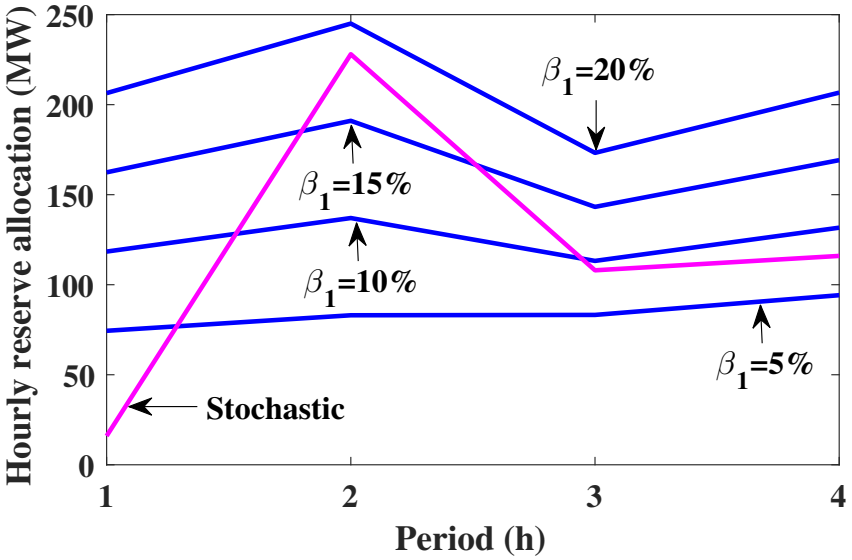

Figure 4.14: Hourly contingency reserve allocation when L5 fails

expensive generators. These results suggest that the 'optimal' scaling factor for the given reserve requirements will lie in [10%,20%]. However, any best guess value should be one that minimizes the expected operation costs induced by the hybrid approach and that will not underestimate the low probability of *LNS*. Nevertheless this value will be difficult to compute efficiently for a large-scale system.

4.5.2 The 118-Bus Test System

In addition to numerical validation with the 6-bus system, it was deemed necessary to test the formulation on a larger network. The same modified IEEE 118-bus system shown in Figure B.5 and used in chapter 3 was considered for this purpose. Three contingencies that represent the outages of unit 16, line 19–34, and line 56–59 were considered. The hybrid algorithm resorted to load shedding in order to reach an equilibrium point in the post-contingency state following the outage line 56-59. However, the system survived the outages of unit 16 and line 19-34 by redispatching the available resources. As a result, the total operating cost rises from \$1937926.08 to \$1945674.09 when unit 16 tripped off-line and \$1955859.06 when line 19-34 failed.

In Figure 4.15, the total cost of the spinning reserve and load shedding are represented when the scaling factor decreases. Note that the stochastic solution has no load shedding, whereas

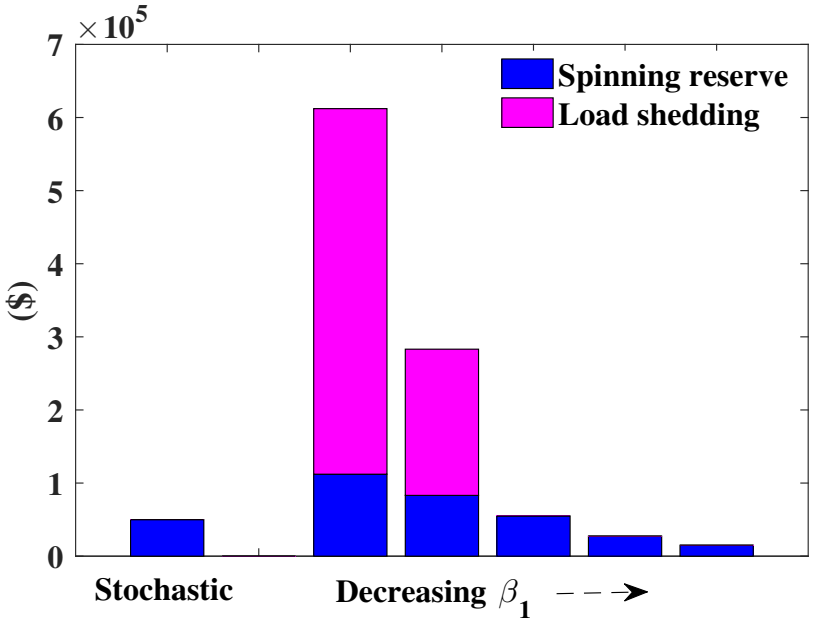

Figure 4.15: Costs of reserve and load shedding, 118-bus system

the hybrid approach exhibits load shedding.

4.6 Conclusion

This chapter proposes a stochastic method to benchmark our proposed hybrid model. A combined SCUC and OPF that explicitly includes wind uncertainty and contingencies by means of probabilities that reflect the relative likelihood of the different states of the system occurring has been devised. We simulated reserve criteria following practices in real-world operations. A comparison of results from both approaches led to a refining of the performance of our hybrid model, by varying its conservativeness with the help of the scaling factor to dial in the amount of spinning reserve due to equipment unreliability.

Conclusion and Future Work

This thesis presented research related to an increasing variability and uncertainty in the short-term power grid operations, emanating from increasing the share of WEGs in the electricity generation mix and competition from electricity markets. In the general introduction the requirements of operating reserves to incorporate higher levels of WEGs against a background of deregulation and increased competition is discussed.

Decisions on the problems addressed in this thesis are taken in the electricity market, while risk mitigation remains the main concern of power grid operations. After a synthesis and analysis of the relevant published works linked to this research, Chapter 1 presents a functional description of the wholesale electricity market, along with a tutorial example that shows how the tight coupling between grid operations and market operations are coordinated under the supervision of the independent system operator.

The model of the WEG used throughout this dissertation is presented in chapter 2. A formula for the stochastic feature of the wind power is established in this chapter to manage the risk borne by the system through the inclusion of WEGs. The main features of the published work presented in chapters 3 and 4 as well as the information on the implementation of the methodology used are also presented in this chapter.

Chapter 3 presents a SCUC OPF suitable for power systems with a large share of WEGs to be used in the day ahead market. The traditional spinning reserve requirement supplemented by an adjustable fraction of the expected shortfall from the supply of WEGs has been computed using the stochastic feature of wind and loosely represented in the security constraint with scenarios. The optimization tool commits and dispatches generating units, while simultaneously determining the geographical procurement of the required spinning reserve, as well as load-following ramping reserve by mixed integer quadratic programming. Case studies

have been used to investigate various effects of grid integration on a reduction in the overall operation costs associated with more wind power in the system.

A benchmark model to the hybrid approach of chapter 3 has been formulated in chapter 4. By modeling the spinning reserve as the upward and downward deviations from an active power contract quantity that limits the range of changes in the output of a generating unit at real-time operation, the reserve requirements are locational and determined endogenously as a function of uncertainty in the system conditions. The output of this approach is then used to vary the conservativeness of the proposed model of chapter 3, thus reducing the impact that the use of such proxy constraints have on the electricity prices.

Future Work

The analysis completed in Chapters 3 and 4 considers the network constraints in the models through a DC load flow representation. Although the linear DC model of line flow allows the problem to be posed as a mixed-integer quadratic program and solved by the state-of-the-art MIQP solver GUROBI, this approximation sacrifices accuracy in the network model. A full AC model of the network which models losses along with voltage and reactive power requirements is an interesting research problem to investigate. This could allow the consideration of synchronized storage devices in the model like synchronous compensators to increase the reliability of the model by controlling the reactive power.

The market clearing algorithm used in the published material of this dissertation, considers generators cost functions and inelastic demand to clear the markets. Practical programs use multiple settlement auctions based on last accepted offers model of pricing and elastic demand to clear the market. Future work should utilize this model of pricing along with elastic demand to analyze the effectiveness of the proposed algorithm.

This thesis considers the integration of wind energy to the transport grid. It will be interesting to consider the solar energy which is an important form of renewable energy. However, the application of the designed tool in the green microgrid could also be studied.

Bibliography

Ahmadi-Khatir A., Conejo A. J., and Cherkaoui R. Multi-area unit scheduling and reserve allocation under wind power uncertainty. *IEEE Trans. Power Syst.*, 29(4):1701–1710, 2014.

Akdağ S.A. and Dinler A. A new method to estimate weibull parameters for wind energy applications. *Energy Convers. Manag.*, 50:1761–1766, 2009.

Al-Hasan M. and Nigmatullin R. R. Identification of the generalized weibull distribution in wind speed data by the eigen-coordinates method. *Renew Energy*, 28:93–110, 2003.

Allan Ronald Norman and Billinton Roy. Probabilistic assessment of power systems. *Proceedings of the IEEE*, 88(2):140–162, 2000.

Ben-Tal A., Ghaoui L. El, and Nemirovski A. *Robust optimization*. Princeton University Press, Princeton, NJ, USA, 2009.

Billinton R. and Wangdee W. Reliability-based transmission reinforcement planning associated with large-scale wind farms. *IEEE Trans. Power Syst.*, 22(1):34–41, 2007.

Billinton Roy and Allan Ronald Norman. *Reliability Evaluation of Power Systems, 2nd ed.* Plenum Press, 1996.

Billinton Roy, Allan Ronald Norman, and Salvaderi Luigi. *Applied reliability assessment in electric power systems*. IEEE press, New York, NY, 1991.

Birge J. R. and Louveaux F. *Introduction to stochastic programming, 2nd ed.* Springer Science & Business Media, New York, NY, USA, 2011.

Borenstein S. and Bushnell J. B. The U.S. electricity industry after 20 years of restructuring. *Annual Review of Economics*, 7(1):437–463, 2015.

Bouffard F. and Galiana F. D. Stochastic security for operations planning with significant wind power generation. *IEEE Trans. Power Syst.*, 23(2):306–316, 2008.

Bradbury L. Wind-power program. Technical report, WINDPOWER program, 2008. http://www.wind-power-program.com/mean_power_calculation.htm.

Brown P., Lopes J., and Matos M. Optimization of pumped storage capacity in an isolated power system with large renewable penetration. *IEEE Trans. Power Syst.*, 23(2):523–531, 2008.

CAISO . In spinning reserve requirement. Technical report, California Electrical System, 2005. http://www.caiso.com/.

Camilo C., Jose D., and Elov D. An approach to determine the weibull parameters for wind energy analysis: the case of galicia (spain). *Energies*, 7(4):2676–2700, 2007.

Capitanescu F., Ramos J. M., Panciatici P., Kirschen D., Marcolini A. M., Platbrood L., and Wehenkel L. State-of-the-art, challenges, and future trends in security constrained optimal power flow. *Electric Power Systems Research*, 81(8):1731–1741, 2011.

Carta J. A., Ramírez P., and Velázquez S. Influence of the level of fit of a density probability function to wind-speed data on the wecs mean power output estimation. *Energy Convers. Manag.*, 49(10):2647–2655, 2008.

Chang T. P. Performance comparison of six numerical methods in estimating weibull parameters for wind energy application. *Appl. Energy*, 88(1):75–84, 2011.

Chen H. *Power grid operation in market environment: Economic efficiency and risk mitigation*. IEEE Press Series on Power Egineering, Wiley, 2016.

Chen J., Wu W., Zhang B., Wang B., and Guo Q. A spinning reserve allocation method for power generation dispatch accommodating large-scale wind power integration. *energies*, 6 (10):5357–5381, 2013.

Conejo A. J., Carrión M., and Morales J. M. *Decision Making under Uncertainty in Electricity Markets*. Springer-Science Business Media, LLC, 2010.

Costa P.A., de Sousa R. Coelho, de Andrade C. Freitas, and da Silva M. Vieira. Comparison of seven numerical methods for determining weibull parameters for wind energy generation in the northeast region of brazil. *Applied Energy*, 89(1):395–400, 2012.

Denny E. and O'Malley M. Wind generation, power system operation, and emissions reduction. *IEEE Trans. Power Syst.*, 21(1):341–347, 2006.

Denny E. and O'Malley M. Quantifying the total net bene¯ts of grid integrated wind. *IEEE Trans. Power Syst.*, 22(2):605–615, 2007.

Dillon T. S., Edwin K. W., and Taud R. J. Integer programming approach to the problem of optimal unit commitment with probabilistic reserve determination. *IEEE Transactions on Power Apparatus and Systems*, PAS-97(6):2154–2166, 1978.

Doostizadeh M., Aminifar F., Lesani H., and Ghasemi H. Multi-area market clearing in wind-integrated interconnected power systems: A fast parallel decentralized method. *Energy Conversion and Management*, 113:131–142, 2016.

Dukpa A., Duggal I., and Venkatesh B. Optimal participation and risk mitigation of wind generators in an electricity market. *IET Renew. Power Gener.*, 4(2):165–175, 2010.

Dupacová J., Gröwe-Kuska N., and Römisch W. Scenario reduction in stochastic programming: An approach using probability metrics. *Mathematical Programming*, 23(A): 493–511, 2003.

Ela E., Milligan M., Kirby B., Lannoye E., Flyynn D., O'Malley M., and Zavadil B. Evolution of operating reserve determination in wind power integration studies. In *IEEE Power and Energy Society General Meeting*, Minneapolis-Minnesota, July 2010.

Ela E., Milligan M., and Kirby B. Operating reserves and variable generation. Technical report, NRLE, 2011. http://www.consultkirby.com.

ENTSO-E . Ucte operation handbook—policy 1: Load-frequency control and performance. Technical report, European Network of Transmission System Operators for Electricity, 2009. http://www.kom.aau.dk/...11.06.../ENTSOE_UCTE_frequency_reserves.pdf.

FCLab . Technical report. http://www.fclab.fr.

Gil H. A. and Joos G. Generalized estimation of average displaced emissions by wind generation. *IEEE Trans. Power Syst.*, 22(3):1035–1043, 2007.

Gooi H. B., Mendes D. P., Bell K. R. W., and Kirschen D. S. Optimal scheduling of spinning reserve. *IEEE Trans. on Power Systems*, 14(4):1485–1492, 1999.

Grigg C., Wong P., Albrecht P., Allan R., Bhavaraju M., Billinton R., Chen Q., Fong C., Haddad S., Kuruganty S., Mukerji R., Patton D., Rau N., Reppen D., k. Schneider , Shahidehpour M., and Singh C. The ieee reliability test system-1996. a report prepared by the reliability test system task force of the application of probability methods subcommittee. *IEEE Trans. Power Syst.*, 14(3):1010–1020, 1999.

Gurobi . Gurobi homepage [online]. Technical report, Gurobi, 2017. http://www.gurobi.com.

Guy J. D. Security constrained unit commitment. *IEEE Transactions on Power Apparatus and Systems*, PAS-90(3):1385–1390, 1971.

GWEC . Global wind report 2017. Technical report, Global Wind Energy Council (GWEC), 2018. http://gwec.net/publications/global-wind-report-2/.

Hamidi V. and Robinson F. Responsive demand in networks with high penetration of wind power. In *In: Proc. of IEEE/PES Transmission and Distribution Conference and Exposition*, Chicago, USA, 2008.

He D., Tan Z., , and Harley R. Chance constrained unit commitment with wind generation and superconducting magnetic energy storages. In *in Proc. 2012 IEEE Power and Energy Society General Meeting*, San Diego, USA, 2012.

Heier S. *Grid integration of wind energy. Third ed.* John Wiley & Sons, New York, NY, USA, 2014.

Holttinen H., Milligan M., and Ela E. Methodologies to determine operating reserves due to increased wind power. *IEEE Trans. Sustain. Energy*, 3(4):713–723, 2012.

IESO . The independent electricity system operator of ontario electrical system. Technical report, Ontario Electrical System, 2004. http://www.ieso.ca/.

Justus C. G., Hargraves W. R., Mikhail A., and Graber D. Methods for estimating wind speed frequency distributions. *J Appl Meteorol*, 17:350–353, 1978.

Kamalinia S. and Shahidehpur M. Generation expansion planning in windthermal power systems. *IET Generation, Transmission & Distribution*, 4(8):940–951, 2010.

Keane A., Tuohy A., Meibom P., Denny E., Flynn D., Mullane A., and O'Malley M. Demand side resource operation on the irish power system with high wind power penetration. *Energy Policy*, 39(5):2925–2934, 2011.

Lavaei J. and Low S. Zero duality gap in optimal power flow problem. *Power Systems, IEEE Transactions on*, 27(1):92–107, 2012.

Li Z., Wu W., Shahidehpour M., and Zhang B. Adaptive robust tie-line scheduling considering wind power uncertainty for interconnected power systems. *IEEE Trans. Power Syst.*, 31(4):2701–2713, 2016.

Liu Y., Ferris M., and Zhao F. Computational study of security constrained economic dispatch with multi-stage rescheduling. *Power Systems, IEEE Transactions on*, 30(2): 920–929, 2015.

Lorca Á. and Sun X. A. Adaptive robust optimization with dynamic uncertainty sets for multi-period economic dispatch under significant wind. *IEEE Trans. Power Syst.*, 30(4): 1702–1713, 2015.

Lun I. Y. and Lam J. C. A study of weibull parameters using long-term wind observations. *Renewable Energy*, 20(2):145–153, 2000.

Lysen E. H. *Introduction to Wind Energy, 2nd Edition*. Consultancy Services Wind Energy Developing Countries, CWO 82, 1983.

Maggio D. J. Impacts of wind-powered generation resource integration on prices in the ercot nodal market. In *Proceedings of 2012 IEEE Power and Energy Society General Meeting*, San Diego-California, USA, 22-26 Jul, 2012.

Mathew S. *Wind Energy: Fundamentals, Resource Analysis and Economics*. Springer Berlin/Heidelberg, Germany, 2006.

Möhrlen C., Jørgensen J., Pinson P., Madsen H., and Kristoffersen Runge. High resolution ensemble for horns rev: A project overview. In *In: Proc. European offshore wind energy conference*, 2007.

Monteiro C., Bessa R., Miranda V., Botterud A., Wang J., and Conzelmann G. Wind power forecasting: State-of-the-art 2009. Technical report, Argonne National Laboratory (ANL), 2009. http://www.ipd.anl.gov/anlpubs/2009/11/65613.pdf.

Morales J. M., Conejo A. J., Madsen H., Pinson P., and Zugno M. *Integrating Renewables Enegy in Electricity Markets*. Springer, 2014.

Murillo-Sánchez C. E., Zimmermann R. D., and Anderson C. L. Secure planning and operations of systems with stochastic sources, energy storage and active demand. *Smart Grid, IEEE Transactions on*, 4(4):2220–2229, 2013a.

Murillo-Sánchez C. E., Zimmermann R. D., Anderson C.L., and Thomas R. J. A stochastic, contingency-based security-constrained optimal power flow for the procurement of energy and distributed reserve. *Decision Support Systems*, 56:1–10, 2013b.

NERC North American Electric Reliability Corporation. Reliability standards for the bulk electric systems of north america. Technical report, NERC, 2009. http://www.nerc.com/pa/.../Reliability.

NYISO New York Independent System Operator. Markets operations. Technical report, NYISO, 2017. http://www.nyiso.com/public/markets_operations/planning/iso_rto.pdf.

Omie . Omi-polo espanol s.a. [online]. Technical report, Omie, 2014. http://www.omel.es/en/inicio,2014.

Onaiwu E. How does bilateral trading differ from electricity pooling. Technical report, University of Dundee, 2010.

Overbye T. J., Cheng X., and Sun Y. A comparison of the ac and dc power flow models for lmp calculations. In *37th Hawaii International Conference on System Sciences*, Hawaii (US), 2004.

Pallabazzer R. Evaluation of wind-generator potentiality. *Solar Energy*, 55(1):49–59, 1995.

Papavasiliou A., Oren S. S., and O'Neill R. P. Reserve requirements for wind power integration: A scenario-based stochastic programming framework. *IEEE Trans. Power Syst.*, 26(4):2197–2206, 2011.

Petkovic D., Shamshirband S., Anuar N.B., Saboohi H., Wahab A.W. Abdul, Protic M., Zalnezhad E., and Mirhashemi S.M. Amin. An appraisal of wind speed distribution prediction by soft computing methodologies: A comparative study. *Energy Conversion and Management*, 84:133–139, 2014.

Pozo D. and Contreras J. A chance-constrained unit commitment with an n-k security criterion and significant wind generation. *IEEE Trans. Power Syst.*, 28(3):2842–2851, 2012.

Purchala K., Meeus L., Dommelen D. V., and Belmans R. Usefulness of dc power flow for active power flow analysis. In *IEEE PES General Meeting*, San Francisco (US), 2005.

REE . In operacion del sistema electrico, red electrica de espana. Technical report, Electrica de Espana, 1998. http://www.ree.es/cap03/pdf/po/PO_resol_30jul1998_b.pdf.

Robitaille A., Kamwa I., and Oussedik A. H. Preliminary impacts of wind power integration in the hydro-quebec system. *Wind Eng.*, 36(1):35–37, 2012.

Rockafellar R. and Uryasev S. Optimization of conditional value-at-risk. *J. Risk*, 2(3):21–42, 2000.

Seguro J. V. and Lambert T. W. Modern estimation of the parameters of the weibull wind speed distribution for wind energy analysis. *J Wind Eng Indus Aerod*, 85:75–84, 2000.

Shahidehpour M., Yamin H., and Li Z. *Market Operations in Electric Power Systems*. John Wiley & Sons, 2002.

Sioshansi F. P. *Evolution of Global Electricity Markets-New paradigms, new challenges, new approaches*. Academic Press, 2013.

Stoft S. *Power System Economics: Designing Markets for Electricity*. Wiley-IEEE Press, New York, 2002.

Stott B., Jardim J., and Alsac O. Dc power flow revisited. *IEEE Trans. Power Syst.*, 24(3): 1290–1301, 2009.

Tai-Her Y. and Li W. A study on generator capacity for wind turbines under various tower heights and rated wind speeds using weibull distribution. *IEEE Trans. Energy Convers.*, 23(2):592–602, 2008.

Tuohy A., Meibom P., Denny E., and O'Malley M. Unit commitment for systems with significant wind penetration. *IEEE Trans. Power Syst.*, 24(2):592–601, 2009.

UCTE . Union for the coordination of transmission of electricity operation handbook. Technical report, California Electrical System, 2004. http://www.ucte.org/pdf/ohb/Operation_Handbook_20.07.3004.pdf.

Ummels B., Gibescu M., Pelgrum E., Kling W., and Brand A. Impacts of wind power on thermal generation unit commitment and dispatch. *IEEE Transactions on Energy Conversion*, 22(1):44–51, 2007.

Vallee F., Lobry J., and Deblecker O. Impact of the wind geographical correlation level for reliability studies. *IEEE Trans. Power Syst.*, 22(4):2232–2239, 2007.

Venkatesh B., Peng Y., Gooi H. B., and Dechen C. Fuzzy milp unit commitment incorporating wind generators. *IEEE Trans. Power Syst.*, 23(4):1738–1746, 2008.

Vrakopoulou M., Margellos K., Lygeros J., and Andersson G. A probabilistic framework for reserve scheduling and n-1 security assessment of systems with high wind power penetration. *IEEE Trans. Power Syst.*, 28(4):3885–3896, 2013.

Wang B. and Hobbs B. F. Real-time markets for flexiramp: A stochastic unit commitment-based analysis. *IEEE Trans. Power Syst.*, 31(2):846–860, 2016.

Wang C., Liu F., Wang J., Qiu F., Wei W., Mei S., and Lei S. Robust risk-constrained unit commitment with large-scale wind generation: An adjustable uncertainty set approach. *IEEE Trans. Power Syst.*, 30(1):109–122, 2016.

Wang J., Wang X., and Wu Y. Operating reserve model in the power market. *IEEE Trans. on Power Systems*, 20(1):223–229, 2005.

Wang J., Botterud A., and Bessa R. Wind power forecasting uncertainty and unit commitment. *Applied Energy*, 88(11):4014–4023, 2011.

Wang Q., Guan Y., and Wang J. A chance-constrained two-stage stochastic program for unit commitment with uncertain wind power output. *IEEE Trans. Power Syst.*, 27(1): 206–215, 2012.

Wood A. J., Wollenberg B. F., and Sheblé G. B. *Power Generation, Operation, and Control, 3rd Edition*. John Wiley & Sons, 2013.

Zhi Z. and Botterud A. Dynamic scheduling of operating reserves in co-optimized electricity markets with wind power. *IEEE Trans. Power Syst.*, 29(1):160–171, 2014.

Zimmerman R. D. Uniform price auctions and optimal power flow, matpower power technical note 1. Technical report, Pserc.cornell, 2010. http://www.pserc.cornell.edu/matpower/TN1-OPF-Auctions.pdf.

Zimmermann R. D., Murillo-Sánchez C. E., and Thomas R. J. Matpower: Steady-state operations, planning and analysis tools for power systems research and education. *Smart Grid, IEEE Transactions on*, 26(1):12–19, 2011.

Appendix A

Mathematical Background

This appendix provides mathematical background material relevant to this dissertation. It includes:

1. The DC load flow used throughout the thesis.
2. The two-parameter Weibull distribution PDFs and CDFs.
3. The fitting Methods of the Weibull Parameters
4. The equivalent linear expressions used in Chapter 4.

A.1 The DC load flow

In a network, the complex power, S_k, at a node k, being composed of the active power P and reactive power Q, is given by the product of the complex voltage, E_k, and the conjugate-complex current, I_k^* , at the node. I_k is given by the voltages and admittances, Y_{nm}, in the network.

$$S_k = P_k + jQ_k = E_k \cdot I_k^* = E_k \sum_l Y_{kl}^* E_l^* \tag{A.1}$$

With $Y_{kl} = G_{kl} + B_{kl}$ and θ_k as phase at node k, the power is calculated as follows

$$P_k + jQ_k = \sum_l |E_k|\,|E_l|\,(G_{kl} - B_{kl}) \exp j(\theta_k - \theta_l) \tag{A.2}$$

With $V_k = |E_k|$, the real power P_k is:[1]

$$P_k = \sum_l V_k V_l \,(G_{kl} \cos(\theta_k - \theta_l) - B_{kl} \sin(\theta_k - \theta_l)) \tag{A.3}$$

[1] The reactive power Q_k, being eliminated by the subsequent assumptions, is not considered any more.

In the following, the DC load flow assumptions are applied. First, the losses are assumed to be zero and the resistance of each branch is negligible compared to its reactance. The conductance G is then zero and the susceptance B is equal to $-1/x$ with x as reactance. Looking at one branch between two nodes, the transmitted power is equal to:

$$P_{kl} = V_k V_l \frac{1}{x_{kl}} \sin(\theta_k - \theta_l) \tag{A.4}$$

Secondly, the difference of the phase angles is considered as small so that the small angle approximation can be applied:

$$P_{kl} = V_k V_l \frac{1}{x_{kl}} (\theta_k - \theta_l) \tag{A.5}$$

Finally, the voltage differences are taken as negligible and all voltages are equal. Setting the base apparent power to 1 and the base voltage to the unique voltage at all nodes, the transmitted power is:

$$P_{kl} = \frac{1}{x_{kl}} (\theta_k - \theta_l) \tag{A.6}$$

The DC load flow (A.6) which is a linearization of the nonlinear AC load flow, is an useful approximation of the transmission especially for large-scale economic models. The losses are neglected but the effects of the constraints are normally much more significant than the effects of the losses (Wood et al., 2013). Detailed comparisons of AC and DC load flow representations are given in several studies (Stott et al., 2009; Overbye et al., 2004; Purchala et al., 2005).

A.2 Fitting Methods of the Weibull Parameters

The most common methods to obtain the scale and shape parameters for a Weibull PDF are hereby described.

A.2.1 Maximum Likelihood Estimation (MLE)

The Weibull parameters are those that maximize their joint probability of occurrence and can be obtained by solving the following:

$$k = \left[\frac{\sum_{i=1}^{n} v_i^k \ln(v_i)}{\sum_{i=1}^{n} v_i^k} - \frac{\sum_{i=1}^{n} \ln(v_i)}{n} \right]^{-1} \quad ; \quad c = \left(\frac{1}{n} \left[\sum_{i=1}^{n} v_i^k \right] \right)^{\frac{1}{k}} \tag{A.7}$$

where v_i are the wind speed data values.

A.2.2 Moment Method (MM)

The Weibull parameters are obtained through statistical moments calculated using wind speed data. When the mean wind speed $\bar{v}$ and the standard deviation σ are available, The MM method is solved through the following equations:

$$c = \frac{\bar{v}}{\Gamma\left(1+\frac{1}{k}\right)}; \quad \sigma = c \left[\Gamma\left(1+\frac{2}{k}\right) - \Gamma^2\left(1+\frac{1}{k}\right) \right]^{\frac{1}{2}} \tag{A.8}$$

where the standard gamma function is given by:

$$\Gamma(x) = \int_0^{\infty} t^{x-1} \exp(-t) dt \tag{A.9}$$

A.2.3 Density Power Method (DPM)

Power density according to the Weibull distribution can be expressed as:

$$P_w = \frac{1}{2} \rho \int_0^{\infty} v^3 f(v) dv \tag{A.10}$$

where ρ is the air density of the region. Considering $c = \frac{\bar{v}}{\Gamma\left(1+\frac{1}{k}\right)}$, the weibull parameter k is related to the power density by the following relation

$$\frac{\bar{v^3}}{(\bar{v})^3} = \frac{\Gamma(1+\frac{3}{k})}{\Gamma(1+\frac{1}{k})^3} \tag{A.11}$$

where $\bar{v^3}$ is the mean of wind speed cubes and $\frac{\bar{v^3}}{(\bar{v})^3}$ is known as ensemble energy pattern factor.

Appendix B

Test Cases Information

This appendix describes the characteristics of the test systems used to examine the scheduling tools proposed in this thesis. Unless stated otherwise in the main body of this dissertation, the characteristics listed next apply integrally. It includes:

1. The 6-Bus Test System.
2. The IEEE Reliability Test System Data.
3. The IEEE 118-Bus Test System Data.

B.1 The 6-Bus Test System

The key features and benefits of our method are demonstrated through a 6-bus test system, comprising two identical 3-bus triangle network tied together. The topology of the test system is picturized in Figure B.1. Two demands at buses 3 and 6 with the profiles shown in Table B.1 are curtailable at \$10000/MWh. The characteristics of the branches and conventional generators are provided in Tables B.2 and B.3, respectively. A WEG with 200 MW nominal output is located at bus 2.

Table B.1: The 6-Bus test system load profile

	1^{st} h	2^{nd} h	3^{rd} h	4^{th} h
D3 (MW)	440	540	300	375
D6 (MW)	440	540	300	375

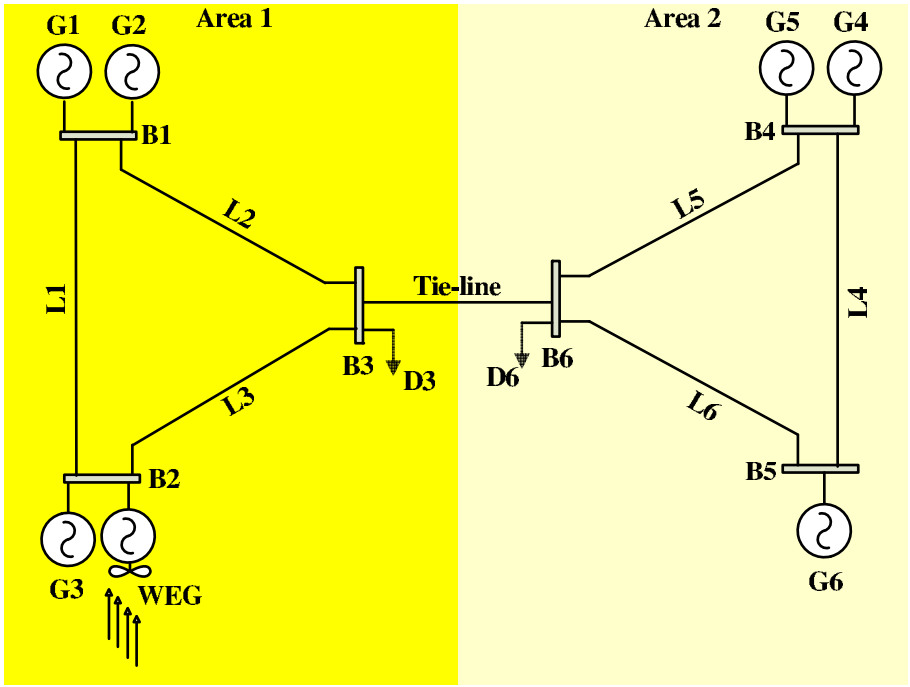

Figure B.1: The interconnected 6-bus test system

Table B.2: The 6-Bus test system transmission lines data

Line #	From node	To node	Resistance (p.u.)	Reactance (p.u.)	Capacity (MVA)
1	1	2	0.005	0.01	300
2	1	3	0.005	0.01	240
3	2	3	0.005	0.01	300
4	4	5	0.005	0.01	300
5	4	6	0.005	0.01	240
6	5	6	0.005	0.01	300
7	3	6	0.005	0.01	150

Table B.3: The 6-Bus test system conventional generators data

Generator g	G1	G2	G3	G4	G5	G6
P^g_{max} (MW)	200	200	500	200	200	500
P^g_{min} (MW)	60	65	60	60	65	60
$R^g_{max^+}$(MW)	100	100	200	100	100	200
$R^g_{max^-}$(MW)	100	100	200	100	100	200
S^g_{on}(\$)	0	200	3000	0	400	6000
S^g_{off}(\$)	0	200	600	0	400	1200
a_g(\$/h)	100	100	100	200	200	200
b_g(\$/MWh)	25	30	40	50	60	80
c_g(\$/MW^{2}h)	.0025	.0030	.0040	.0050	.0060	.0080
d_g(\$/MWh)	1	3	5	2	6	10
e_{g_+}(\$/MWh)	2	4	6	4	8	12
e_{g_-}(\$/MWh)	2	4	6	4	8	12
f_{g_+}(\$/MWh)	1	3	5	2	6	10
f_{g_-}(\$/MWh)	1	3	5	2	6	10
τ^g_+(h)	1	3	1	1	3	1
τ^g_-(h)	1	1	1	1	1	1

B.2 IEEE Reliability Test System Data

The IEEE Reliability Test System is modified to a version that can be readily used for electricity markets and power system operation studies. In order to fully describe the model used, we only elaborate on certain modifications of the original model. The reader, however, is referred to the original reference (Grigg et al., 1999) for a greater discussion of this data and the bases for its creation.

B.2.1 IEEE-RTS Topology

The 24-bus power system is illustrated in Figure B.2. Due to increases in interregional transactions among different electricity systems, multi-area reliability test system has been developed by linking various single-area RTS-96 networks as shown in Figures B.3 and B.4, where, two single-area RTS-96 systems have been merged into a two-area system through three interconnections defined as below:

- 51 mile 230 kV transmission line connecting Bus 123 and Bus 217,
- 52 mile 230 kV transmission line connecting Bus 113 and Bus 215,
- 42 mile 138 kV transmission line connecting Bus 107 and Bus 203,

the resulting two-area system thereafter has been also merged to another third single-area RTS-96 network to form a three-area test system, using the following interconnections:

- 52 mile 230 kV transmission line connecting Bus 121 to Bus 323,
- 67 mile 230 kV transmission line connecting Bus 223 to Bus 318.

B.2.2 Network data

Since all three areas have identical topology, the network data is given based on the one-area RTS-96 and the interconnections between them. Each single-area test system comprises 24 buses and 34 transmission lines as the double-circuit lines in (Grigg et al., 1999) have been

replaced by equivalent single circuit ones. The slack bus of the system is node 213. Line resistances are null and thus, active power losses are disregarded. The values of reactance and capacity of transmission lines for the single-area and interconnections are listed in Table B.4 and Table B.5, respectively. Line reactances are given in per unit on a 100-MVA base.

B.2.3 Load data

The IEEE one-area RTS-96 test system represented in Figure B.2 has 17 loads. The nodal location of these loads and their contribution in percentage to the total system demand are listed in Table B.6. Moreover, the load profile for the considered 24-hour scheduling horizon is provided in Table B.7. The hourly load data correspond to the Thursday of winter week 45 with a peak load of 2850 MW for each area (5700 MW for the two-area system and 8550 MW for the three-area system).

B.2.4 Unit data

Tables B.8-B.11 present the generating units data of the single-area power system. Table B.11 provides the technical data of generating units, Table B.8 shows the node location of generating units, Table B.9 categorizes the units in different types. In our simulations, units with the same type and on the same bus have been merged. In doing so, each single-area has 12 generating units and the system wide total number of units is 36, numbered from 1 to 36 with unit # 1 located in Area 1. Note that the input-output function of generating units are derived from the heat rate data provided in (Grigg et al., 1999), fitted by quadratic functions as shown in Table B.11. Moreover, the unit fuel cost function is derived from multiplying the input-output function by the fuel marginal cost data of generating units as listed in Table B.10. The nuclear and hydro generators are assumed to be must-run units.

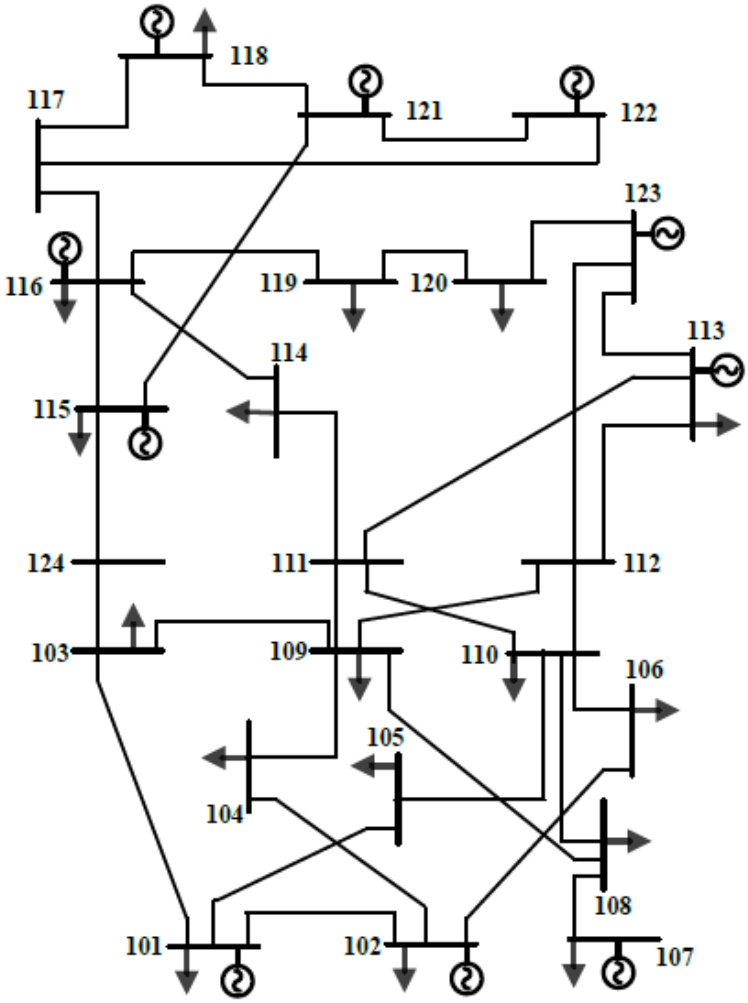

Figure B.2: IEEE one-area RTS-96.

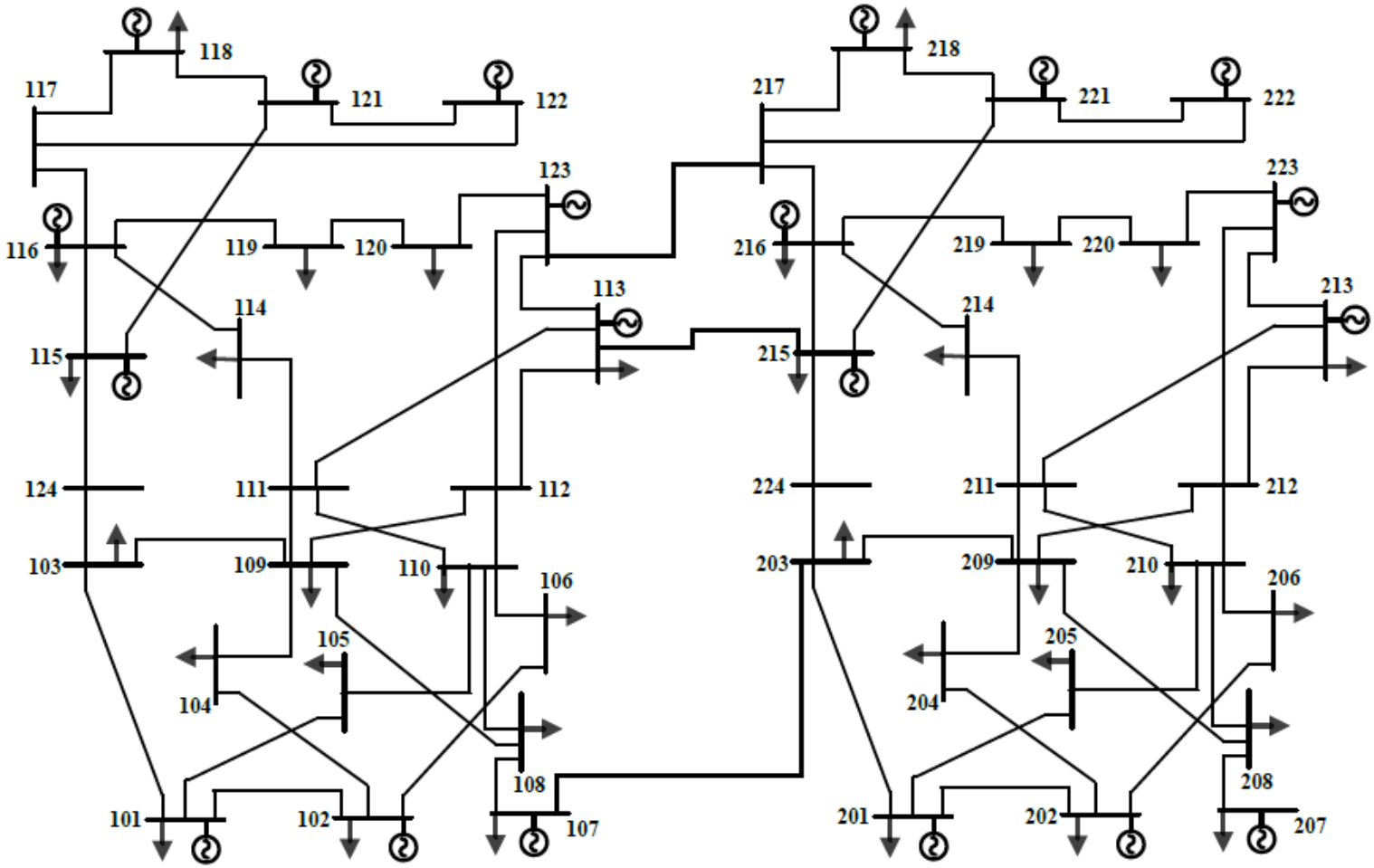

Figure B.3: IEEE two-area RTS-96.

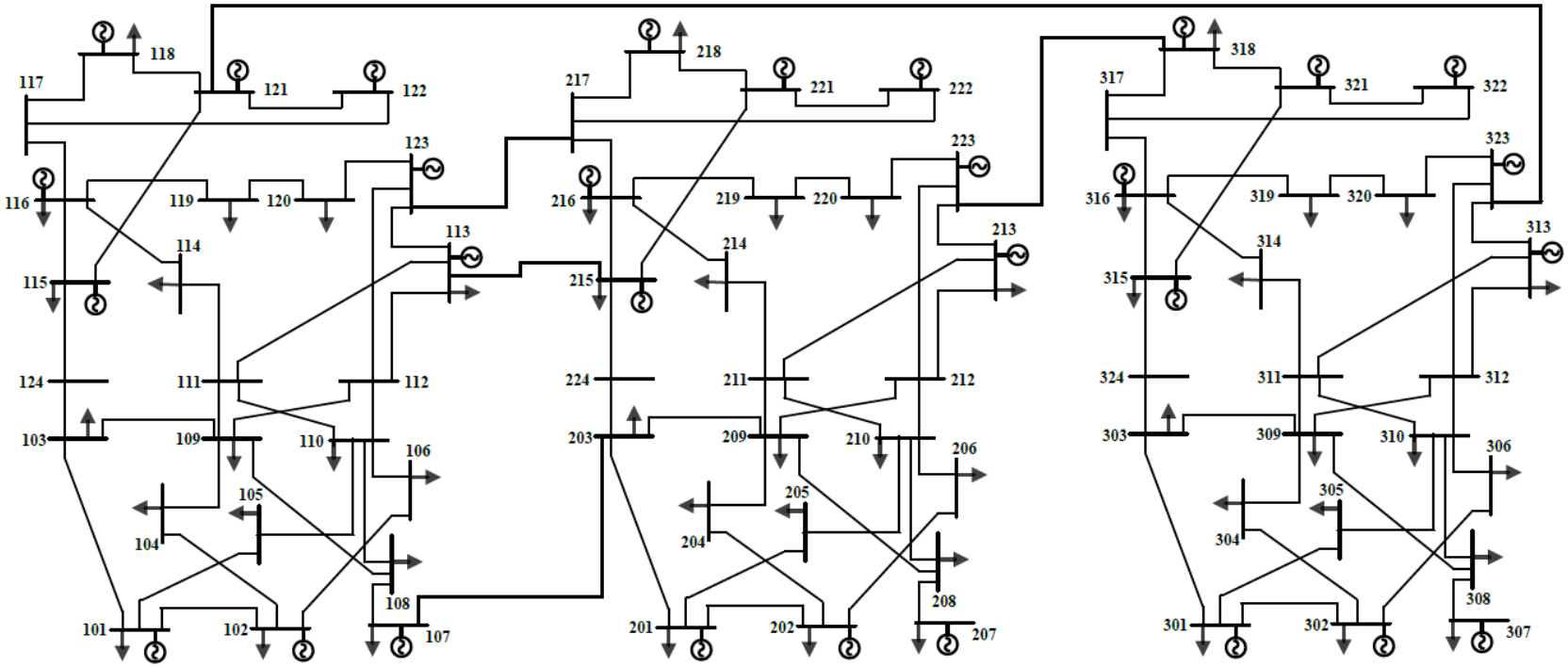

Figure B.4: IEEE three-area RTS-96.

Table B.4: IEEE One-area RTS-96: Reactance and capacity of transmission lines

From node	To node	Reactance (p.u.)	Capacity (MVA)
101	102	0.014	175
101	103	0.211	175
101	105	0.085	175
102	104	0.127	175
102	106	0.192	175
103	109	0.119	175
103	124	0.084	400
104	109	0.104	175
105	110	0.088	175
106	110	0.061	175
107	108	0.061	175
108	109	0.165	175
108	110	0.165	175
109	111	0.084	400
109	112	0.084	400
110	111	0.084	400
110	112	0.084	400
111	113	0.048	500
111	114	0.042	500
112	113	0.048	500
112	123	0.097	500
113	123	0.087	500
114	116	0.059	500
115	116	0.017	500
115	121	0.025	1000
115	124	0.052	500
116	117	0.026	500
116	119	0.023	500
117	118	0.014	500
117	122	0.105	500
118	121	0.013	1000
119	120	0.020	1000
120	123	0.011	1000
121	122	0.068	500

Table B.5: Interconnections among areas: Reactance and capacity of transmission lines

From node	To node	Reactance (p.u.)	Capacity (MVA)
107	203	0.161	175
113	215	0.075	500
123	217	0.074	500
121	323	0.097	500
223	318	0.104	500

Table B.6: Node location and distribution of the total system demand: Area 1

Load #	Node	% of system load	Load #	Node	% of system load
1	101	3.8	10	110	6.8
2	102	3.4	11	113	9.3
3	103	6.3	12	114	6.8
4	104	2.6	13	115	11.1
5	105	2.5	14	116	3.5
6	106	4.8	15	118	11.7
7	107	4.4	16	119	6.4
8	108	6.0	17	120	4.5
9	109	6.1			

Table B.7: Load profile: Area 1

Hour	Demand (MW)	Hour	Demand (MW)	Hour	Demand (MW)
1	1622.3112	9	2300.292	17	2397.1464
2	1525.4568	10	2324.5056	18	2421.36
3	1452.816	11	2324.5056	19	2421.36
4	1428.6024	12	2300.292	20	2324.5056
5	1428.6024	13	2300.292	21	2203.4376
6	1452.816	14	2300.292	22	2009.7288
7	1791.8064	15	2251.8648	23	1767.5928
8	2082.3696	16	2276.0784	24	1525.4568

Table B.8: Generating unit locations: IEEE one-area RTS-96

Bus	Unit #1	Unit #2	Unit #3	Unit #4	Unit #5	Unit #6
101	U76	U76				
102	U76	U76				
107	U100	U100	U100			
113	U197	U197	U197			
115	U12	U12	U12	U12	U12	U155
116	U155					
118	U400					
121	U400					
122	U50	U50	U50	U50	U50	U50
123	U155	U155	U350			

Table B.9: Unit type

Unit type	Unit(s)
Oil-steam	U12 U100 U197
Coal-steam	U76 U155 U350
Nuclear	U400
Hydro	U50

Table B.10: Fuel marginal cost data

Fuel Type	Oil-steam	Coal-steam	Nuclear	Hydro
Cost ($/MBtu)	2.30	1.20	0.60	0

Table B.11: Technical data of generating units: IEEE one-area RTS-96

Units Group	P^g_{max} (MW)	P^g_{min} (MW)	c_g (MBtu/MW^{2}h)	b_g (MBtu/MWh)	a_g (MBtu/h)	$R^g_{max^+}$ (MW)	$R^g_{max^-}$ (MW)	Δ^g_+ (MW/h)	Δ^g_- (MW/h)	τ^g_+ (h)	τ^g_- (h)
U12	12	2.4	0.158141	8.674834	16.80916	12	12	12	12	4	2
U50	50	0	0	0	0	10	10	50	50	1	1
U76	76	15.2	0.030919	7.859749	134.0325	20	20	60	60	8	4
U100	100	25	0.011923	7.504672	129.6655	25	25	100	100	8	8
U155	155	54.25	0.005561	7.541385	184.2571	30	30	155	155	8	8
U197	197	68.95	0.004972	7.651967	189.491	60	60	80	80	12	10
U350	350	140	0.003261	7.428056	323.3268	40	40	240	240	24	48
U400	400	100	0.000983	8.582228	406.6257	50	50	280	280	48	48

B.3 IEEE 118-Bus Test System Data

The system data are given at `http://www.motor.ece.iit.edu/data/SCUC_118test.xls` however, the topology of the test system is depicted below.

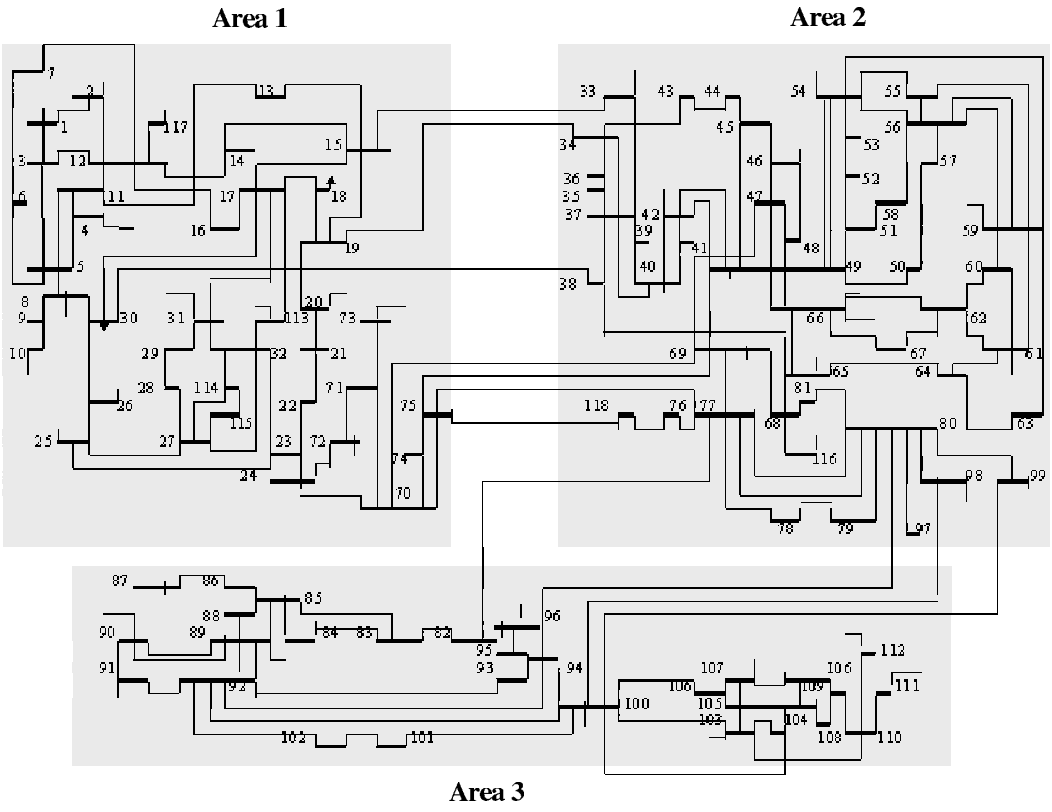

Figure B.5: IEEE 118-bus three-area test system.

Appendix C

Description of Matlab Codes

In Chapter 3 and 4, multiperiod, stochastic, contingency constrained, optimal power flow (where network constraints are represented through a DC load flow) problems with linear constraints and unit commitment are proposed and formulated. The objective of this appendix is to help the reader to implement these models. For this reason, a description of the Matlab code sources used are included in this appendix.

C.1 Background

These simulations are based on two free-open source packages for the Matlab language, namely:
- Matpower, a steady state power flow simulation and optimization for Matlab and Octave
- Most, the Matpower Optimal Scheduling Tool (installed with MATPOWER).

In order to run these simulations, you need a high-performance MIP solver. I used Gurobi, which is supported by Matpower for Matlab and is available via a free license for academic use.

C.2 Getting Started

I solve the quadratic programming problem (2.20) as described in subsection 2.7.3 of chapter 2. The difference between the two models being in:

-the representation of security constraints (3.9), (3.10), (3.12) and (3.22) for chapter 3 against (4.1g)-(4.1j) for chapter 4

-the consideration of the number of scenarios and contingencies, only one scenario and no contingency in chapter 3 against three base scenarios and a list of selected contingencies for chapter 4.

Keeping in mind these different features, the structure of the codes are as follows:

1- Inputs

a) Construct all data needed for the optimization problem as shown in Figure 1.2 namely, the matpower case **mpc**, the transition probability matrices **transmat**, the extra generator data **xgt**, the contingency table **contab** and the **profiles** for time-varying parameters.

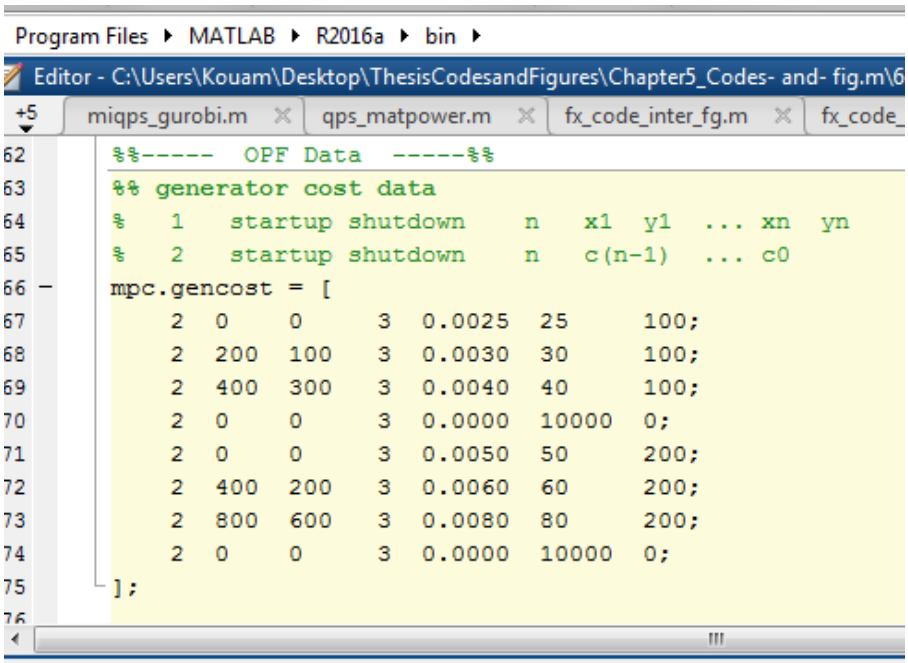

Figure C.1: The 6-bus test system mpc generator cost data

For example, the generator cost data from the illustrative 6-bus test system used throughout the thesis is reported in Figure C.1, where the three last columns represent in the same order, the quadratic, the linear and the no load cost coefficients of the generating units. Lines 4 and 8 in this table are fictitious units cost data, located at load buses to mimic load shedding. Note that mpc.gencost is one of the four tables contain in the data structure **mpc**

of the case under studied. The format of the data is similar to the PTI format described in http://www.ee.washington.edu/research/pstca/formats/pti.txt. **transmat** is a cell array containing the transition probability matrices. In chapter 4 model with three base scenarios for low, medium and high wind realizations, **transmat** handles the transitions from period $t-1$ to period t. **xgt** contain the per-generator data required for the problem and that are not included in the **mpc**. This includes UC data, ramping cost or reserve offer data. **contab** is a contingency table with a master set of contingencies used for security throughout entire horizon. **contab** struct is used only in chapter 4 while the failure of a generating unit in chapter 3 is manually handled by setting its status to 0 in the **xgt** struct. **profiles** are used to specify how parameters vary from period to period and are defined in terms of changes to a base value.

b) Assemble all the above data structures as an input to Most using the **loadmd** function. In Matpower, this is done by calling a Most data struct as the first argument:

```
mdi = loadmd(mpc, transmat, xgd, contab, profiles);
```

The types of arguments to the **loadmd** function are typical of the nature of the problem. For example, in chapter 3, **loadmd** will not contain **contab** as an argument.

c) Specify Most run options, **mpopt**, i.e., - how Most is run and - the solver to use and the phases of the problem building and solving to be included. At this stage, the reader should assume that **mpopt** is a Matpower options struct and that the define_constants has already been executed in order to avoid having to remember column numbers and to allow code to be more robust against potential future changes to the Matpower case data format.

```
mpopt = mpoption('verbose', 2, 'most.solver', 'GUROBI');
```

with verbose printing of the algorithm progress.

In our study the MIQP problem is built at this step, both constraints and standard costs and store in **mdo**.QP field, where **mdo** is the Most data struct output. The DC model of load flow is also specified here as well as the Gurobi for the solver. In building the model the reader can implement the exogenous security constraint or the local determination of reserve by including the **contab** data struct or not. However, he should pay a great attention in defining the different reserve zones of chapter 3 as the fields for their requirement, zone, cost and quantity are to be specified.

2- Solving the case

Assuming the input data have been loaded into the input Most Data struct **mdi** and the Matpower options set in **mpopt**, the solver can be called as follows.

```
mdo = most(mdi, mpopt);
```